D-Serine, an emerging biomarker of kidney diseases, is a hidden substrate of sodium-coupled monocarboxylate transporters

Pattama Wiriyasermkul[1], Satomi Moriyama[1], Yoko Tanaka[1], Pornparn Kongpracha[1], Nodoka Nakamae[1], Masataka Suzuki[2], Tomonori Kimura[3,4], Masashi Mita[5], Jumpei Sasabe[2], Shushi Nagamori[1,#]

[1]Department of Collaborative Research for Biomolecular Dynamics, Nara Medical University, Nara, Japan

[2]Department of Pharmacology, Keio University School of Medicine, Tokyo, Japan

[3]KAGAMI Project, [4]Reverse Translational Research Project, Center for Rare Disease Research, National Institutes of Biomedical Innovation, Health and Nutrition (NIBIOHN). Osaka, Japan

[5]KAGAMI Inc., Osaka, Japan

Corresponding contact information: snagamori@nagamori-lab.jp

Keywords: transporter, proteome, ischemia-reperfusion injury (IRI), acute kidney injury (AKI), chronic kidney diseases (CKD), membrane

Abstract

Delay in diagnosis of renal injury has profound impacts on morbidity and mortality. Damage of proximal tubules by the injury impairs not only individual membrane transport proteins but also coordinated transport systems. In this study, we analyzed the proteome of apical membranes of proximal tubular epithelium from the mouse kidney with early ischemia-reperfusion injury (IRI), a well-known acute kidney injury (AKI) model. The proteome showed drastic elevations of the injury-responsive proteins and depressions of abundant transporters, leading to the prediction of biomarkers for early IRI. As the benchmark of our in-depth analysis from the proteome, we characterized transporters for D-serine, a promising renal diseases' biomarker. Using cell-based and cell-free methods, we identified sodium-coupled monocarboxylate transporters (SMCTs) as the D-serine transporters. This finding enlightens the role of non-canonical substrate transport and clarifies the D-serine transport systems in the kidney. Our approaches can be applied for investigation of other membrane transport systems.

Impact statement

Proteomics and biochemical analysis reveal D-serine as a non-canonical substrate of sodium-coupled monocarboxylate transporter SMCTs

43 **Introduction**

44 The renal system, where membrane transport proteins are the most diverse and
45 abundant, plays crucial roles in body homeostasis, thereby often being the most impacted from
46 critical illness and vulnerability to the subtle changes in molecular substances. Acute kidney
47 injury (AKI) and chronic kidney diseases (CKD), which are common diseases worldwide,
48 cause severe health problems but encounter the limitations on standard diagnosis and
49 classification (Zhang and Parikh, 2019). AKI and CKD are considered as interconnected
50 syndromes. Although AKI happens suddenly and is reversible, the extension of the injury and
51 incomplete repairment of renal tubular cells consecutively lead to CKD progression (Devarajan
52 and Jefferies, 2016). Hence, the gold-standard diagnosis at the early stages of AKI is an
53 important key factor needed in order to maximize the therapeutic success and minimize CKD
54 development. Conventional markers for AKI diagnosis include measuring serum creatinine
55 levels and estimated Glomerular filtration rate (eGFR). Still, both methods are limited in their
56 specificity, lack of standardized quantification, variation in individuals, and limited usage in
57 patients with comorbidities (Ostermann and Joannidis, 2016). Lately, systemic analysis using
58 innovative technologies, such as Integrative Omics and Next-Generation Sequencing, have
59 opened new possibilities for detecting biomarkers of AKI and CKD. Yet, the new biomarkers
60 have restrictions on their application and efficacy due to the specificity and the unclear
61 characterization of the underlying molecular mechanism (Eddy et al., 2020; Kirita et al., 2020;
62 Liu et al., 2020; Marx et al., 2018; Thongboonkerd, 2020; Zhang and Parikh, 2019).

63 Proximal tubule, the main part for reabsorption and secretion of metabolites and organic
64 compounds in the kidney, is the primary target of AKI and CKD progression (Chevalier, 2016).
65 Thus, apical (luminal) membrane proteins from proximal tubular epithelium would represent
66 significant pathological membrane transport proteins that are the underlying mechanisms of
67 metabolite biomarkers for AKI and CKD. D-Serine, a dextro isomer of serine, is discovered as

68 one of the promising biomarkers for AKI and CKD detections using the 2D-HPLC method
69 (Hesaka et al., 2019; Kimura et al., 2020, 2016; Sasabe et al., 2014; Sasabe and Suzuki, 2018).
70 In the normal condition, D-serine is in high ratio to urine but low in plasma. Contrarily, the
71 plasma D-serine is elevated in patients and animal models with CKD and AKI, while the
72 luminal D-serine is decreased. The amount of D-serine is strongly associated with kidney
73 function and progression of these diseases. Transport of D-serine takes place at the proximal
74 tubule (Kragh-Hansen and Sheikh, 1984; Sasabe and Suzuki, 2018; Shimomura et al., 1988;
75 Silbernagl et al., 1999). However, such a corresponding transporter in both physiological and
76 pathological conditions has not been clearly explained.

77 D-Serine was firstly found highly abundant in the brain. Extensive studies have revealed
78 that D-serine plays important roles in neurotransmitter modulation by acting as an obligatory
79 physiological co-agonist of *N*-methyl-D-aspartate receptors (NMDARs) (Wolosker, 2018).
80 Until now, three amino acid transporters, SLC1A4/ASCT1, SLC1A5/ASCT2, and
81 SLC7A10/Asc-1 are recognized to mediate D-serine transport in the brain (Foster et al., 2016;
82 Rosenberg et al., 2013). Despite the role and transport system of D-serine in brain, little is
83 known about D-serine in peripheral tissues. Mammals acquire D-serine by biosynthesis via
84 serine racemase function and absorption from dietary and gut microbiota via intestinal transport
85 system(s) (Sasabe et al., 2016; Sasabe and Suzuki, 2018). The D-serine homeostasis in the
86 plasma is controlled by luminal-membrane transporters and DAAO activities in the intestine
87 and kidney. In the kidney, D-serine from blood, which passed through the renal glomeruli, is
88 reabsorbed at proximal tubules. Subsequently, intracellular D-serine is degraded by DAAO,
89 which is located in the proximal tubular cells, thereby maintaining the plasma D-serine at low
90 levels (Sasabe et al., 2014). It is suggested by the serum and urinary D/L serine profile of the
91 CKD patients and AKI animal models that the renal D-serine transport properties in

92 physiological conditions and in pathological conditions are different and have distinct
93 stereoselectivity (Sasabe and Suzuki, 2018).

94 The reabsorption and excretion of a substance in the kidney is co-operated by multiple
95 plasma membrane transport proteins (Chu et al., 2016; Ghezzi et al., 2018; Kandasamy et al.,
96 2018). Malfunction of a single type of membrane transport protein causes a fluctuation in the
97 chemical gradient of the substrates and affects other transport systems that also transport the
98 same substance. Therefore, it is necessary to consider that renal dysfunction is caused by not
99 only the breaking down of several transport systems themselves but also the disruption of the
100 coordination between each transport system. Here, we applied proteomics of apical membranes
101 from renal proximal tubules of the mice with ischemia-reperfusion injury (IRI), a well-known
102 model for AKI and AKI-CKD transition (Fu et al., 2018; Sasabe et al., 2014), to reveal the
103 membrane transport proteins that are responsible for the transport of AKI metabolite
104 biomarkers, especially the D-serine transport system as a paradigm. By further screening and
105 kinetic analysis, we identified two D-serine transport systems at the apical membranes of
106 proximal tubules—sodium-coupled monocarboxylate transporters (SMCTs) and neutral amino
107 acid transporter ASCT2, which explain the mechanism of chiral selection and elevation of D-
108 serine transport in AKI and CKD.

109 # Results

110 **Membrane proteome of renal proximal tubules of the IRI model**

111 To understand the molecular pathophysiology of AKI, we characterized proteomes of
112 renal brush border membrane vesicles (BBMVs), the membrane fraction representing the
113 apical membranes of proximal tubular epithelium, from the IRI mouse model. We analyzed the
114 samples from 4 hours and 8 hours after ischemia-reperfusion (4h IRI and 8h IRI) because these
115 time points are considered as early stages of AKI, where serum creatinine levels are slightly
116 increased, and urine KIM-1 remains unchanged (Sasabe et al., 2014). The proteome of IRI
117 samples was calculated as ratios of the negative control group (sham), yielding two groups of
118 comparative proteome data: 4h IRI/sham (4h) and 8h IRI/sham (8h). In total, 4,426 proteins
119 were identified in which 1,186 proteins were categorized as plasma membrane proteins and
120 extracellular matrix proteins (Table supplement 1, Figure supplement 1A). Among them, 1,110
121 proteins were predicted to possess more than one transmembrane domain (Table supplement
122 1). We observed a great increase of two well-known early AKI biomarkers—CCN1 (CYR61:
123 matrix-associated heparin-binding protein; the ratio of 4h/sham = 41.4; the ratio of 8h/sham =
124 29.9) and NGAL (LCN2: Neutrophil gelatinase-associated lipocalin; the ratio of 4h/sham =
125 1.8; the ratio of 8h/sham = 9.5), which confirmed the reliability of our proteomics on the IRI
126 model for early AKI (Table supplement 1) (Marx et al., 2018). To characterize pathological
127 changes in IRI, we selected 318 proteins which passed a cut-off value of 1.5 fold change ($\log_2$
128 fold of IRI/sham = 0.58: both increased and decreased) with p-value ≤ 0.05 ($-\log_{10}$ p-value $\geq$
129 1.3) and further analyzed the biological functions and toxicity functions by using IPA. Top-10
130 toxicity functions verified the damages of the kidney due to the injury and inflammation
131 (Figure supplement 1B). Hierarchical heatmaps of the organ pathologies prognosticate various
132 defects in the kidney which include tubule dilation, nephritis, kidney injury and damage, and

133 renal failure (Figure supplement 1C). Besides the renal pathologies, IPA also indicated the
134 injury and damage in the liver and heart as several corresponding proteins are shared among
135 the organs (Figure supplement 1C).

136 Analysis of biological functions showed the proteome was highly involved in cellular
137 compromise, cell survival, molecular transport, and system development (Figure 1A-B). The
138 hierarchical heatmap exhibited that most of the biological functions are increased (with a
139 decrease of cell death), which indicated the mechanisms related to the injury responses rather
140 than the pathophysiological functions (Figure 1C). We categorized the injury responses into
141 three groups: *rapid responses*, *prolonged responses*, and *slow responses*. The first group, *rapid*
142 *responses*, shows biological functions are highly increased at 4h IRI but gradually reduced at
143 8h IRI. The responses related to pro-inflammation and innate immunity, which include the
144 complementary system, free radical scavenging, metal ion elevation, lipid synthesis, lipid
145 transport, and lipid metabolism (Figure 1C). The second group is involved in the biological
146 functions that are rapidly increased at 4h IRI and maintained to 8h IRI, named *prolonged*
147 *responses*. Cell viability and homeostasis, cell-cell interaction, epithelial cell movement, and
148 vascularization are the biological functions in the *prolonged responses* in order to sustain an
149 effective immune response (Figure 1C). The third group called *slow responses* are those
150 increased functions at 8h IRI, including the adaptive immunity—leukocyte/lymphocyte
151 migration and phagocytosis, immune cell and connective tissue adhesion, and endothelial
152 tissue development (Figure 1C). At 8h, we observed the significant increase of cellular
153 compromise and tissue development, implying the initiation of the repairment systems (Figure
154 1A-B). Analysis of diseases relevant to biological functions showed the remarkable elevation
155 of the inflammatory response at both 4h and 8h IRI, confirming the significant contribution of
156 the *rapid, prolonged, and slow responses* (Figure 1D). Although the immune-related responses
157 and tissue repairment were progressive, we still observed the tissue abnormality, tissue damage,

158 and inflammation (Figure 1D). From the results, we concluded the biological functions in early
159 AKI (both 4h and 8h IRI) as follows: 1) the immune system rapidly and extensively responded
160 to the injury since 4h IRI, 2) the processes of tissue development and repair were initiated at
161 8h IRI, and 3) the pathological features of the injured kidney were prolonged observed since
162 4h IRI.

163 Next, we predicted a series of protein biomarkers to detect early stages of the kidney
164 injury and found 34 proteins significant altered at both 4h and 8h IRI (Figure 1E). Table 1
165 summarizes the physiological function and previous applications of these proteins. The protein
166 biomarkers previously proposed for AKI, CKD, and related kidney diseases are CCN1/CYR61,
167 LTF, FPR2, CYBB, SERPINF1, and C5AR1. In this study, we predicted 28 protein biomarkers
168 (Figure 1E, Table 1). The protein biomarkers are categorized into four types according to their
169 physiological functions. BTF3, ZFP36L1, TPT1, CDA, RPSA, EIF3D, and RPS27A, which
170 were increased in IRI, are molecules that play a role in protein synthesis. DCTN4, ARL3,
171 PAFAH1B2, OCLN, PCOLCE, GPC4, and CMKLR1 are molecules involved in cell structure,
172 cell-cell interaction, and tissue development. LDLR, ESYT1, and APOA2 are correlated with
173 lipid transport and homeostasis. The last group of candidates which were mostly found
174 decreased in IRI are membrane transport proteins: SLC15A2/PEPT2, SLC19A3/THTR2,
175 SLC5A8/SMCT1, PLXDC2, SLC22A7/OAT2, CYB5B, SLCO4C1/OATP-M1, AQP7,
176 SLC2A5/GLUT5, PIEZO1, and KCNAB2.

177 We analyzed the biological networks and found two top-scoring networks were related
178 to the *rapid responses* (Figure 2A-B), while another network related to the *prolonged responses*
179 (Figure 2C). Networks at the *slow responses* (8h IRI) have less scoring than the *rapid* and
180 *prolonged* responses (Figure supplement 2). Although we did not examine the total proteome,
181 we could predict the master regulators of the networks from our membrane proteome. In the
182 networks of the *rapid responses*, NF-κB, PI3K, and Myc are likely the key regulators (Figure

183 2A-B). HDL complex was found to be a central regulator for the *prolonged responses* and Akt
184 was predicted to be involved (Figure 2C). BCL2, ANXA1, and integrin complex are important
185 regulators for tissue development and repair in the *slow responses* (Figure supplement 2).

186 **Alterations of membrane transport proteins in the kidney of the IRI model**

187 To unveil the renal pathophysiological defect behind the injury responses, we analyzed
188 the whole proteome without any cutoff to recognize slight changes of the silent molecules. The
189 analysis depicted a high scoring of pathological functions related to kidney diseases and the
190 circulatory system (Figure supplement 3). These data intimate that the proximal tubular
191 membrane proteins involved in IRI pathological mechanisms altered less in the amounts than
192 the injury-responsive proteins but were abundant in the membrane proteome. Among these
193 membrane proteins, membrane transport proteins were one of the leading groups. Because the
194 substrates of these membrane transport proteins are well-used metabolite biomarkers for AKI,
195 CKD, and other diseases, we further investigated membrane transport proteins to unveil the
196 pathogenic mechanisms. We selected the 319 membrane transport proteins comprising ATP-
197 binding cassette (ABC) transporters, solute-carriers (SLCs), ATPase pumps, and channels to
198 analyze their biological functions by IPA without any cutoff. The analysis unveiled two
199 transport groups based on the types of substrates; 1) ions and 2) organic compounds (Figure
200 3A). The ions are composed of inorganic ions (Figure 3A: lower left) and charged organic
201 compounds (Figure 3A: right). The organic compounds comprise both charged and uncharged
202 compounds (Figure 3A: right). IPA analysis showed that the transport of ions remained
203 unchanged at 4h IRI and slightly increased at 8h IRI. The sum of ions which indicated less
204 change was actually made up from the combination of anions and cations in which both of
205 them altered in some degrees at the opposite direction (Figure 3A: left). In particular, sum of
206 ions which showed small alteration was caused by the dynamic alteration of various inorganic

207 ion transport proteins (both inorganic cations and inorganic anions; Figure 3B). Accordingly,
208 the cells are suggested to have neural pH at 4h IRI and slight pH change at 8h. We suggest that
209 the injured cells attempted to preserve cellular pH and ion homeostasis, which was a foundation
210 for the function of organic compound transporters and substantial protein functions. In contrast
211 to the ion transport group, the protein group that transports organic compounds was strongly
212 decreased at 4h and gradually recovered at 8h (Figure 3A: right). Most proteins in this group
213 were found to be decreased, indicating that their defect was from the damaged brush border
214 membranes and delayed in recovery (Figure 3B). The levels of less alteration in membrane
215 transport proteins also imply the low expression levels compared to the proteins in the injury
216 responses.

217 **Screening of candidate molecules for D-serine transporters**

218 Membrane transport proteins derived from our proteome represent a good collection
219 for identification of transport systems for the anticipated metabolite biomarkers of renal injury
220 with unknown transporter(s) or novel metabolite biomarkers. Since D-serine has been proposed
221 as an effective biomarker for AKI and CKD yet unknown transport mechanism, we aimed to
222 characterize the D-serine transport system in the kidney. From the membrane proteome, we
223 detected the increases of ASCT2 at both 4h and 8h IRI (Figure 4A, Table 2). Using HAP1 cells
224 carrying CRISPR/CAS-mediated *ASCT2* knockout, we examined D-serine uptake and
225 confirmed that ASCT2 is a D-serine transporter (Figure supplement 4A). ASCT2 is located at
226 the apical membranes of all proximal tubular segments and transports serine with high affinity
227 (K_m of 167 μM for D-serine in oocyte system) but weak stereoselectivity (Foster et al., 2016).
228 However, the previous studies demonstrated D-serine transport systems in S1-S2 and S3
229 segments are different and their kinetics are in mM range (Kragh-Hansen and Sheikh, 1984;
230 Silbernagl et al., 1999). Silbernagl et al. also suggested ASCT2 is not (or not only) a D-serine

231 transporter at pars recta (Silbernagl et al., 1999). Notably, the serum and urinary D/L serine
232 profile from CKD and AKI samples indicated the stereoselective transporter(s) (Sasabe and
233 Suzuki, 2018). We thus postulated the existence of (an)other D-serine transporter(s). To screen
234 and identify D-serine transporters, we choose ASCT2 as a pivotal molecule to make the cut-off
235 line in our membrane proteomics data. We selected membrane transport proteins that altered
236 more than ASCT2 at both 4h and 8h IRI (Figure 4A). To further focus on the reabsorption
237 system at the lumen, we omitted transporters that are reported to be in basolateral membranes
238 and organelles. Membrane transport proteins that recognize only inorganic ions were excluded.
239 SLC36A1/PAT1 and SLC6A18/B^0AT3, known small amino acid transporters, were included,
240 although they only passed the cut-off value at one of the time points, either 4h or 8h.
241 SLC5A12/SMCT2 was also included in the list with less significant alteration because SMCT1,
242 another member of sodium-coupled monocarboxylate (SMCT) family, was selected. SMCT2
243 has a comparable role with SMCT1 in monocarboxylate reabsorption at apical membranes, but
244 they localize at different segments of proximal tubules. Finally, ten candidates of D-serine
245 transporters were listed (Table 2).

246 HEK293 cell line was used for the development of the screening method of D-serine
247 transporters because the cells exhibited high transfection efficiency. First, we identified amino
248 acid transporters from membrane proteome of HEK293 cells (Table supplement 2). Then, we
249 examined which transporters are responsible for D-serine transport in the cells. From the results,
250 D-serine transport in HEK293 cells required Na^+ and was inhibited by ASCT2 substrates (L-
251 Ser, L-Thr, and L-Met) (Figure supplement 4B-C). Inhibition by Ben-Cys and GPNA in
252 HEK293 cells showed a similar pattern to that of ASCT2-expressed cells (Bröer et al., 2016),
253 but MeAIB (system A inhibitor) had no effect (Figure supplement 4C). Using siRNA to
254 knockdown ASCT2, we verified that ASCT2 is a main D-serine transporter in HEK293 cells
255 (Figure 4B-C). A previous study showed that treatment with D-serine in a human proximal

256 tubular cell line impaired the growth (Okada et al., 2017). We found that this growth defect
257 occurred in HEK293 cells and was due to the ASCT2 function. Although L-serine showed no
258 effect, D-serine reduced cell growth in a concentration-dependent manner with IC_{50} of 17.4
259 mM (Figure supplement 4D). In the ASCT2-knockdown cells, the growth inhibition by D-
260 serine was attenuated (Figure 4D), indicating the D-serine taken up by ASCT2 contributes to
261 the D-serine-suppressed cell growth.

262 Based on the findings above, we investigated the candidate transporters from the
263 proteome data by the D-serine effect on cell growth. With D-serine treatment at both 15 mM
264 (near the IC_{50} concentration) and 25 mM (high concentration), Asc-1 transfected cells (positive
265 control) showed significantly lower growth than the Mock cells, confirming this assay is
266 effective to screen D-serine transporters. Among the ten candidates, PAT1 and B^0AT3
267 attenuated growth suppression while SMCT1 and SMCT2 exaggerated growth suppression
268 over Mock at both 15 and 25 mM D-serine treatment (Figure 5A-B), suggesting that both
269 SMCTs transport D-serine into the cells. Accordingly, SMCT1 and SMCT2 are primarily
270 selected for further analysis (Figure supplement 5).

271 **Characterization of D-serine transport in SMCTs.**

272 SMCTs are sodium-dependent monocarboxylate symporters. Their canonical
273 substrates are short-chain fatty acids and monocarboxylates such as lactate, propionate, and
274 nicotinate (Ganapathy et al., 2008). To characterize D-serine transport in both SMCT1 and
275 SMCT2, we generated Flp-In T-REx 293 cells stably expressing human SMCT1 (FlpInTR-
276 SMCT1) and SMCT2 (FlpInTR-SMCT2). Expression of SMCTs in FlpInTR-SMCT1 and
277 FlpInTR-SMCT2 was verified by Western blot using anti-FLAG antibody to detect FLAG-
278 tagged on SMCTs. SMCT1 and SMCT2 expression remain unchanged upon ASCT2
279 knockdown (Figure supplement 6A). The transport function of SMCTs was verified by

280 [^{14}C]nicotinate uptake (Figure supplement 6B-C). Ibuprofen, an SMCT inhibitor, was used to
281 verify the growth inhibition effect by SMCTs. Unlike Mock in which ibuprofen has no effect,
282 the growth inhibition by D-serine treatment were gradually attenuated by ibuprofen in both
283 FlpInTR-SMCT1 and FlpInTR-SMCT2 cells (Figure 5C).

284 Transport of D-[^{3}H]serine was measured in the SMCT stable cell lines. Both SMCT1
285 and SMCT2 cells showed an increase of D-[^{3}H]serine transport compared to Mock with or
286 without ASCT2 knockdown (Figure 6A and supplement 6D). The D-[^{3}H]serine transport in
287 both SMCT1 and SMCT2 was inhibited by NSAIDs (ibuprofen and acetylsalicylate: SMCT
288 inhibitors) (Figure 6B) (Gopal et al., 2007; Itagaki et al., 2006). D-Serine and nicotinate also
289 inhibited D-[^{3}H]serine uptake in the SMCT1 cells but much less effective in the SMCT2 cells
290 suggesting the low affinity of D-serine in SMCT2 than SMCT1 (Figure 6B).

291 **Transport properties and kinetics of D-serine in SMCT1**

292 Kinetics of D-[^{3}H]serine transport in SMCT1 was measured in FlpInTR-SMCT1 cells
293 in the presence of ASCT2 knockdown. SMCT1 transported D-[^{3}H]serine in a concentration-
294 dependent manner, and the curve fitted to Michaelis−Menten kinetics with the apparent K_m of
295 5.0 mM (Figure 6C, supplement 6E).

296 Because there were the high backgrounds of D-serine transport in cells, even in the
297 ASCT2-knockdown condition, we assumed that endogenous transporters, including
298 uncharacterized molecules, and metabolites impede the examination of the SMCT1 properties
299 precisely. We then characterized the D-serine transport properties of the purified SMCT1 in
300 SMCT1-reconstituted proteoliposomes. Liposomes are spherical-shaped vesicle made from
301 lipid mixtures to mimic the membrane lipid bilayer. The proteoliposomes are the liposomes
302 with a protein incorporated. With the proteoliposome system, both internal and external
303 substances can be squarely defined. 3xFLAG-tagged SMCT1 was purified from Expi293F cells

304 transfected with pCMV14-SMCT1 by anti-FLAG affinity column. Purified SMCT1 showed a
305 single band on SDS-PAGE corresponding to the expected size (Figure 7A), and the protein
306 was confirmed by Western blot using anti-FLAG antibody (Figure supplement 7A). SDS-
307 PAGE showed the successful incorporation of the purified SMCT1 in the proteoliposomes
308 (SMCT1-PL) (Figure 7A). We measured the uptake of L- and D-[^{3}H]serine in SMCT1-PL. In
309 the presence of external Na^+, SMCT1 transported both L- and D-[^{3}H]serine as well as the
310 canonical substrates ([^{3}H]lactate and [^{3}H]propionate) (Figure 7B, supplement 7B). The
311 transport was dramatically inhibited by ibuprofen, confirming the function of SMCT1 (Figure
312 7B, supplement 7B). The time courses of D-[^{3}H]serine uptake were measured in both Na^+ and
313 Na^+-free buffers. The results showed that SMCT1 transported D-[^{3}H]serine in Na^+-dependent
314 condition (Figure 7C and supplement 7C). The uptake value in Na^+-free buffer is a result of
315 non-specific accumulation in liposomes/proteoliposomes, which is slightly linear upon the
316 incubation time (Figure supplement 7C). SMCT1 recognized both L- and D-serine over other
317 small amino acids (L- and D-alanine), acidic amino acids (L- and D-glutamate), or large neutral
318 amino acids (L- and D-tyrosine) (Figure 7D). Uptake of L- and D-serine was approximately 30%
319 and 60% of lactate, respectively (Figure 7D). These results indicated that SMCT1 transported
320 serine with lower affinity than its canonical substrates, and the recognition is more
321 stereoselective to D- than L- isomer.

322 **D-Serine reabsorption in renal proximal tubular cells**

323 To investigate the function of transporters at the apical membranes of proximal tubules
324 under controlled conditions of chemical gradients, we used mouse brush border membrane
325 vesicles (BBMVs), which enriched the apical membrane transporters. D-Serine transport in
326 mouse BBMVs was examined in different conditions to distinguish the contribution of ASCT2
327 and SMCTs. Because ASCT2 functions as an antiporter that influxes one amino acid with an

328 efflux of L-glutamine while SMCTs are symporters (Ganapathy et al., 2008; Scalise et al.,
329 2018), we performed D-serine transport assay in BBMVs with or without L-glutamine
330 preloading. In L-glutamine-preloaded BBMVs, transport of D-[^{3}H]serine arose quickly and
331 reached the saturated point at 20 sec (Figure 8A, supplement 8A). The uptake was ibuprofen-
332 insensitive at 10 – 30 sec and became partially ibuprofen-sensitive at 1 min (Figure 8A). In
333 contrast, transport of D-[^{3}H]serine in BBMVs without the preloading increased slowly (Figure
334 8B). D-[^{3}H]Serine transport was initiated after 30 sec and reached the optimum at 2 min (Figure
335 8B, supplement 8B). Notably, the transport was largely inhibited by ibuprofen which is a
336 SMCT inhibitor, but not by L-threonine which is an ASCT2 substrate (Figure 8B-C). These
337 results suggested that, in the L-glutamine preloading condition, positive D-[^{3}H]serine transport
338 at 10 - 30 sec was derived from the antiport mode of Asct2, which occurred rapidly. Meanwhile,
339 SMCTs function started slowly at 60 sec as seen in the non-preloading condition. As a result,
340 D-[^{3}H]serine transport at 1 min in L-glutamine preloading condition was from the
341 combinational functions of both ASCT2 and SMCTs (Figure 8A).

342 Previous studies described the localization of SMCT1 at S3 segment. SMCT2 is found
343 in all segments and enriched in S1 of proximal tubules (Gopal et al., 2007; Kirita et al., 2020).
344 Although ASCT2 has been intensively studied in cells or other organs, the localization and
345 function in the kidney have not been well characterized. We generated affinity-purified Asct2
346 antibodies to recognize both N-terminus (NT) and C-terminus (CT) of Asct2 (Figure
347 supplement 8C) and detected Asct2 in mouse kidney. Asct2 was co-immunostained with both
348 Sglt2 (Slc5a2; sodium/glucose cotransporter 2) and Agt1 (slc7a13, aspartate/glutamate
349 transporter 1), which are apical membrane markers for S1+S2 and S3 segments, respectively
350 (Figure 8D-E) (Ghezzi et al., 2018; Nagamori et al., 2016a). In contrast, Asct2 did not co-
351 localize with Na^+/K^+-ATPase, which is a basolateral membrane marker (Figure 8F). The results
352 demonstrated that Asct2 is localized at the apical side in all segments of proximal tubules.

353 **Discussion**

354 Our membrane proteome revealed two major groups of the proteins classified by
355 biological functions. The first group is involved in injury/inflammatory responses and tissue
356 repairs. Most proteins in this group exhibited high degrees of elevation and various subcellular
357 localization. Many of them are often found in the omics research and the list of protein
358 biomarkers in kidney diseases (Eddy et al., 2020; Marx et al., 2018; Thongboonkerd, 2020;
359 Zhang and Parikh, 2019). On the other hand, the second group is rather specific to the
360 pathogenic proteins in IRI. The dominant protein types in the second group are membrane
361 transport proteins. Many of the membrane transport proteins showed low degrees of alteration
362 in IRI, adding difficulty to their identification from the whole-cell/tissue proteome and
363 transcriptome. In this study, we succeeded in identifying multiple membrane proteins, in
364 particular transporters located at the apical membranes of proximal tubules. The membrane
365 proteome allows us to examine how transporters play roles in the normal condition or in the
366 injured condition.

367 Based on the proteome data, we utilized the intensive biochemical assays including "*in*
368 *vitro*" cultured cells, "cell-free" proteoliposomes, and "*ex vivo*" BBMV methods to identify
369 SMCT1, SMCT2, and ASCT2 as D-serine transporters at the apical membranes of renal
370 proximal tubules. SMCT1 has preference on D-serine over L-serine and other amino acids
371 (Figure 7D). The apparent K_m of D-serine transport in SMCT1 is 5.0 mM which is considered
372 to be low affinity (Figure 6C). We attempted to examine the kinetics of D-serine transport in
373 SMCT2. However, the uptake values at high D-serine concentration were low and concealed
374 by the high background, indicating a lower affinity of SMCT2 than that of SMCT1. These
375 results are in agreement with the physiological properties of SMCT1 and SMCT2 as the low-
376 affinity transporters for their canonical substrates although the affinity of SMCT1 is higher
377 than that of SMCT2 (Ganapathy et al., 2008). We conclude that SMCT1 and SMCT2 transport

378 D-serine with low affinity and high stereoselectivity toward the D- isomer. On the contrary,
379 ASCT2 transports D-serine with high affinity (μM range) although approximately 8 folds less
380 than L-serine (Foster et al., 2016).

381 It is surprising, but reasonable once we found that SMCTs transport D-serine. Several
382 studies reported the transport of non-canonical substrates by membrane transport proteins
383 especially the recognition between amino acids, carboxylates and amines among SLC
384 transporters (de Carvalho and Quick, 2011; Matsuo et al., 2008; Metzner et al., 2005;
385 Schweikhard and Ziegler, 2012; Wei et al., 2016). D-Serine structure consists of a
386 hydroxypropionic acid with an amino group at the α-carbon. It is likely that the
387 hydroxypropionic acid residue on D-serine is the main part to interact with SMCTs because
388 hydroxypropionic acid shares similar moiety to lactic acid and propionic acid of SMCT
389 canonical substrates.

390 Previous studies indicated D-serine transport takes place at the proximal tubules by the
391 distinct transport systems between S1-S2 and S3 segments. Although the transport properties
392 of each system were not clearly distinguished, both systems exhibited the characteristics of Na^+
393 dependency, electrogenicity, low affinity (mM range), and partial stereoselectivity (Kragh-
394 Hansen and Sheikh, 1984; Shimomura et al., 1988; Silbernagl et al., 1999). These D-serine
395 transport properties suit well to SMCTs and convince the contribution of SMCTs to renal D-
396 serine transport in addition to ASCT2. It was reported that a fair amount of D-serine from gut
397 microbiota mitigates AKI (Nakade et al., 2018). However, a high dose of D-serine
398 administration induces nephrotoxicity by targeting proximal tubules and confining at the S3
399 segment (Hasegawa et al., 2019; Morehead et al., 1945; Silbernagl et al., 1999). It is most likely
400 that the D-serine-induced proximal tubular damage is (partly) due to the absorption of D-serine
401 by SMCTs, in particular by SMCT1 at the S3 segment. Ibuprofen minimized D-serine transport

402 and attenuated D-serine-induced toxicity in SMCTs-expressing cells (Figure 5C, 6B), implying
403 the efficiency of ibuprofen to alleviate D-serine-induced nephrotoxicity.

404 What is the physiological importance of D-serine reabsorption? Although ASCT2
405 transports D-serine with high affinity *in vitro* (Foster et al., 2016), the amount of ASCT2 in the
406 kidney is much lower than those of SMCTs (Table 2: abundance in Sham) indicating the low
407 capacity of D-serine reabsorption. In contrast, the high abundance and low affinity of SMCTs
408 demonstrate a high capacity of D-serine transport. It is most likely that the main contributor for
409 D-serine reabsorption is SMCTs. However, in the physiological conditions where the canonical
410 substrates of SMCTs exist, the amount of reabsorbed D-serine via SMCTs would be relatively
411 low because the luminal D-serine amount is low and D-serine competes with SMCTs' canonical
412 substrates. Possibly, SMCTs take up D-serine by chance, and the reabsorbed D-serine may not
413 be important for carbon-source supplement or particular renal activities as the reabsorbed D-
414 serine is also degraded by DAAO. Despite the inconspicuous merit of reabsorbed D-serine,
415 functional activity of SMCTs to transport D-serine is significant in order to preserve the low-
416 level of serum D-serine.

417 *De novo* cells, stem cells, and cancer cells share common characteristics of high
418 proliferative rate and metabolic demands. In the IRI condition where the damaged proximal
419 tubules attempt to recover their function by tissue development and repair, functions of high-
420 affinity transporters would denote great benefit to supply enormous nutrients in a short time.
421 In these regards, ASCT2 is a good candidate for the cellular response mechanism. ASCT2 is
422 found in placenta for fetus development and highly expressed in cancer cells and stem cells
423 (Formisano and Van Winkle, 2016; Kandasamy et al., 2018; Scalise et al., 2018). ASCT2 plays
424 a key role in regulation of mammalian target of rapamycin (mTOR) signaling pathway and
425 glutamine-mediated metabolism (Kandasamy et al., 2018; Scalise et al., 2018). Our proteome

426 data detected the continued elevation of ASCT2 (Figure 3C, 4A). Conceivably, ASCT2
427 upregulation is a result of a proliferative pathway for cell growth and repair.

428 Taken all together, we propose a model of D-serine transport in renal proximal tubules
429 (Figure 8G). In physiological conditions, SMCT1 and SMCT2 mainly contribute to D-serine
430 transport with low affinity. Intracellular D-serine is then catalyzed by DAAO in the proximal
431 tubule. As a consequence, the meager amount of D-serine is detected in serum (Sasabe et al.,
432 2014). In contrast, both SMCTs were decreasing while ASCT2 was upregulating in the IRI
433 model (Table 2, Figure supplement 5). The increase and high affinity of ASCT2 bring about
434 larger D-serine reabsorption. Thus, luminal D-serine is decreased in the pathophysiological
435 conditions (Figure 8G). Recently, SMCT2 was reported as a protein indicator for kidney repair
436 from the injury. Prolonged SMCT2 down-expression indicated the failed repair of proximal
437 tubular cells in IRI (Kirita et al., 2020). The prolonged decrease of SMCT2 during the injury
438 in-turn supports the merit of luminal D-serine as a metabolite biomarker for AKI and CKD.

439 In this study, we principally focused on the D-serine transport system at the luminal
440 side of proximal tubules and explained the low urinary D-serine in IRI. Combination of ASCT2
441 induction and DAAO reduction may result in the elevation of serum D-serine. Future study on
442 the D-serine transport system at the basolateral side is necessary to explain the increase of
443 serum D-serine and complete the picture of D-serine transport system in renal proximal tubules.

444 D-Serine treatment in PAT1- and B^0AT3-expressing cells showed an increase in cell
445 growth (Figure 5A). PAT1, which is localized at both lysosome and plasma membrane, was
446 reported to transport D-serine while the ability of B^0AT3 in D-serine uptake is unknown. Both
447 PAT1 and B^0AT3 may play a role in D-serine secretion in cells. In kidney, PAT1 is located at
448 both apical membranes and inside of the epithelium (maybe also on the basolateral side) of S1
449 segment (The Human Protein Atlas: https://www.proteinatlas.org; updated on Mar 6th, 2020;
450 Thwaites and Anderson, 2011; Vanslambrouck et al., 2010). B^0AT3 is found at the apical

451 membranes of S3 segment (Vanslambrouck et al., 2010). The contribution of D-serine transport
452 by PAT1 and B^0AT3 in the kidney needs to be further examined.

453 For the detection of membrane transport proteins which require post-translational
454 modification and translocation, proteomics provides a direct association toward the protein
455 function than the transcriptomics does. Although proteomics has been intensively applied for
456 AKI and CKD studies, to our knowledge, none of the studies emphasized the analysis of
457 membrane proteins at the lumen of proximal tubules of the IRI model. Membrane transport
458 proteins are one of the most important targeting groups in the proteomic analysis of AKI
459 because they are directly linked to the metabolites and molecular substances. Our proteomics
460 provides a great hint on membrane transport proteins at hierarchical levels: from individual
461 proteins to systemic scale. The proteome data clearly indicated that homeostasis of inorganic
462 ions is rescued within a short time. On the contrary, the defect of organic compounds is
463 prolonged and requires extensive time to be fully recovered (Figure 3A). These data support
464 the usefulness of the metabolite biomarkers for diagnosis and prognosis of kidney diseases
465 because most metabolite biomarkers are organic compounds which exhibit prolonged defects
466 during IRI. Herein, we predict a new series of membrane transport proteins as biomarkers
467 (Table 2). Since most of them are decreased in the IRI model, their substrates are promising
468 candidates for AKI and CKD metabolite biomarkers, such as substrates of GLUT5, AQP7,
469 OATP-M1, OAT2, THTR2, and PEPT2.

470 One good example of the usefulness of our proteome is the prediction of transport
471 systems for creatinine, a well-known AKI and CKD biomarker. At the apical membranes,
472 creatinine is excreted by transporters MATE1/SLC47A1 and MATE2-K/SLC47A2 and likely
473 transported by OCTN1/SLC22A4, OCTN2/SLC22A5, and OAT2 (Chu et al., 2016; Tanihara
474 et al., 2007). Our proteome data indicated the reduction of MATE1 (Figure 3B), convincing
475 the importance of MATE1 over MATE2-K in creatinine efflux. Decrease of OCTN1, OCTN2,

476 and OAT2 in IRI also leads to speculation of their contribution in creatinine transport (Figure
477 3, Table 1-2). Another example is the glucose transport system. In physiological conditions,
478 SGLTs reabsorb glucose and GLUT5 reabsorbs fructose at the luminal side (Ghezzi et al.,
479 2018; Szablewski, 2017). From the proteome, we found a decrease in SGLT1/SLC5A1 and
480 GLUT5 but an increase in GLUT3/SLC2A3 (Figure 3B). GLUT3 exhibits the highest affinity
481 among GLUTs but very low expression in physiological conditions (Simpson et al., 2008).
482 Accordingly, GLUT3 might be a key transporter for metabolic activities in the repair processes.

483 Apart from the kidney, D-serine transport in the brain is contributed by multiple
484 transport systems. The affinity of D-serine transport in astrocyte and retinal glia cultures was
485 found to be in the millimolar range (Dun et al., 2007; Foster et al., 2016). SMCT1 is expressed
486 in neurons, astrocytes, and retinal cells, while SMCT2 is rather restricted to retina (Martin et
487 al., 2007, 2006). Meta-data analysis demonstrated the interaction of SMCT1 and five types of
488 NMDARs (https://amp.pharm.mssm.edu/Harmonizome/; Rouillard et al., 2016). SMCTs are
489 also found in the colon, intestine, and thyroid organs (Ganapathy et al., 2008; Paroder et al.,
490 2006). It is worthwhile to investigate the contribution of SMCTs on D-serine transport systems
491 in those tissues.

492 Here, we utilize a multi-hierarchical approach to identify D-serine as a hidden substrate
493 of SMCTs. This finding clarifies the physiological transport system of D-serine at the apical
494 membranes of proximal tubules and proposes the D-serine transport in IRI. Our strategy can be
495 applied to the investigation of any transport systems with hidden physiological substrates.

496 # Materials and Methods

497 ## Materials, animals and graphical analysis

498 General chemicals and cell culture media were purchased from Wako Fujifilm.
499 Chemicals used in mass spectrometry were HPLC or MS grades. Flp-In T-Rex 293 cells,
500 Expi293F cells, Expi293 Expression medium, Lipofectamine 3000, fluorescent-labeled
501 secondary antibodies, and Tyramide SuperBoost kit were from Thermo. Amino acids, fetal
502 bovine serum (FBS), anti-FLAG antibody and anti-FLAG M2 column were from Sigma.
503 Secondary antibodies with HRP conjugated were from Jackson ImmunoResearch. L-[^{3}H]Serine,
504 D-[^{3}H]serine, L-[^{3}H]alanine, and D-[^{3}H]alanine were from Moravek. L-[^{3}H]Glutamic acid, D-
505 [^{3}H]glutamic acid, L-[^{14}C]tyrosine, D-[^{14}C]tyrosine, DL-[^{3}H]lactic acid, [^{3}H]propionic acid,
506 [^{14}C]nicotinic acid and [^{14}C]uric acid were from American Radiolabeled Chemicals. Anti-
507 SGLT2 and anti-Na^+/K^+-ATPase antibodies were obtained from Santa Cruz Biotechnology.
508 All animal experiments were carried out following institutional guidelines under
509 approval by the Animal Experiment Committees of Nara Medical University and Keio
510 University, Japan.

511 Unless otherwise indicated, data shown in all figures are mean ± standard error of the
512 representative data from three independent experiments. Statistical differences and p-values
513 were determined using the unpaired Student *t* test. Graphs, statistical significance, and kinetics
514 were analyzed and plotted by GraphPad Prism 8.3.

515 ## Plasmid construction

516 In this study, we used the cDNA of human SLC5A8/SMCT1 clone "NM_145913". We
517 generated the clone NM_145913 from the clone AK313788 (NBRC, NITE, Kisarazu, Japan).
518 At first, SMCT1 from AK313788 was subcloned into p3XFLAG-CMV14 (Sigma) via *Hind*III

519 and *Bam*HI sites. The clone "pCMV14-SMCT1" NM_145913 was subsequently generated by
520 mutagenesis of p3XFLAG-CMV14-SMCT1_AK313788 at I193V, T201A and I490M
521 (variants between NM_145913 and AK313788) by HiFi DNA Assembly Cloning (NEB) and
522 site-directed mutagenesis. Human SLC5A12/SMCT2 cDNA (NM_178498; Sino Biological
523 Inc.) was amplified by PCR and cloned into p3XFLAG-CMV14 via *Kpn*I and *Bam*HI sites to
524 generate "pCMV14-SMCT2". Human expression clones of SLC7A10/Asc-1 (NM_019849),
525 SLC7A1/CAT1 (NM_003045), SLC36A1/PAT1 (NM_078483), SLC2A5/GLUT5
526 (NM_003039), SLCO4C1/OATP-M1 (NM_180991), SLC22A13/OAT10 (NM_004256),
527 SLC22A7/OAT2 (NM_153320), SLC6A18/B^0AT3 (NM_182632), SLC15A2/PEPT2
528 (NM_021082), and TMEM27/Collectrin (NM_0202665) were obtained from GenScript and
529 RIKEN BRC through the National BioResource Project of the MEXT/AMED, Japan. Mouse
530 Asct2 (mAsct2, NM_009201) TrueORF clone was obtained from OriGene. p3XFLAG-
531 CMV14 empty vector was used for Mock production. pcDNA5-SMCT1 and pcDNA5-SMCT2
532 used for generation of SMCT1- and SMCT2-stable cell lines, respectively, were constructed
533 by assembling the PCR products of SMCT1 or SMCT2 into pcDNA5/FRT/TO (Thermo) by
534 HiFi DNA Assembly Cloning kit.

535 **Antibody (Ab) production**

536 Anti-human ASCT2 (hASCT2) and anti-mAsct2 Abs were self-produced. First, we
537 generated pET47b(+)-GST. The fragment encoding GST was amplified by using pET49b(+)
538 as the template. The GST fragment was cloned into pET47b(+) via *Not*I and *Xho*I restriction
539 sites. To obtain the antigen for anti-hASCT2 Ab, the PCR products corresponding to amino
540 acid residues 7-20 of hASCT2 were amplified and cloned into pET47b(+)-GST to obtain GST-
541 fusion protein. For antigens from mAsct2, both N-terminal (mAsct2(NT), amino acid residues
542 1 – 38) and C-terminal (mAsct2(CT), amino acid residues 521 – 553) fragments were fused
543 with GST by cloning into pET47b(+)-GST or pET49b(+), respectively (Cosmo Bio Co., Ltd).

544 The GST-fusion antigens were expressed in *E. coli* BL21(DE3) and purified by Glutathione
545 Sepharose 4B (GE Healthcare) as described previously (Nagamori et al., 2016a). The antigens
546 were used to immunize rabbits to obtain anti-sera were obtained (Cosmo Bio).

547 Anti-hASCT2 Ab was purified from the anti-sera using HiTrap Protein G HP (GE
548 Healthcare) following the manufacturer's protocol. After purification, the antibody was
549 dialyzed against PBS pH 7.4 and adjusted concentration to 1 mg/mL.

550 Anti-mAsct2(NT) and anti-mAsct2(CT) Abs were purified by using two-step
551 purifications. First, affinity columns of GST-fused mAsct2(NT)-antigen and GST-fused
552 mAsct2(CT)-antigen were made by conjugated the antigens with HiTrap NHS-activated HP
553 (GE Healthcare) following the manufacturer's protocol. To purify anti-mAsct2(NT) Ab, the
554 anti-sera was subjected to the first purification by using the GST-fused mAsct2(NT)-antigen
555 column. The elution fraction was dialyzed and subsequently subjected to the second column of
556 GST-fused mAsct2(CT)-antigen column. The flowthrough fraction corresponding to the
557 affinity-purified anti-mAsct2(NT) Ab was obtained. Purification of anti-mAsct2(CT) Ab was
558 performed in the same way as mAsct2(NT) Ab but used GST-fused mAsct2(CT)-antigen
559 column followed by GST-fused mAsct2(NT)-antigen column.

560 **Ischemia-reperfusion injury (IRI) model and isolation of brush border membrane**
561 **vesicles (BBMVs) for mass spectrometry analysis**

562 C57BL/6J (CLEA Japan) male mice between 12 – 16 weeks old underwent
563 experimental procedures for the IRI model. Ischemia-reperfusion was performed as previously
564 described (Sasabe et al., 2014). Before IRI induction, right kidney was removed. After 12 days,
565 the mice were grouped by randomization. Ischemia was operated for 45 min by clamping the
566 vessel under anesthesia with pentobarbital. After that, the vessel clamp was removed, and the
567 abdomen was closed. Sham-operated control mice were treated identically except for clamping.

568 At 4 and 8 hours after reperfusion, mice were anesthetized with isoflurane and euthanized by
569 perfusion with PBS pH 7.4. The kidney was removed and stored at -80 °C until use.

570 BBMVs were prepared by calcium precipitation method (Modified from Biber et al.,
571 2007). Frozen kidneys were minced into fine powders by using a polytron-type homogenizer
572 (Physcotron, Microtec) in the homogenization buffer containing 20 mM Tris-HCl, pH 7.6, 250
573 mM sucrose, 1 mM EDTA and cOmplete EDTA-free protease inhibitor cocktail (Roche). After
574 low-speed centrifugation at 1,000 ×g and 3,000 ×g, the supernatant was collected and incubated
575 with 11 mM $CaCl_2$ for 20 min on ice with mild shaking. The supernatant was ultra-centrifuged
576 at 463,000 ×g for 15 min at 4 °C. The pellet was resuspended in the homogenization buffer and
577 repeated the steps of $CaCl_2$ precipitation. Finally, the pellet of BBMVs was resuspended in 20
578 mM Tris-HCl pH 7.6 and 250 mM sucrose. Membrane proteins of BBMVs were enriched by
579 the urea wash method (Uetsuka et al., 2015). The urea-washed BBMV samples were subjected
580 to sample preparation for mass spectrometry.

581 **Cell culture, transfection, and generation of stable cell lines**

582 HEK293 and Flp-In T-Rex 293 cells were cultured in DMEM supplemented with 10 %
583 (v/v) FBS, 100 units/mL penicillin G, and 100 μg/mL streptomycin (P/S), and routinely
584 maintained at 37 °C, 5 % CO_2 and humidity. For transfection experiments, the cells were
585 seeded in antibiotic-free media for one day prior to transfection to obtain approximately 40%
586 confluence. DNA transient transfection and ASCT2-siRNA (ID#s12916; Ambion) transfection
587 were performed by using Lipofectamine 3000 following the manufacturer's protocol. The ratio
588 of DNA : P3000 : Lipofectamine 3000 is 1.0 μg : 2.0 μL : 1.5 μL. The ratio of siRNA :
589 Lipofectamine 3000 is 10 pmol : 1 μL. The cells were further maintained in the same media
590 for 2 days and used for the experiments.

591 Flp-In T-REx 293 stably expressing SMCT1 (FlpInTR-SMCT1) and SMCT2
592 (FlpInTR-SMCT2) were generated by co-transfection of pOG44 and pcDNA5-SMCT1 or
593 pcDNA5-SMCT2 and subsequently cultured in the media containing 5 mg/L blasticidin and
594 150 mg/L hygromycin B for positive clone selection. Mock cells were generated in the same
595 way using the empty plasmid. Expressions of SMCT1 in FlpInTR-SMCT1 and SMCT2 in
596 FlpInTR-SMCT2 were induced by adding 1 mg/L doxycycline hyclate (Dox; Tet-ON system)
597 one day after seeding. The cells were further cultured for two days prior to performing
598 experiments.

599 Wild-type and *ASCT2*-knockout HAP1 cells (Horizon Discovery) were cultured in
600 IMDM supplemented with 10 % (v/v) FBS, P/S, and routinely maintained at 37 °C, 5 % CO_2
601 and humidity.

602 Expi293F cells were cultured in Expi293 Expression medium at 37 °C, 8 % CO_2, and
603 humidity. To express SMCT1 transiently, the cells were transfected with pCMV14-SMCT1
604 using PEI MAX pH 6.9 (MW 40,000; Polysciences) and cultured for two days.

605 **Mass spectrometry**

606 Mass spectrometry of mouse BBMVs was performed as described previously with
607 some modification (Uetsuka et al., 2015). After preparing urea-washed BBMVs, the samples
608 were fractionated into four fractions by SDB-XC StageTips and desalted by C18-StageTips.
609 Mass spectrometry was performed using the Q Exactive (Thermo) coupled with Advance
610 UHPLC (Michrom Bioresources). The HPLC apparatus was equipped with a trap column (L-
611 column ODS, 0.3 x 5 mm, CERI) and a C18 packed tip column (100 µm ID; Nikkyo Technos).
612 Raw data from four fractions were analyzed using Proteome Discoverer 2.2 (Thermo) and
613 Mascot 2.6.2 (Matrix Science). Data from four fractions were combined and searched for
614 identified proteins from the UniProt mouse database (released in March 2019). The maximum
615 number of missed cleavages, precursor mass tolerance, and fragment mass tolerance were set

616 to 3, 10 ppm and 0.01 Da, respectively. The carbamidomethylation Cys was set as a fixed
617 modification. Oxidation of Met and deamidation of Asn and Gln were set as variable
618 modifications. A filter (false discovery rate < 1%) was applied to the resulting data. For each
619 mouse sample, the analysis was conducted twice and the average was used. One data set was
620 composed of 3 samples from each operation condition (n = 3).

621 Mass spectrometry of HEK293 cells was analyzed from crude membrane fractions.
622 Membrane fractions from HEK293 cells were prepared from 3-day cultured cells as described
623 (Nagamori et al., 2016b). Membrane proteins were enriched by the urea wash method, and
624 tryptic peptides were subject for analysis as described above.

625 **Proteome data analysis and availability**

626 Protein localization and functional categories were determined by Ingenuity pathway
627 analysis (IPA, Qiagen). The prediction of transmembrane regions was acquired using the
628 transmembrane hidden Markov model (TMHMM) Server v. 2.0. Localization in kidney
629 segments was evaluated based on related literature and The Human Protein Atlas
630 (http://www.proteinatlas.org: updated Dec 19, 2019).

631 The biological functions, the toxicity functions (diseases and organ pathologies), and
632 the biological networks were analyzed using IPA. Molecules from the dataset that met the
633 cutoff of the Ingenuity Knowledge Base were considered for the analysis. A right-tailed
634 Fisher's Exact Test was used to calculate the p-value determining the probability (z-scores) of
635 the biological function or the toxicity function assignment (IPA). The networks derived from
636 IPA were simplified by omitting the proteins in canonical pathways that were not detected and
637 not key regulators. Networks with the shared regulators were merged and displayed in the
638 Figures.

639 All proteomics data have been deposited in Japan Proteome Standard
640 Repository/Database: JPST000929 and JPST000931.

641 **Effect of cell D-serine on cell growth**

642 HEK293 cells were seeded into 96-well-plate at 10,000 cells/well. Transient
643 transfection was performed 12 hours after seeding followed by L- or D-serine treatment 12
644 hours after that. In the case of FlpInTR-stable cell lines, ASCT2 siRNA was transfected 12
645 hours after seeding, if needed. Dox was added one day after seeding followed by treatment
646 with L- or D-serine (in the presence or absence of ibuprofen as indicated) 10 hours after adding
647 Dox. The cells were further maintained for 2 days. Cell growth was examined by XTT assay.
648 In one reaction, 50 μL of 1 mg/mL XTT (2,3-Bis-(2-Methoxy-4-Nitro-5-Sulfophenyl)-2*H*-
649 Tetrazolium-5-Carboxanilide) (Biotium) was mixed with 5 μL of 1.5 mg/mL phenazine
650 methosulfate. The mixture was applied to the cells and incubated for 4 hours at 37 °C in the
651 cell culture incubator. Cell viability was evaluated by measuring the absorbance at 450 nm.
652 Cell growth in serine treatment samples was compared to the control (without serine treatment).
653 For transporter screening, the growth of the transfected cells at a specific D-serine concentration
654 was compared to that of Mock after normalization with no treatment.

655 **Transport assay in cultured cells**

656 Transport assay in cells was performed as described previously with some
657 modifications (Nagamori et al., 2016b). Briefly, for D-[^{3}H]serine transport in HEK293 cells,
658 the cells were seeded into poly-D-lysine-coated 24-well plates at 1.2 x 10^5 cells/well and
659 cultured for three days. Uptake of 10 μM (100 Ci/mol) or 100 μM (10 Ci/mol) D-[^{3}H]serine
660 was measured in PBS pH 7.4 at 37 °C at the indicated time points. After termination of the
661 assay, the cells were lysed. An aliquot was subjected to measure protein concentration, and the
662 remaining lysate was mixed with Optiphase HiSafe 3 (PerkinElmer). The radioactivity was
663 monitored using a β-scintillation counter (LSC-8000, Hitachi). In the transport assay with or
664 without Na^+, Na^+-HBSS, or Na^+-free HBSS (choline-Cl substitution) were used instead of PBS.

665 Transport assay in FlpInTR-stable cell lines was performed in a similar way to HEK293
666 cells. After cell seeding for one day, SMCT1 and SMCT2 expression were induced by adding
667 Dox for two days. For the ASCT2 knockdown experiment, ASCT2-siRNA was transfected 12
668 hours prior to Dox induction. The time course of 100 μM D-[^{3}H]serine transport (10 Ci/mol)
669 was measured 37 °C for 5 – 20 min. Inhibition assay was performed by adding the test
670 inhibitors at the same time with D-[^{3}H]serine substrate. Kinetics of D-[^{3}H]serine transport were
671 examined by the uptake of D-[^{3}H]serine at the concentration of 0.5 – 8 mM (0.125 – 2 Ci/mol)
672 for 10 min at 37 °C.

673 Transport of D-[^{3}H]serine in wild-type and *ASCT2*-knockout HAP1 was performed in
674 a similar way to HEK293 and FlpInTR-stable cells but without the process of transfection.

675 **hSMCT1 purification, proteoliposome reconstitution, and transport assay**

676 hSMCT1 was purified from SMCT1-expressing Expi293F cells. Membrane fraction
677 and purification processes were performed as previously described with small modifications
678 (Nagamori et al., 2016a). First, cell pellets were resuspended in 20 mM Tris-HCl pH 7.4, 150
679 mM NaCl, 10% (v/v) glycerol, and protease inhibitor cocktail (Roche). The crude membrane
680 fraction was derived from sonication and ultracentrifugation (sonication method). Membrane
681 proteins were extracted from the crude membrane fraction with 2% (w/v) DDM and
682 ultracentrifugation. hSMCT1 was purified by anti-FLAG M2 affinity column. Unbound
683 proteins were washed out by 20 mM Tris-HCl pH 7.4, 200 mM NaCl, 10% (v/v) glycerol, and
684 0.05% (w/v) DDM then hSMCT1 was eluted by 3xFLAG peptide in the washing buffer.
685 Purified hSMCT1 was concentrated by Amicon Ultra Centrifugal Filters 30K (Millipore).

686 The reconstitution of proteoliposomes was performed as described with minor
687 modifications (Lee et al., 2019). The purified hSMCT1 was reconstituted in liposomes (made
688 from 5:1 (w/w) of type II-S PC : brain total lipid) at a protein-to-lipid ratio of 1:100 (w/w) in
689 20 mM MOPS-Tris pH 7.0 and 100 mM KCl.

690 Transport assay in proteoliposomes was conducted by the rapid filtration method (Lee
691 et al., 2019). Uptake reaction was conducted by dilution of 1 μg SMCT1 proteoliposomes in
692 100 μL uptake buffer (20 mM MOPS-Tris pH 7.0, 100 mM NaCl for Na^+-buffer or KCl for
693 Na^+-free buffer, 1 mM $MgSO_4$ and 1 mM $CaCl_2$) containing radioisotope-labeled substrates.
694 The reaction was incubated at 25 °C for an indicated time. The radioisotope-labeled substrates
695 were used as follows: 5 Ci/mol for [^{14}C]uric acid, L-[^{14}C]tyrosine and D-[^{14}C]tyrosine; 10
696 Ci/mol for DL-[^{3}H]lactic acid, L-[^{3}H]alanine, D-[^{3}H]alanine, L-[^{3}H]serine, D-[^{3}H]serine, L-
697 [^{3}H]glutamic acid and D-[^{3}H]glutamic acid; and 20 Ci/mol for [^{3}H]propionic acid. In the
698 inhibition assay, 1 mM ibuprofen was applied at the same time with the radioisotope-labeled
699 substrates.

700 **Transport assay in mouse BBMVs**

701 Both left and right kidneys were taken out from the 8 weeks old male wild-type
702 C57BL/6J mice (Japan SLC) after PBS perfusion and frozen until use. After mincing and
703 homogenizing the frozen kidneys (as in the above section) in the buffer containing 20 mM Tris-
704 HCl pH 7.6, 150 mM mannitol, 100 mM KCl, 1 mM EDTA, and protease inhibitor cocktail,
705 the BBMVs were prepared by magnesium precipitation method (Biber et al., 2007). The pellet
706 of BBMVs was resuspended in the suspension buffer (10 mM Tris-HCl, pH 7.6, 100 mM
707 mannitol, and 100 mM KCl). In the L-glutamine preloading experiment, the BBMVs were
708 mixed with 4 mM L-glutamine on ice for 3 hours, centrifuged at 21,000 ×*g* for 20 min, and
709 resuspended in the suspension buffer.

710 Transport assay was performed by rapid filtration. Prior to initiating the reaction, 5 μM
711 valinomycin was added into the BBMV samples and the BBMVs were kept at room
712 temperature for 2 minutes. Transport assay was examined by diluting 100 μg BBMVs in 100
713 μL of the uptake buffer (10 mM Tris-HCl pH 7.6, 150 mM NaCl for Na^+ condition or KCl for

714 Na^+-free condition, 50 mM mannitol and 5 μM valinomycin) containing 10 μM D-[^{3}H]serine
715 (100 Ci/mol). The reaction was incubated at 30 °C at an indicated time, then terminated by the
716 addition of ice-cold buffer containing 10 mM Tris-HCl pH 7.6 and 200 mM mannitol, and
717 filtered through 0.45 μm nitrocellulose filter (Millipore), followed by washing with the same
718 buffer once. The membranes were soaked in Clear-sol I (Nacalai Tesque), and the radioactivity
719 on the membrane was monitored. For the inhibition experiments, the tested inhibitors were
720 added into the D-[^{3}H]serine substrate solution at the same time.

721 **Western Blot analysis**

722 Expressions of targeting proteins from membrane fractions were verified by Western
723 blot analysis as described (Nagamori et al., 2016b). Membrane fractions from cultured cell
724 pellets were prepared by sonication. BBMVs were prepared by the magnesium precipitation
725 method. Membrane proteins were dissolved in 1% w/v DDM prior to the addition of the SDS-
726 PAGE sample buffer. Signals of chemiluminescence (Immobilon Forte Western HRP
727 substrate; Millipore) were visualized by ChemiDoc MP Imaging system (Bio-Rad).

728 **Immunofluorescent staining of mouse kidneys**

729 The 8 weeks old male wild-type C57BL/6J mice (Japan SLC) were anesthetized and
730 fixed by anterograde perfusion via the aorta with 4% w/v paraformaldehyde in 0.1 M sodium
731 phosphate buffer pH 7.4. The kidneys were dissected, post-fixed in the same buffer for two
732 days, and cryoprotected in 10 %, 20 %, and 30 % w/v sucrose. Frozen kidney sections were
733 cut at 7 μm thickness in a cryostat (Leica) and mounted on MAS-coated glass slides
734 (Matsunami). The sections were placed in antigen retrieval buffer (10 mM citrate and 10 mM
735 sodium Citrate), autoclaved at 121 °C for 5 min and washed by TBS-T (Tris-buffered saline
736 (TBS) with 0.1 % v/v Tween 20). Immunostaining was done by serial incubation with each
737 antibody as below.

738 For mAsct2 and mSglt2 co-immunostaining, the samples were incubated with 3 %
739 hydrogen peroxide solution for 10 min, washed with TBS, and incubated in Blocking One
740 Histo (Nacalai tesque) for 15 min. The samples were then incubated with mouse anti-SGLT2
741 antibody diluted in immunoreaction enhancer B solution (Can Get Signal immunostain,
742 TOYOBO) overnight at 4 °C. Signal was enhanced by Alexa Fluor 568 Tyramide SuperBoost
743 (TSA) kit, goat anti-mouse IgG, following the manufacture's instruction (Thermo). The
744 antibodies were then stripped by citrate/acetate-based buffer, pH 6.0, containing 0.3% w/v SDS
745 at 95 °C for 10 min (Buchwalow et al., 2018), washed by TBS, and incubated with Blocking
746 One Histo. mSglt2 staining was done by conventional staining method (Nagamori et al., 2016b).
747 The samples were incubated with rabbit anti-mAsct2(NT) antibody diluted in immunoreaction
748 enhancer A solution (Can Get Signal immunostain) overnight at 4 °C. After washing with TBS-
749 T, the specimens were incubated with Alexa Fluor 488-labeled donkey anti-rabbit IgG.

750 For mAsct2 and mAgt1 co-immunostaining, signals of both antibodies were enhanced
751 by TSA kit. First, the specimens were incubated with rabbit anti-mAGT1(G) antibody
752 (Nagamori et al., 2016a) overnight at 4 °C followed by Alexa Fluor 568 TSA kit, goat anti-
753 rabbit. The antibodies were then stripped. The specimens were incubated with rabbit anti-
754 mAsct2(NT) overnight at 4 °C and then repeated the steps of TSA kit using Alexa Fluor 488,
755 goat anti-rabbit.

756 Staining of mAsct2 and Na^+/K^+-ATPase was performed without TSA enhancement.
757 After blocking by Blocking One Histo, the samples were incubated with rabbit anti-
758 mAsct2(NT) antibody diluted in immunoreaction enhancer A solution overnight. The samples
759 were washed with TBS-T, incubated with Alexa Fluor488-labeled donkey anti-rabbit IgG, and
760 washed again. Non-specific staining was blocked by Blocking One Histo and the specimens
761 were then incubated with mouse anti-Na^+/K^+-ATPase antibody diluted in immunoreaction

762 enhancer B solution overnight at 4 °C. The specimens were washed with TBS-T, incubated
763 with Alexa Fluor568-labeled goat anti-mouse IgG for 1 hour.
764 All specimens were washed with TBS-T and mounted with Fluoromount (Diagnostic
765 Biosystems). Imaging was detected using a KEYENCE BZ-X710 microscope. Images were
766 processed by using ImageJ ver. 1.51 (NIH).

Acknowledgments

We greatly appreciate Noriyoshi Isozumi for preliminary proteomic analysis and Rikako Furuya for crucial discussion. We would like to thank Saki Takeshita, Yuki Mori, Junko Iwatani, and Yuika Shimo for technical assistance. We are especially grateful to Yoshinori Moriyama for critical reading and suggestions. This work is partly supported by MEXT/JSPS KAKENHI under grant number 19K07373 to P.W.; research grants from Shiseido Company, Ltd. and AMED under grant numbers JP20ek031001 and JP20gm0810010 to S.N.

Competing interests

A patent has been applied by KAGAMI Inc., Nara Medical University, and NIBIOHN with P.W., S.M., P.K., T.K., M.M., and S.N. as inventors based on this research. KAGAMI Inc. was founded in 2019 to implement the technologies in medicine.

Author contributions

Pattama Wiriyasermkul—Conceptualization, Methodology, Investigation, Validation, Formal analysis, Data curation, Visualization, Writing—original draft, Writing—review and editing

Satomi Moriyama—Investigation, Validation, Formal analysis, Visualization

Yoko Tanaka—Investigation, Validation, Formal analysis

Pornparn Kongpracha—Investigation, Validation, Formal analysis, Data curation

Nodoka Nakamae—Investigation, Formal analysis

Masataka Suzuki—Investigation, Resources

Tomonori Kimura—Resources, Methodology

Masashi Mita—Conceptualization, Funding acquisition

Jumpei Sasabe—Investigation, Resources, Methodology

Shushi Nagamori—Conceptualization, Methodology, Validation, Data curation, Supervision, Resources, Funding acquisition, Project administration, Writing—original draft, Writing—review and editing

All authors contributed to the final manuscript.

795 **References**

796 Biber J, Stieger B, Stange G, Murer H. 2007. Isolation of renal proximal tubular brush-border
797 membranes. *Nature Protocols* **2**:1356–1359. doi:10.1038/nprot.2007.156

798 Bröer A, Rahimi F, Bröer S. 2016. Deletion of amino acid transporter ASCT2 (SLC1A5)
799 reveals an essential role for transporters SNAT1 (SLC38A1) and SNAT2 (SLC38A2)
800 to sustain glutaminolysis in cancer cells. *J Biol Chem* **291**:13194–13205.
801 doi:10.1074/jbc.M115.700534

802 Buchwalow I, Samoilova V, Boecker W, Tiemann M. 2018. Multiple immunolabeling with
803 antibodies from the same host species in combination with tyramide signal
804 amplification. *Acta Histochemica* **120**:405–411. doi:10.1016/j.acthis.2018.05.002

805 Bukhari FJ, Moradi H, Gollapudi P, Ju Kim H, Vaziri ND, Said HM. 2011. Effect of chronic
806 kidney disease on the expression of thiamin and folic acid transporters. *Nephrology*
807 *Dialysis Transplantation* **26**:2137–2144. doi:10.1093/ndt/gfq675

808 Cheng G, Zhong M, Kawaguchi R, Kassai M, Al-Ubaidi M, Deng J, Ter-Stepanian M, Sun H.
809 2014. Identification of PLXDC1 and PLXDC2 as the transmembrane receptors for the
810 multifunctional factor PEDF. *eLife* **3**:e05401. doi:10.7554/eLife.05401

811 Chevalier RL. 2016. The proximal tubule is the primary target of injury and progression of
812 kidney disease: role of the glomerulotubular junction. *American Journal of Physiology-*
813 *Renal Physiology* **311**:F145–F161. doi:10.1152/ajprenal.00164.2016

814 Chu X, Bleasby K, Chan GH, Nunes I, Evers R. 2016. The complexities of interpreting
815 reversible elevated serum creatinine levels in drug development: Does a correlation
816 with inhibition of renal transporters exist? *Drug Metabolism and Disposition* **44**:1498–
817 1509. doi:10.1124/dmd.115.067694

818 de Carvalho FD, Quick M. 2011. Surprising substrate versatility in SLC5A6: Na^+-coupled I^-
819 transport by the human Na^+/multivitamin transporter (hSMVT). *Journal of Biological*
820 *Chemistry* **286**:131–137. doi:10.1074/jbc.M110.167197

821 Devarajan P, Jefferies JL. 2016. Progression of chronic kidney disease after acute kidney injury.
822 *Progress in Pediatric Cardiology* **41**:33–40. doi:10.1016/j.ppedcard.2015.12.006

823 DiGiacomo V, Meruelo D. 2016. Looking into laminin receptor: critical discussion regarding
824 the non-integrin 37/67-kDa laminin receptor/RPSA protein: Looking into laminin
825 receptor. *Biological Reviews* **91**:288–310. doi:10.1111/brv.12170

826 Djamali A, Vidyasagar A, Adulla M, Hullett D, Reese S. 2008. Nox-2 is a modulator of
827 fibrogenesis in kidney allografts: Nox-2 and kidney allograft fibrosis. *American*
828 *Journal of Transplantation* **9**:74–82. doi:10.1111/j.1600-6143.2008.02463.x

829 Douard V, Ferraris RP. 2008. Regulation of the fructose transporter GLUT5 in health and
830 disease. *American Journal of Physiology-Endocrinology and Metabolism* **295**:E227–
831 E237. doi:10.1152/ajpendo.90245.2008

832 Dun Y, Mysona B, Itagaki S, Martin-Studdard A, Ganapathy V, Smith SB. 2007. Functional
833 and molecular analysis of D-serine transport in retinal Müller cells. *Experimental Eye*
834 *Research* **84**:191–199. doi:10.1016/j.exer.2006.09.015

835 Eddy S, Mariani LH, Kretzler M. 2020. Integrated multi-omics approaches to improve
836 classification of chronic kidney disease. *Nature Review Nephrology*.
837 doi:10.1038/s41581-020-0286-5

838 Emond MJ, Louie T, Emerson J, Zhao W, Mathias RA, Knowles MR, Wright FA, Rieder MJ,
839 Tabor HK, Nickerson DA, Gibson RL, Bamshad MJ. 2012. Exome sequencing of
840 extreme phenotypes identifies DCTN4 as a modifier of chronic Pseudomonas

841 aeruginosa infection in cystic fibrosis. *Nature Genetics* **44**:886–889.
842 doi:10.1038/ng.2344

843 Famulski KS, Reeve J, de Freitas DG, Kreepala C, Chang J, Halloran PF. 2013. Kidney
844 transplants with progressing chronic diseases express high levels of acute kidney injury
845 transcripts: AKI signal in transplants with CKD. *American Journal of Transplantation*
846 **13**:634–644. doi:10.1111/ajt.12080

847 Formisano TM, Van Winkle LJ. 2016. At least three rransporters likely mediate threonine
848 uptake needed for mouse embryonic stem cell proliferation. *Frontiers in Cell and*
849 *Developmental Biology* **4**:17. doi:10.3389/fcell.2016.00017

850 Foster AC, Farnsworth J, Lind GE, Li Y-X, Yang J-Y, Dang V, Penjwini M, Viswanath V,
851 Staubli U, Kavanaugh MP. 2016. D-Serine is a substrate for neutral amino acid
852 transporters ASCT1/SLC1A4 and ASCT2/SLC1A5, and is transported by both
853 subtypes in rat hippocampal astrocyte cultures. *PLoS ONE* **11**:e0156551.
854 doi:10.1371/journal.pone.0156551

855 Fu Y, Tang C, Cai J, Chen G, Zhang D, Dong Z. 2018. Rodent models of AKI-CKD transition.
856 *American Journal of Physiology-Renal Physiology* **315**:F1098–F1106.
857 doi:10.1152/ajprenal.00199.2018

858 Furusho K, Shibata T, Sato R, Fukui R, Motoi Y, Zhang Y, Saitoh S, Ichinohe T, Moriyama
859 M, Nakamura S, Miyake K. 2019. Cytidine deaminase enables Toll-like receptor 8
860 activation by cytidine or its analogs. *International Immunology* **31**:167–173.
861 doi:10.1093/intimm/dxy075

862 Ganapathy V, Thangaraju M, Gopal E, Martin PM, Itagaki S, Miyauchi S, Prasad PD. 2008.
863 Sodium-coupled monocarboxylate transporters in normal tissues and in cancer. *The*
864 *AAPS Journal* **10**:193. doi:10.1208/s12248-008-9022-y

865 Ghezzi C, Loo DDF, Wright EM. 2018. Physiology of renal glucose handling via SGLT1,
866 SGLT2 and GLUT2. *Diabetologia* **61**:2087–2097. doi:10.1007/s00125-018-4656-5

867 Gopal E, Umapathy NS, Martin PM, Ananth S, Gnana-Prakasam JP, Becker H, Wagner CA,
868 Ganapathy V, Prasad PD. 2007. Cloning and functional characterization of human
869 SMCT2 (SLC5A12) and expression pattern of the transporter in kidney. *Biochimica et*
870 *Biophysica Acta (BBA) - Biomembranes* **1768**:2690–2697.
871 doi:10.1016/j.bbamem.2007.06.031

872 Hasegawa H, Masuda N, Natori H, Shinohara Y, Ichida K. 2019. Pharmacokinetics and
873 toxicokinetics of D-serine in rats. *Journal of Pharmaceutical and Biomedical Analysis*
874 **162**:264–271. doi:10.1016/j.jpba.2018.09.026

875 Hesaka A, Sakai S, Hamase K, Ikeda T, Matsui R, Mita M, Horio M, Isaka Y, Kimura T. 2019.
876 D-Serine reflects kidney function and diseases. *Scientific Reports* **9**:5104.
877 doi:10.1038/s41598-019-41608-0

878 Itagaki S, Gopal E, Zhuang L, Fei Y-J, Miyauchi S, Prasad PD, Ganapathy V. 2006. Interaction
879 of ibuprofen and other structurally related NSAIDs with the sodium-coupled
880 monocarboxylate transporter SMCT1 (SLC5A8). *Pharmaceutical Research* **23**:1209–
881 1216. doi:10.1007/s11095-006-0023-1

882 James R, Searcy JL, Bihan TL, Martin SF, Gliddon CM, Povey J, Deighton RF, Kerr LE,
883 McCulloch J, Horsburgh K. 2012. Proteomic analysis of mitochondria in APOE
884 transgenic mice and in response to an ischemic challenge. *Journal of Cerebral Blood*
885 *Flow & metabolism* **32**:164-176. DOI:10.1038/jcbfm.2011.120

886 Kamal MA, Keep RF, Smith DE. 2008. Role and relevance of PEPT2 in drug disposition,
887 dynamics, and toxicity. *Drug Metabolism and Pharmacokinetics* **23**:236–242.
888 doi:10.2133/dmpk.23.236

889 Kandasamy P, Gyimesi G, Kanai Y, Hediger MA. 2018. Amino acid transporters revisited:
890 New views in health and disease. *Trends in Biochemical Sciences* **43**:752–789.
891 doi:10.1016/j.tibs.2018.05.003

892 Karihaloo A, Kale S, Rosenblum ND, Cantley LG. 2004. Hepatocyte growth factor-mediated
893 renal epithelial branching morphogenesis is regulated by glypican-4 expression.
894 *Molecular and Cell Biology* **24**:8745–8752. doi:10.1128/MCB.24.19.8745-8752.2004

895 Karim AS, Reese SR, Wilson NA, Jacobson LM, Zhong W, Djamali A. 2015. Nox2 is a
896 mediator of ischemia reperfusion injury: Nox2 and IRI. *American Journal of*
897 *Transplantation* **15**:2888–2899. doi:10.1111/ajt.13368

898 Kimura T, Hamase K, Miyoshi Y, Yamamoto R, Yasuda K, Mita M, Rakugi H, Hayashi T,
899 Isaka Y. 2016. Chiral amino acid metabolomics for novel biomarker screening in the
900 prognosis of chronic kidney disease. *Scientific Reports* **6**:26137.
901 doi:10.1038/srep26137

902 Kimura T, Hesaka A, Isaka Y. 2020. Utility of D-serine monitoring in kidney disease.
903 *Biochimica et Biophysica Acta (BBA) - Proteins and Proteomics* **1868**:140449.
904 doi:10.1016/j.bbapap.2020.140449

905 Kirita Y, Wu H, Uchimura K, Wilson PC, Humphreys BD. 2020. Cell profiling of mouse acute
906 kidney injury reveals conserved cellular responses to injury. *Proceeding of the National*
907 *Academy of Sciences of the United States of America* **117**:15874–15883.
908 doi:10.1073/pnas.2005477117

909 Kovacevic L, Lu H, Caruso JA, Govil-Dalela T, Thomas R, Lakshmanan Y. 2017. Marked
910 increase in urinary excretion of apolipoproteins in children with nephrolithiasis
911 associated with hypercalciuria. *Pediatric Nephrology* **32**:1029–1033.
912 doi:10.1007/s00467-016-3576-1

913 Kragh-Hansen U, Sheikh MI. 1984. Serine uptake by luminal and basolateral membrane
914 vesicles from rabbit kidney. *The Journal of Physiology* **354**:55–67.
915 doi:10.1113/jphysiol.1984.sp015361

916 Kruzel ML, Zimecki M, Actor JK. 2017. Lactoferrin in a context of inflammation-induced
917 pathology. *Frontiers in Immunology* **8**:1438. doi:10.3389/fimmu.2017.01438

918 Lee S-Y, Shin J-A, Kwon HM, Weiner ID, Han K-H. 2011. Renal ischemia–reperfusion injury
919 causes intercalated cell-specific disruption of occludin in the collecting duct.
920 *Histochemistry and Cell Biology* **136**:637–647. doi:10.1007/s00418-011-0881-4

921 Lee Y, Wiriyasermkul P, Jin C, Quan L, Ohgaki R, Okuda S, Kusakizako T, Nishizawa T, Oda
922 K, Ishitani R, Yokoyama T, Nakane T, Shirouzu M, Endou H, Nagamori S, Kanai Y,
923 Nureki O. 2019. Cryo-EM structure of the human L-type amino acid transporter 1 in
924 complex with glycoprotein CD98hc. *Nature Structural & Molecular Biology* **26**:510–
925 517. doi:10.1038/s41594-019-0237-7

926 Liu C, Wang J, Hu J, Fu B, Mao Z, Zhang H, Cai G, Chen X, Sun X. 2020. Extracellular
927 vesicles for acute kidney injury in preclinical rodent models: a meta-analysis. *Stem Cell*
928 *Research & Therapy* **11**:11. doi:10.1186/s13287-019-1530-4

929 Lu Y, Chen Xiaoniao, Yin Z, Zhu S, Wu D, Chen Xiangmei. 2016. Screening for potential
930 serum biomarkers in rat mesangial proliferative nephritis. *Proteomics* **16**:1015–1022.
931 doi:10.1002/pmic.201500405

932 Luan H, Wang C, Sun J, Zhao L, Li L, Zhou B, Shao S, Shen X, Xu Y. 2020. Resolvin D1
933 protects against ischemia/reperfusion-induced acute kidney injury by increasing Treg
934 percentages via the ALX/FPR2 pathway. *Frontiers in Physiology* **11**:285.
935 doi:10.3389/fphys.2020.00285

936 Ma C, Guo Y, Zhang Y, Duo A, Jia Y, Liu C, Li B. 2018. PAFAH1B2 is a HIF1a target gene
937 and promotes metastasis in pancreatic cancer. *Biochemical and Biophysical Research*
938 *Communications* **501**:654–660. doi:10.1016/j.bbrc.2018.05.039

939 Makridakis M, Kontostathi G, Petra E, Stroggilos R, Lygirou V, Filip S, Duranton F, Mischak
940 H, Argiles A, Zoidakis J, Vlahou A. 2020. Multiplexed MRM-based protein
941 quantification of putative prognostic biomarkers for chronic kidney disease progression
942 in plasma. *Scientific Reports* **10**:4815. doi:10.1038/s41598-020-61496-z

943 Martin PM, Gopal E, Ananth S, Zhuang L, Itagaki S, Prasad BM, Smith SB, Prasad PD,
944 Ganapathy V. 2006. Identity of SMCT1 (SLC5A8) as a neuron-specific Na^+-coupled
945 transporter for active uptake of L-lactate and ketone bodies in the brain. *Journal of*
946 *Neurochemistry* **98**:279–288. doi:10.1111/j.1471-4159.2006.03878.x

947 Martin PM, Dun Y, Mysona B, Ananth S, Roon P, Smith SB, Ganapathy V. 2007. Expression
948 of the sodium-coupled monocarboxylate transporters SMCT1 (SLC5A8) and SMCT2
949 (SLC5A12) in retina. *Investigative Ophthalmology & Visual Science* **48**:3356.
950 doi:10.1167/iovs.06-0888

951 Martins JR, Penton D, Peyronnet R, Arhatte M, Moro C, Picard N, Kurt B, Patel A, Honoré E,
952 Demolombe S. 2016. Piezo1-dependent regulation of urinary osmolarity. *Pflugers*
953 *Archiv - European Journal of Physiology* **468**:1197–1206. doi:10.1007/s00424-016-
954 1811-z

955 Marx D, Metzger J, Pejchinovski M, Gil RB, Frantzi M, Latosinska A, Belczacka I, Heinzmann
956 SS, Husi H, Zoidakis J, Klingele M, Herget-Rosenthal S. 2018. Proteomics and
957 metabolomics for AKI diagnosis. *Seminars in Nephrology* **38**:63–87.
958 doi:10.1016/j.semnephrol.2017.09.007

959 Matsuo H, Chiba T, Nagamori S, Nakayama A, Domoto H, Phetdee K, Wiriyasermkul P,
960 Kikuchi Y, Oda T, Nishiyama J, Nakamura T, Morimoto Y, Kamakura K, Sakurai Y,
961 Nonoyama S, Kanai Y, Shinomiya N. 2008. Mutations in glucose transporter 9 gene
962 SLC2A9 cause renal hypouricemia. *The American Journal of Human Genetics* **83**:744–
963 751. doi:10.1016/j.ajhg.2008.11.001

964 Metzner L, Kottra G, Neubert K, Daniel H, Brandsch M. 2005. Serotonin, L-tryptophan, and
965 tryptamine are effective inhibitors of the amino acid transport system PAT1. *FASEB*
966 *Journal* **19**:1468–1473. doi:10.1096/fj.05-3683com

967 Mocker A, Hilgers KF, Cordasic N, Wachtveitl R, Menendez-Castro C, Woelfle J, Hartner A,
968 Fahlbusch FB. 2019. Renal chemerin expression is induced in models of hypertensive
969 nephropathy and glomerulonephritis and correlates with markers of inflammation and
970 fibrosis. *International Journal of Molecular Sciences* **20**:6240.
971 doi:10.3390/ijms20246240

972 Morehead RP, Fishman WH, Artom C. 1945. Renal injury in the rat following the
973 administration of serine by stomach tube. *The American Journal of Pathology* **21**:803–
974 815.

975 Nagamori S, Wiriyasermkul P, Guarch ME, Okuyama H, Nakagomi S, Tadagaki K, Nishinaka
976 Y, Bodoy S, Takafuji K, Okuda S, Kurokawa J, Ohgaki R, Nunes V, Palacín M, Kanai
977 Y. 2016a. Novel cystine transporter in renal proximal tubule identified as a missing
978 partner of cystinuria-related plasma membrane protein rBAT/SLC3A1. *Proceeding of*
979 *the National Academy of Sciences of the United States of America* **113**:775–780.
980 doi:10.1073/pnas.1519959113

981 Nagamori S, Wiriyasermkul P, Okuda S, Kojima N, Hari Y, Kiyonaka S, Mori Y, Tominaga
982 H, Ohgaki R, Kanai Y. 2016b. Structure–activity relations of leucine derivatives reveal

983 critical moieties for cellular uptake and activation of mTORC1-mediated signaling.
984 *Amino Acids* **48**:1045–1058. doi:10.1007/s00726-015-2158-z

985 Nakade Y, Iwata Y, Furuichi K, Mita M, Hamase K, Konno R, Miyake T, Sakai N, Kitajima
986 S, Toyama T, Shinozaki Y, Sagara A, Miyagawa T, Hara A, Shimizu M, Kamikawa Y,
987 Sato K, Oshima M, Yoneda-Nakagawa S, Yamamura Y, Kaneko S, Miyamoto T,
988 Katane M, Homma H, Morita H, Suda W, Hattori M, Wada T. 2018. Gut microbiota–
989 derived D-serine protects against acute kidney injury. *JCI Insight* **3**:e97957.
990 doi:10.1172/jci.insight.97957

991 Okada A, Nangaku M, Jao T-M, Maekawa H, Ishimono Y, Kawakami T, Inagi R. 2017. D-
992 serine, a novel uremic toxin, induces senescence in human renal tubular cells via GCN2
993 activation. *Scientific Reports* **7**:11168. doi:10.1038/s41598-017-11049-8

994 Ostermann M, Joannidis M. 2016. Acute kidney injury 2016: diagnosis and diagnostic workup.
995 *Critical Care* **20**:299. doi:10.1186/s13054-016-1478-z

996 Özkan G, Güzel S, Atar RV, Fidan Ç, Kara SP, Ulusoy Ş. 2019. Elevated serum levels of
997 procollagen C-proteinase enhancer-1 in patients with chronic kidney disease is
998 associated with a declining glomerular filtration rate. *Nephrology* nep.13521.
999 doi:10.1111/nep.13521

1000 Paroder V, Spencer SR, Paroder M, Arango D, Schwartz S, Mariadason JM, Augenlicht LH,
1001 Eskandari S, Carrasco N. 2006. Na^+/monocarboxylate transport (SMCT) protein
1002 expression correlates with survival in colon cancer: Molecular characterization of
1003 SMCT. *Proceedings of the National Academy of Sciences of the United States of*
1004 *America* **103**:7270–7275. doi:10.1073/pnas.0602365103

1005 Pinkaew D, Fujise K. 2017. Fortilin: A Potential target for the prevention and treatment of
1006 human diseasesAdvances in clinical chemistry. *Advances in Clinical Chemistry*
1007 **82**:265–300. doi:10.1016/bs.acc.2017.06.006

1008 Rodríguez A, Catalán V, Gómez-Ambrosi J, Frühbeck G. 2011. Aquaglyceroporins serve as
1009 metabolic gateways in adiposity and insulin resistance control. *Cell Cycle* **10**:1548–
1010 1556. doi:10.4161/cc.10.10.15672

1011 Rosenberg D, Artoul S, Segal AC, Kolodney G, Radzishevsky I, Dikopoltsev E, Foltyn VN,
1012 Inoue R, Mori H, Billard J-M, Wolosker H. 2013. Neuronal D-serine and glycine release
1013 via the Asc-1 transporter regulates NMDA receptor-dependent synaptic activity.
1014 *Journal of Neuroscience* **33**:3533–3544. doi:10.1523/JNEUROSCI.3836-12.2013

1015 Rouillard AD, Gundersen GW, Fernandez NF, Wang Z, Monteiro CD, McDermott MG,
1016 Ma'ayan A. 2016. The harmonizome: a collection of processed datasets gathered to
1017 serve and mine knowledge about genes and proteins. *Database* **2016**:baw100.
1018 doi:10.1093/database/baw100

1019 Saheki Y, Bian X, Schauder CM, Sawaki Y, Surma MA, Klose C, Pincet F, Reinisch KM, De
1020 Camilli P. 2016. Control of plasma membrane lipid homeostasis by the extended
1021 synaptotagmins. *Nature Cell Biology* **18**:504–515. doi:10.1038/ncb3339

1022 Sanduja S, Blanco FF, Dixon DA. 2011. The roles of TTP and BRF proteins in regulated
1023 mRNA decay: TTP and BRF proteins in regulated mRNA decay. *WIREs RNA* **2**:42–57.
1024 doi:10.1002/wrna.28

1025 Sasabe J, Suzuki M, Miyoshi Y, Tojo Y, Okamura C, Ito S, Konno R, Mita M, Hamase K, Aiso
1026 S. 2014. Ischemic acute kidney injury perturbs homeostasis of serine enantiomers in
1027 the body fluid in mice: Early detection of renal dysfunction using the ratio of serine
1028 enantiomers. *PLoS ONE* **9**:e86504. doi:10.1371/journal.pone.0086504

1029 Sasabe J, Miyoshi Y, Rakoff-Nahoum S, Zhang T, Mita M, Davis BM, Hamase K, Waldor
1030 MK. 2016. Interplay between microbial D-amino acids and host D-amino acid oxidase
1031 modifies murine mucosal defence and gut microbiota. *Nature Microbiology* **1**:16125.
1032 doi:10.1038/nmicrobiol.2016.125

1033 Sasabe J, Suzuki M. 2018. Distinctive roles of D-amino acids in the homochiral world: Chirality
1034 of amino acids modulates mammalian physiology and pathology. *The Keio Journal of*
1035 *Medicine* **68**:1–16. doi:10.2302/kjm.2018-0001-IR

1036 Scalise M, Pochini L, Console L, Losso MA, Indiveri C. 2018. The human SLC1A5 (ASCT2)
1037 amino acid transporter: From function to structure and role in cell biology. *Frontiers in*
1038 *Cell and Developmental Biology* **6**:96. doi:10.3389/fcell.2018.00096

1039 Schrick JJ, Vogel P, Abuin A, Hampton B, Rice DS. 2006. ADP-Ribosylation Factor-Like 3 is
1040 involved in kidney and photoreceptor development. *The American Journal of*
1041 *Pathology* **168**:1288–1298. doi:10.2353/ajpath.2006.050941

1042 Schweikhard ES, Ziegler CM. 2012. Amino acid secondary transporters: Toward a common
1043 transport system. *Current Topics in Membranes* **70**:1–28. doi:10.1016/B978-0-12-
1044 394316-3.00001-6

1045 Shen H, Feng S, Lu Y, Jiang L, Yang T, Wang Z. 2020. Correlation between plasma proprotein
1046 convertase subtilisin/kexin type 9 and blood lipids in patients with newly diagnosed
1047 primary nephrotic syndrome. *Renal Failure* **42**:405–412.
1048 doi:10.1080/0886022X.2020.1756846

1049 Shen H, Lai Y, Rodrigues AD. 2017. Organic anion transporter 2: An enigmatic human solute
1050 carrier. *Drug Metabolism and Disposition* **45**:228–236. doi:10.1124/dmd.116.072264

1051 Shimomura A, Carone FA, Peterson DR. 1988. Contraluminal uptake of serine in the proximal
1052 nephron. *Biochimica et Biophysica Acta (BBA) - Biomembranes* **939**:52–56.
1053 doi:10.1016/0005-2736(88)90046-6

1054 Shrestha P, van de Sluis B, Dullaart RPF, van den Born J. 2019. Novel aspects of PCSK9 and
1055 lipoprotein receptors in renal disease-related dyslipidemia. *Cellular Signaling* **55**:53–
1056 64. doi:10.1016/j.cellsig.2018.12.001

1057 Silbernagl S, Völker K, Dantzler WH. 1999. D-Serine is reabsorbed in rat renal pars recta.
1058 *American Journal of Physiology - Renal Physiology* **276**:F857–F863.
1059 doi:10.1152/ajprenal.1999.276.6.F857

1060 Simpson IA, Dwyer D, Malide D, Moley KH, Travis A, Vannucci SJ. 2008. The facilitative
1061 glucose transporter GLUT3: 20 years of distinction. *American Journal of Physiology -*
1062 *Endocrinology and Metabolism* **295**:E242–E253. doi:10.1152/ajpendo.90388.2008

1063 Sohara E, Rai T, Sasaki S, Uchida S. 2006. Physiological roles of AQP7 in the kidney: Lessons
1064 from AQP7 knockout mice. *Biochimica et Biophysica Acta (BBA) - Biomembranes*
1065 **1758**:1106–1110. doi:10.1016/j.bbamem.2006.04.002

1066 Suzuki T, Toyohara T, Akiyama Y, Takeuchi Y, Mishima E, Suzuki C, Ito S, Soga T, Abe T.
1067 2011. Transcriptional regulation of organic anion transporting polypeptide SLCO4C1
1068 as a aew therapeutic modality to prevent chronic kidney disease. *Journal of*
1069 *Pharmaceutical Sciences* **100**:3696–3707. doi:10.1002/jps.22641

1070 Szablewski L. 2017. Distribution of glucose transporters in renal diseases. *Journal of*
1071 *Biomedical Science* **24**:64. doi:10.1186/s12929-017-0371-7

1072 Tang M, Zhang Kun, Li Y, He Q, Li G, Zheng Q, Zhang Ke-qin. 2018. Mesenchymal stem
1073 cells alleviate acute kidney injury by down-regulating C5a/C5aR pathway activation.

1074 *International Urology and Nephrology* **50**:1545–1553. doi:10.1007/s11255-018-1844-
1075 7

1076 Tanihara Y, Masuda S, Sato T, Katsura T, Ogawa O, Inui K. 2007. Substrate specificity of
1077 MATE1 and MATE2-K, human multidrug and toxin extrusions/H^+-organic cation
1078 antiporters. *Biochemical Pharmacology* **74**:359–371. doi:10.1016/j.bcp.2007.04.010

1079 Thongboonkerd V. 2020. Roles for exosome in various kidney diseases and disorders.
1080 *Frontiers in Pharmacology* **10**:1655. doi:10.3389/fphar.2019.01655

1081 Thwaites DT, Anderson CM. 2011. The SLC36 family of proton-coupled amino acid
1082 transporters and their potential role in drug transport: SLC36 proton-coupled amino
1083 acid transporter family. *British Journal of Pharmacology* **164**:1802–1816.
1084 doi:10.1111/j.1476-5381.2011.01438.x

1085 Uetsuka S, Ogata G, Nagamori S, Isozumi N, Nin F, Yoshida T, Komune S, Kitahara T,
1086 Kikkawa Y, Inohara H, Kanai Y, Hibino H. 2015. Molecular architecture of the stria
1087 vascularis membrane transport system, which is essential for physiological functions of
1088 the mammalian cochlea. *European Journal of Neuroscience* **42**:1984–2002.
1089 doi:10.1111/ejn.12973

1090 Vanslambrouck JM, Bröer A, Thavyogarajah T, Holst J, Bailey CG, Bröer S, Rasko JEJ. 2010.
1091 Renal imino acid and glycine transport system ontogeny and involvement in
1092 developmental iminoglycinuria. *Biochemical Journal* **428**:397–407.
1093 doi:10.1042/BJ20091667

1094 Vaziri ND. 2016. HDL abnormalities in nephrotic syndrome and chronic kidney disease.
1095 *Nature Reviews Nephrology* **12**:37–47. doi:10.1038/nrneph.2015.180

1096 Wei L, Tominaga H, Ohgaki R, Wiriyasermkul P, Hagiwara K, Okuda S, Kaira K, Kato Y,
1097 Oriuchi N, Nagamori S, Kanai Y. 2016. Transport of 3-fluoro-L-α-methyl-tyrosine
1098 (FAMT) by organic ion transporters explains renal background in [^{18}F]FAMT positron
1099 emission tomography. *Journal of Pharmacological Sciences* **130**:101–109.
1100 doi:10.1016/j.jphs.2016.01.001

1101 Wei L, Yu SP, Gottron F, Snider BJ, Zipfel GJ, Choi DW. 2003. Potassium channel blockers
1102 attenuate hypoxia- and ischemia-induced neuronal death In Vitro and In Vivo. *Stroke*
1103 **34**:1281–1286. doi:10.1161/01.STR.0000065828.18661.FE

1104 Wolosker H. 2018. The nof D-serine signaling. *Advances in Pharmacology* **82**:325–348.
1105 doi:10.1016/bs.apha.2017.08.010

1106 Yang H, Zhang X, Xin G. 2018. Investigation of mechanisms of mesenchymal stem cells for
1107 treatment of diabetic nephropathy via construction of a miRNA-TF-mRNA network.
1108 *Renal Failure* **40**:136–145. doi:10.1080/0886022X.2017.1421556

1109 Yin Y, Long J, Sun Y, Li H, Jiang E, Zeng C, Zhu W. 2018. The function and clinical
1110 significance of eIF3 in cancer. *Gene* **673**:130–133. doi:10.1016/j.gene.2018.06.034

1111 Zhang WR, Parikh CR. 2019. Biomarkers of acute and chronic kidney disease. *Annual Review*
1112 *of Physiology* **81**:309–333. doi:10.1146/annurev-physiol-020518-114605

1113 Zhang Y, Gross N, Li Z, Yin G, Zhong Q, Liu C, Huang Z. 2019. Upregulation of BTF3 affects
1114 the proliferation, apoptosis, and cell cycle regulation in hypopharyngeal squamous cell
1115 carcinoma. *Biomedicine & Pharmacotherapy* **118**:109211.
1116 doi:10.1016/j.biopha.2019.109211

1117 Zheng X, Zhang X, Feng B, Sun H, Suzuki M, Ichim T, Kubo N, Wong A, Min LR, Budohn
1118 ME, Garcia B, Jevnikar AM, Min W-P. 2008. Gene silencing of complement C5a

1119 receptor using siRNA for preventing ischemia/reperfusion injury. *The American*
1120 *Journal of Pathology* **173**:973–980. doi:10.2353/ajpath.2008.080103
1121

1122 **Figures**

Figure 1: Wiriyasermkul, et al.

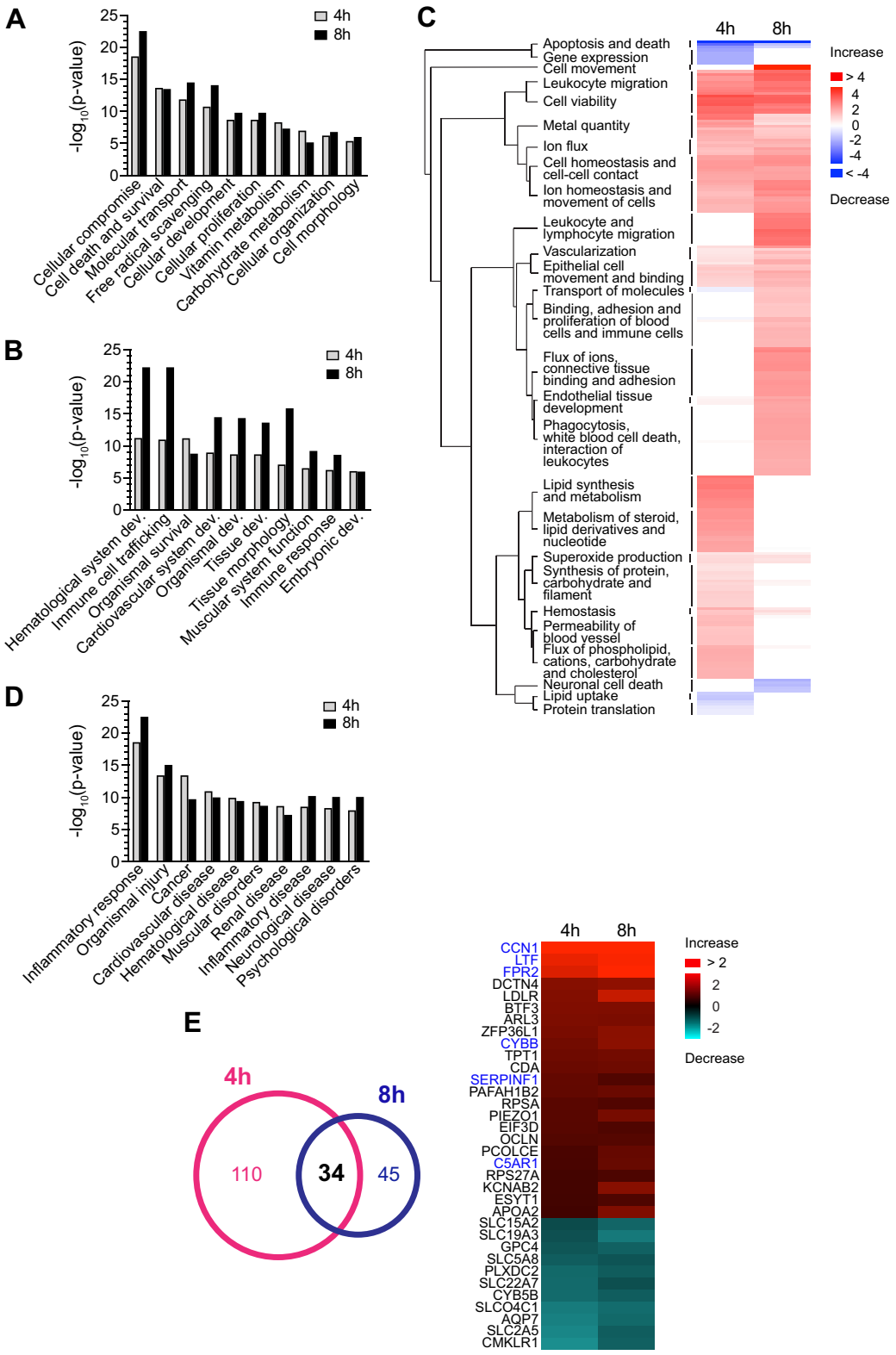

1123 **Figure 1: Proteomics uncovers cellular functions and the relevant diseases altered in the**
1124 **renal IRI model**

1125 Proteome of BBMVs from mouse kidneys after ischemia operation for 4 hours or 8 hours was
1126 normalized to that of sham operation. Proteins with a ratio of 4h IRI/sham (4h) and 8h IRI/sham
1127 (8h) passing 1.5-fold change and 0.05 p-value were subjected to analyze cellular functions and
1128 the relevant diseases by IPA. Top-10 cellular functions (A) and systemic functions (B) that are
1129 significantly altered in both 4h and 8h IRI are shown. dev. = development. C) Hierarchical
1130 heatmap of functional pathways corresponding to cellular and systemic functions in A - B.
1131 Colors indicate predicted functions. D) Top-10 diseases resulting from altered proteins. E)
1132 Area-proportional Venn diagrams (left) of biomarkers predicted by IPA. Thirty-four
1133 biomarkers found in both 4h and 8h are shown as a heatmap of protein expression (right).
1134 Colors indicated $\log_2$ fold of 4h IRI/sham (4h) or 8h IRI/sham (8h). Proteins highlighted in
1135 blue are previously predicted biomarkers for IRI and/or CKD.

Figure 2: Wiriyasermkul, et al.

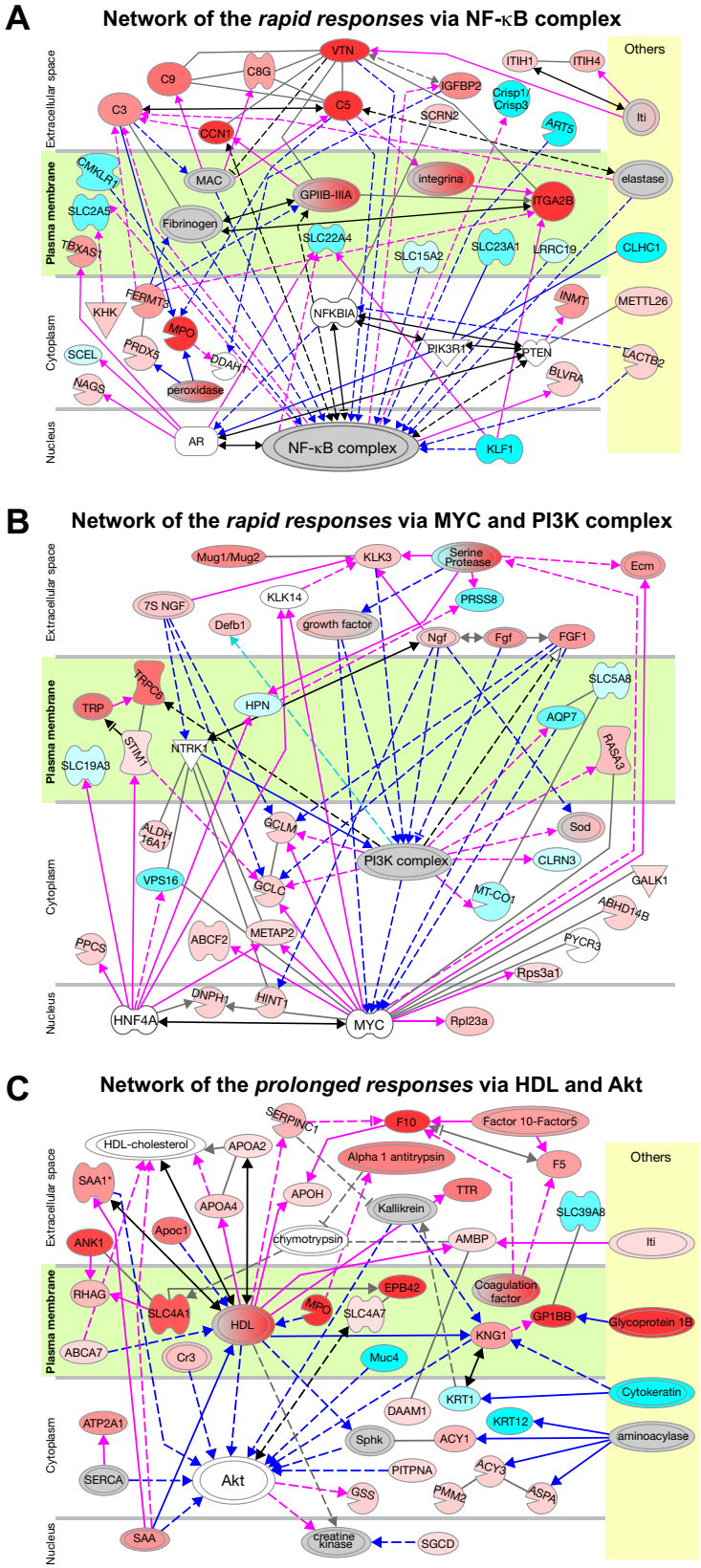

1136 **Figure 2: Predicted pathways in response to 4h, and combination of 4h and 8h IRI**

1137 Identified proteins from renal BBMVs, which are significantly altered more or less than 1.5-
1138 fold change (p-value < 0.05) in 4h and 8h IRI, were curated into networks by IPA and literatures.
1139 Top-3 networks (A - C) with the highest scores and molecule numbers are presented. Protein
1140 expressions, that are upregulated and downregulated, are shown in red and cyan, respectively,
1141 with intensity shading corresponding to the degrees of fold change. Proteins are shaped by
1142 categories, and double cycles indicate protein complexes. Solid and dash lines represent direct
1143 and indirect interactions, respectively. Lines are colored for contrast observation in which blue
1144 and magenta lines imply activation to regulators and targeting proteins, respectively. A)
1145 Network of the *rapid responses* via NF-κb regulator at 4h IRI. Network is highly involved in
1146 innate immune system, cellular movement, and cell cycle in response to the injury, tissue
1147 disorder, and defect of molecular transport. B) Network of the *rapid responses* at 4h IRI. The
1148 increase of several growth factors from organismal injury and abnormalities apparently
1149 regulate PI3K- and MYC-related pathways. C) Network of the *prolonged responses* during 4h
1150 – 8h IRI via HDL complex and Akt. Significant proteins at 4h and 8h IRI are shown. Proteins
1151 in the network are highly involved in injury-response, cell death and survival, coagulation,
1152 apolipoprotein profile, and antioxidants.

Figure 3: Wiriyasermkul, et al.

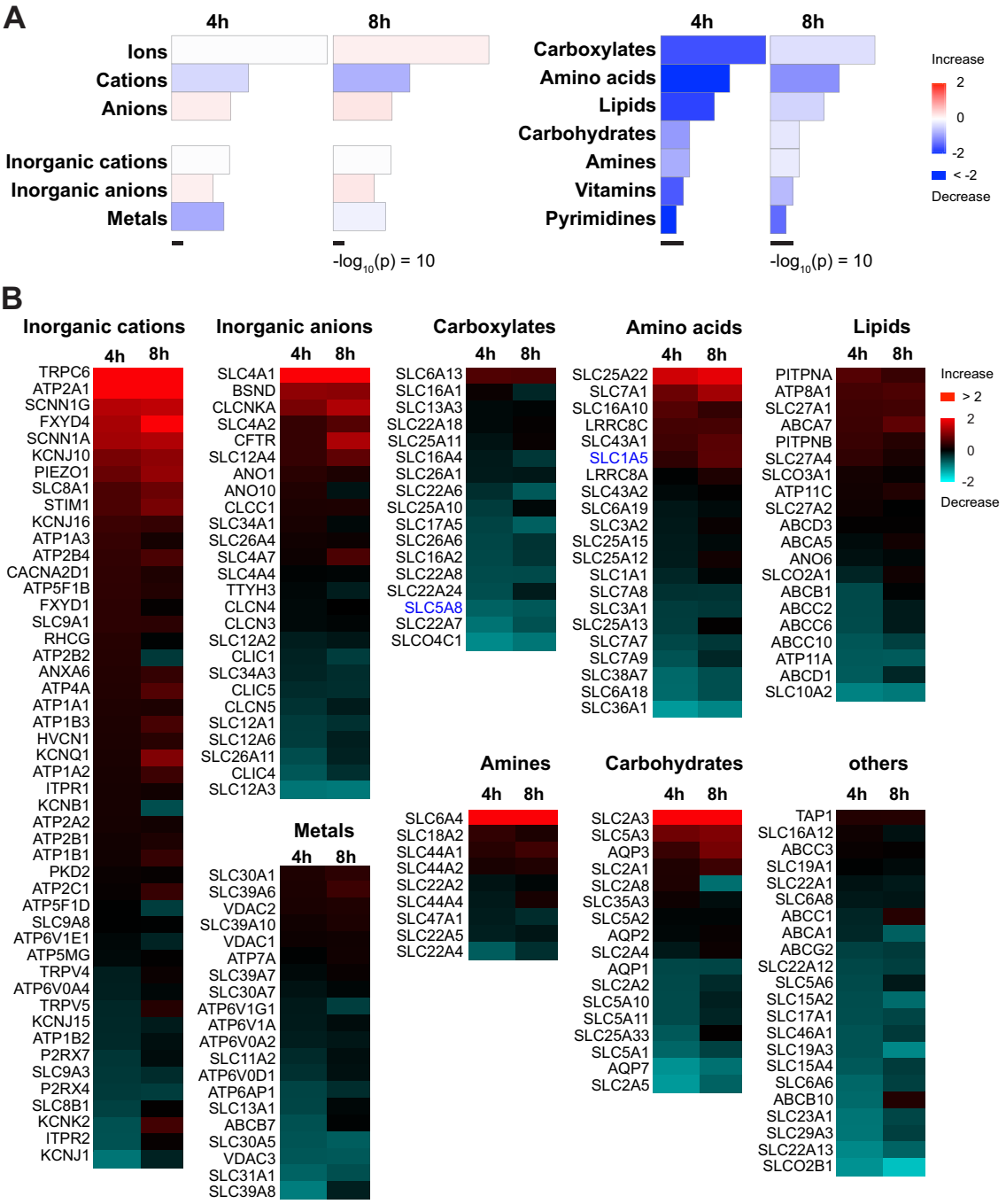

1153 **Figure 3: Proteome analysis of membrane transport proteins**

1154 A) Heatmap of predicted transport function analyzed from membrane transport proteins (319
1155 identified proteins). Transport function is categorized by types of substrates. Ion transport is a
1156 group of inorganic ions (lower left) and charged organic compounds (right). Transport of

1157 organic compounds (right) comprises both charged and uncharged compounds (right). Area
1158 and colors represent -$\log_{10}$(p-value) and predicted function (z-score), respectively. B) Heatmap
1159 of membrane transport proteins categorized by types of their canonical substrates. The "Others"
1160 category includes vitamin and nucleobase transporters. Colors indicate $\log_2$ fold of 4h IRI/sham
1161 (4h) or 8h IRI/sham (8h).

Figure 4: Wiriyasermkul, et al.

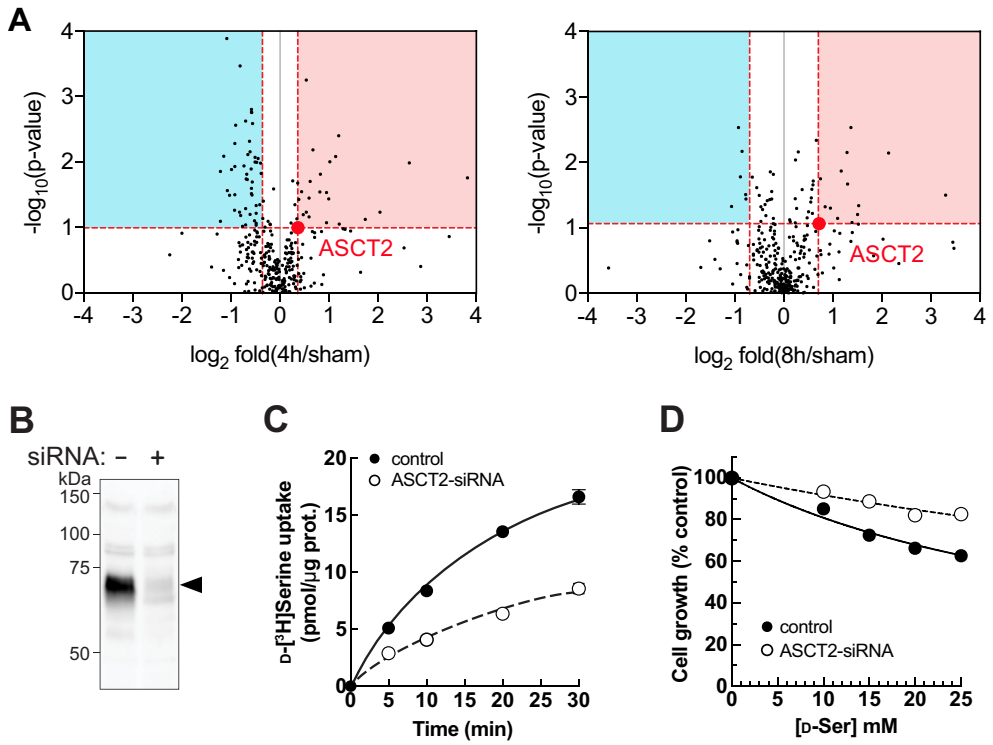

1162 **Figure 4: ASCT2 is a D-serine transporter**

1163 A) Volcano plots of 319 membrane transport proteins identified from the BBMV proteome of
1164 the IRI model. The $\log_2$ fold of 4h IRI/sham (left) or 8h IRI/sham (right) were plotted against
1165 $-\log_{10}$ of p-value. The value of Asct2 (red dot) was set as a cut-off value (red lines) to select
1166 candidates of D-serine transporters. Candidates with increased or decreased expression were
1167 shown in red and cyan areas, respectively. B) Western blot of ASCT2 from the membrane
1168 fraction of HEK293 transfected with ASCT2-siRNA indicated the suppression of ASCT2
1169 expression. ASCT2 was detected by using anti-hASCT2 antibody. C) Transport of 100 µM D-
1170 [^{3}H]serine was measured in ASCT2-knockdown (ASCT2-siRNA) in comparison to Mock cells.
1171 Uptake was measured in PBS (Na^+-buffer). n = 3. D) Cell-growth measurement (XTT assay)
1172 of HEK293 cells treated with D-serine. Prior to treatment, the cells were transfected with
1173 ASCT2-siRNA or without siRNA (control). After transfection, the cells were treated with D-

1174 serine at the indicated concentration for two days. Data represent percent cell growth compared
1175 to the non-treated cells. The graphs were fitted to inhibition kinetics (Dose-response –
1176 Inhibition). n = 5.

Figure 5: Wiriyasermkul, et al.

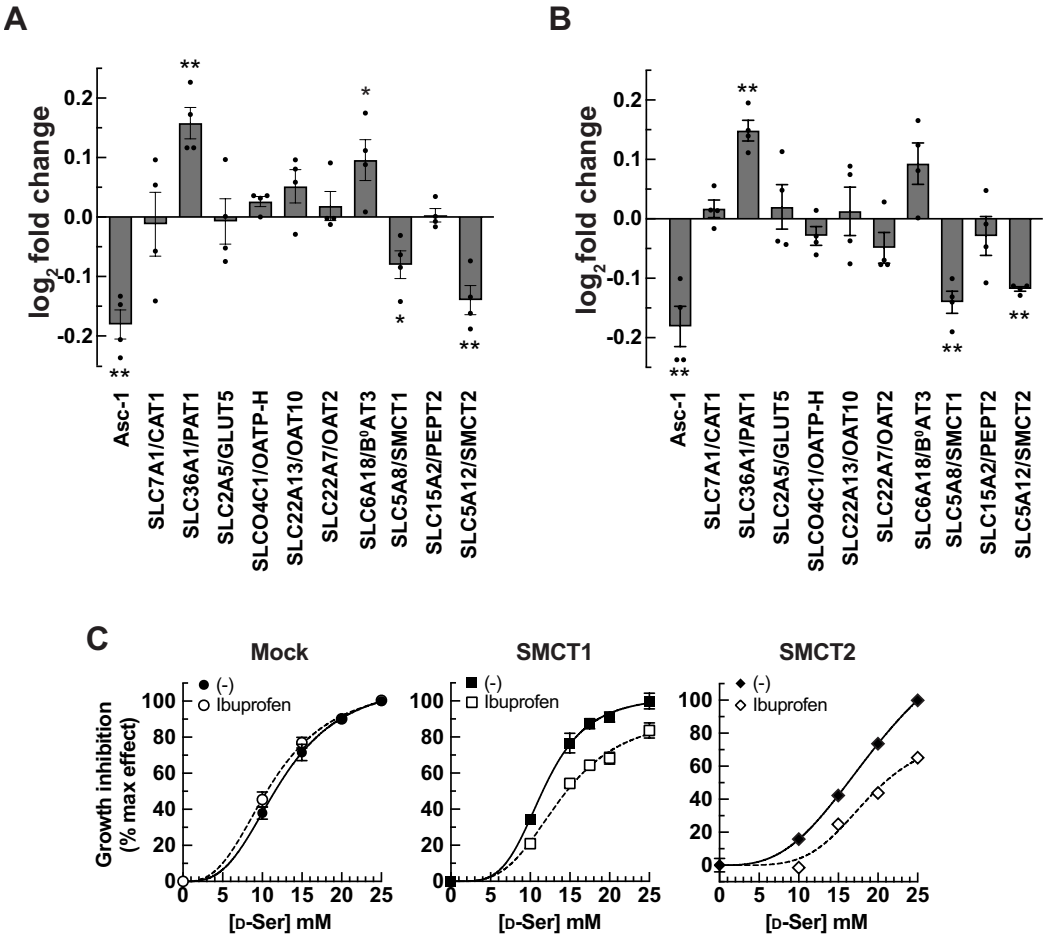

Figure 5: Identification of SMCTs as candidates of D-serine transporters

Candidates of D-serine transporters were screened by cell growth determination. HEK293 cells were transfected with various cDNA clones, as indicated. After transfection, the cells were treated with either 15 mM (A) or 25 mM (B) D-serine for two days and cell growth was examined by XTT assay. The growth effect by D-serine treatment in both transfected cells and Mock was normalized with that of no treatment. Subsequently, the normalized growth of the transfected cells was calculated as "fold change" compared to that of Mock at the same D-serine concentration and plotted as $\log_2$fold change. The order of clones was rearranged according to Table 1. *$p < 0.05$; **$p < 0.01$; n = 4. C). Inhibition effect of ibuprofen on D-

1186 serine-induced cell growth. FlpInTR-SMCT1 (SMCT1), FlpInTR-SMCT2 (SMCT2) and
1187 FlpInTR-Mock (Mock) cells were preincubated with 0.5 mM ibuprofen prior to treated with
1188 D-serine at indicated concentration for 2 days. Cell growth was measured by XTT assay. For
1189 comparison, the maximum growth inhibition by 25 mM D-serine treatment was set as 100 %
1190 inhibition and no D-serine treatment was set as 0 % inhibition. The graphs were fitted to
1191 inhibition kinetics (Dose-response – Inhibition). n = 5.

Figure 6: Wiriyasermkul, et al.

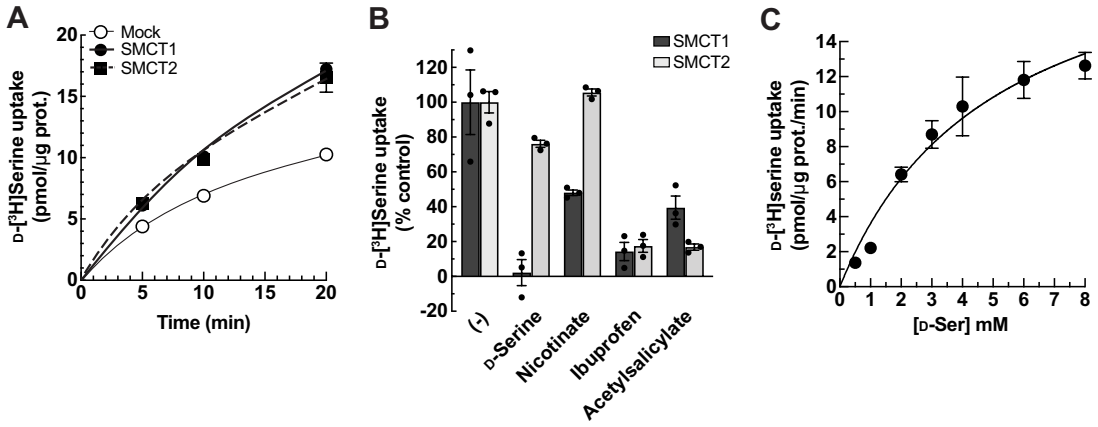

Figure 6: Characterization of SMCT1 and SMCT2 as D-serine transporters using SMCTs-stably expressing cell lines

A) Time course of 100 µM D-[^{3}H]serine uptake in FlpInTR-SMCT1 (SMCT1), FlpInTR-SMCT2 (SMCT2) and Mock cells with ASCT2 knockdown. Prior to measure D-[^{3}H]serine transport, the cells were transfected with ASCT2-siRNA for two days. n = 4. B) Inhibition of 20 µM D-[^{3}H]serine uptake by several inhibitors. Transport of D-[^{3}H]serine by ASCT2-siRNA transfected FlpInTR stable cell lines were measured in the absence (-) or presence of 5 mM inhibitors as indicated. Uptake was incubated for 10 min. Graphs represented the uptake data subtracted with those of Mock cells. n = 3. C) Concentration dependence of D-[^{3}H]serine transport in FlpInTR-SMCT1 cells. The cells were transfected with ASCT2-siRNA and cultured for two days prior to measuring the transport. Uptake of D-[^{3}H]serine (0.5 – 8 mM) was measured for 10 min in PBS. The graph represented D-[^{3}H]serine transport in FlpInTR-SMCT1 subtracted with those of Mock cells. The uptake values were fitted to Michaelis-Menten plot, with apparent K_m of 5.0 mM and V_{max} of 21.6 pmol/µg protein/min. n = 3 - 4.

Figure 7: Wiriyasermkul, et al.

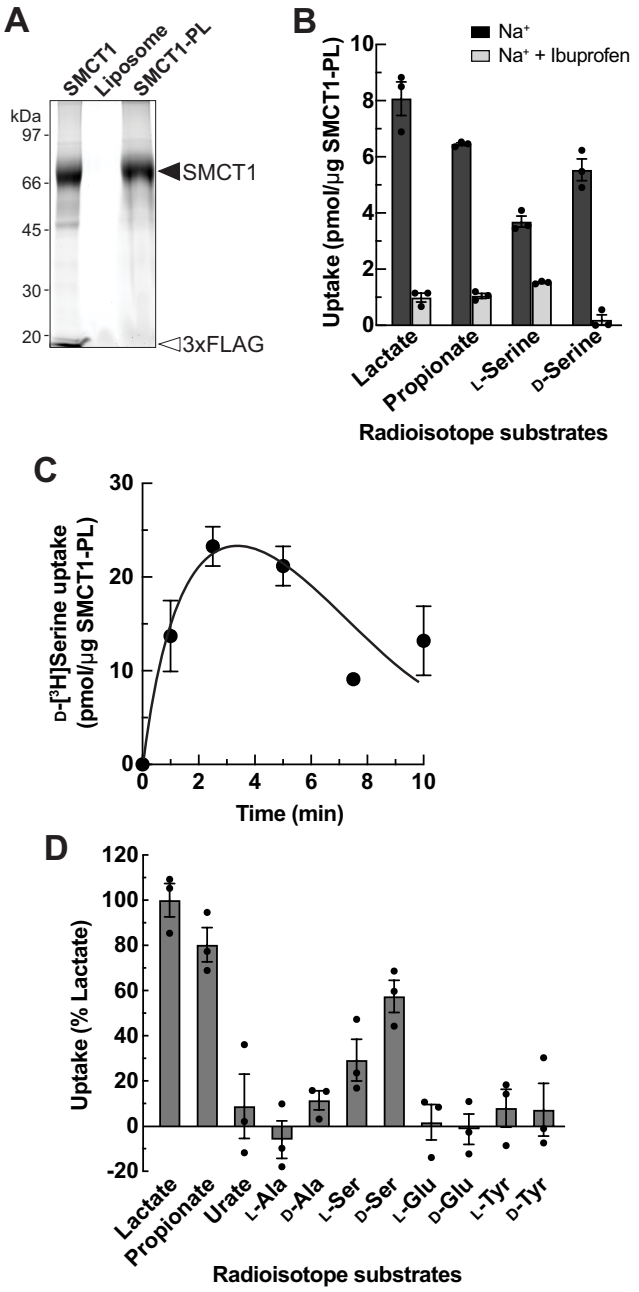

Figure 7: Characterization of SMCT1 as a D-serine transporter using SMCT1-reconstituted proteoliposomes

A) Stain-free SDS-PAGE gel (Bio-Rad) shows SMCT1 (SMCT1) purified from pCMV14-SMCT1-transfected Expi293F cells, reconstituted empty liposomes (Liposome) and SMCT1 proteoliposomes (SMCT1-PL). Closed arrowhead indicates SMCT1, whereas opened

1211 arrowhead indicates 3xFLAG peptides, which were used to elute the purified SMCT1. B)
1212 Ibuprofen effect on the uptake of [^{3}H]lactate, [^{3}H]propionate, L-[^{3}H]serine, and D-[^{3}H]serine in
1213 SMCT1 proteoliposomes (SMCT1-PL). Uptakes of 50 μM radiolabeled substrates were
1214 measured in the presence or absence of 1 mM ibuprofen for 5 min. The graphs represent uptake
1215 values in Na^+- buffer (Na^+), which were subtracted with those in Na^+-free buffer. n = 3. C)
1216 Time course of D-[^{3}H]serine transport in SMCT1 proteoliposomes. D-[^{3}H]Serine transport (200
1217 μM) was measured in the SMCT1 proteoliposomes in Na^+-buffer. All uptake values were
1218 subtracted with the uptake in Na^+-free buffer. n = 3. D) Substrate selectivity of SMCT1-PL.
1219 The uptakes of 50 μM radiolabeled substrates were measured in SMCT1 proteoliposomes for
1220 5 min. The uptake of each substrate in Na^+- buffer was subtracted with those in Na^+-free buffer,
1221 and calculated as % lactate uptake. Bar graphs represent mean ± standard error from 3
1222 independent experiments. n = 2 – 4 in each experiment.

Figure 8: Wiriyasermkul, et al.

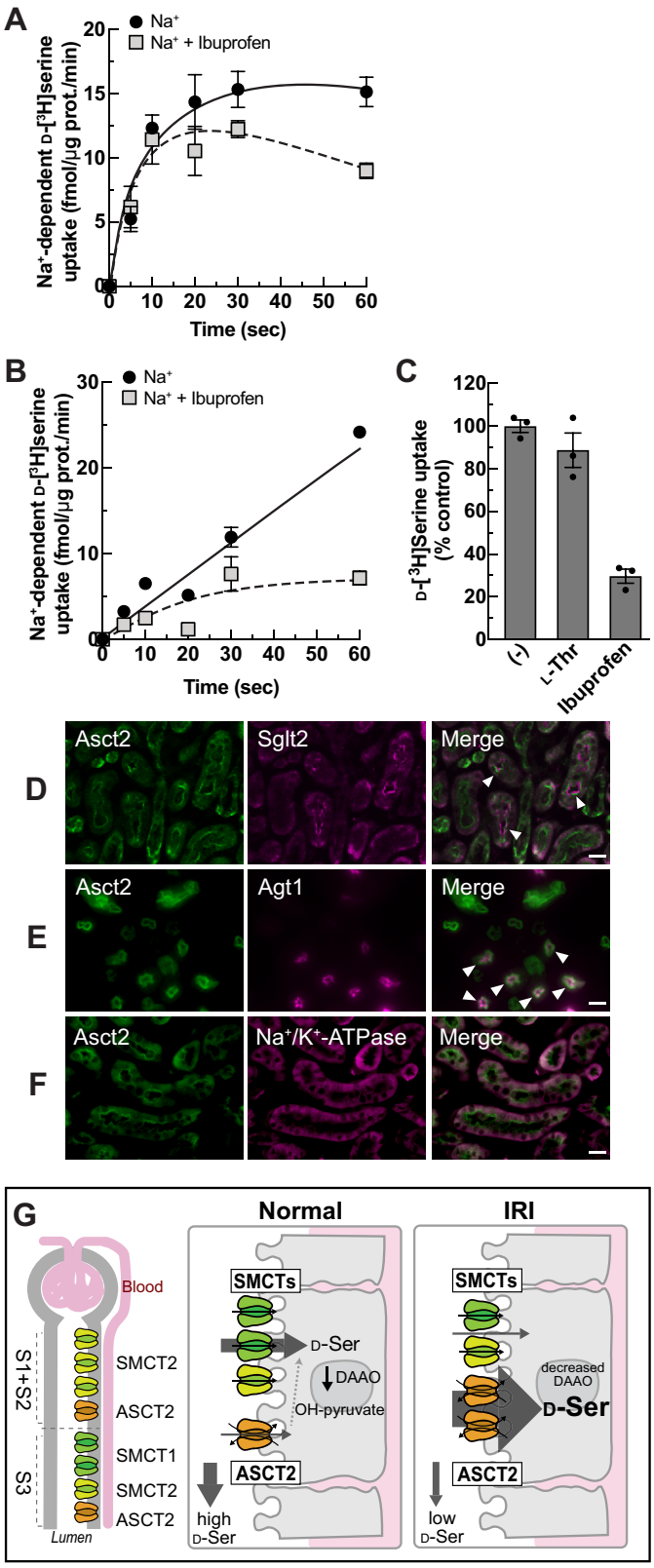

Figure 8: Characterization of D-serine transport at the apical membrane of renal proximal tubules

1225 A) D-[^{3}H]Serine transport in BBMVs preloaded with 4 mM L-glutamine. Time courses of 10
1226 μM D-[^{3}H]serine transport in L-glutamine-preloaded BBMVs were measured in the presence
1227 or absence of 1 mM ibuprofen. The graphs represented uptake data in Na^+-buffer (Na^+)
1228 subtracted with those in Na^+-free buffer. n = 3 – 4. B) D-[^{3}H]Serine transport in BBMVs
1229 without amino acid preloading. Transports of D-[^{3}H]serine were measured in a similar way to
1230 A) but the experiment was carried out in BBMVs without any amino acid preloading. n = 3 –
1231 4. C) Inhibition of D-[^{3}H]serine transport in BBMVs. Uptake of 10 μM D-[^{3}H]serine was
1232 measured in the presence or absence of 1 mM inhibitors for 1 min. n = 3. D - F) Localization
1233 of Asct2 in mouse kidney by immunofluorescent staining. Mouse kidney slide was co-stained
1234 with anti-mAsct2(NT) antibody (Asct2; green) and protein markers for renal proximal tubule
1235 segments: anti-Sglt2 antibody (D: Sglt2, apical membrane marker of S1 - S2 segment), anti-
1236 Agt1 antibody (E: Agt1, apical membrane marker of S3 segment), and anti-Na^+/K^+-ATPase
1237 antibody (F: Na^+/K^+-ATPase, basolateral membrane marker). Merge image is shown in the
1238 right pictures with DAPI (blue) staining. Scale bar = 20 μm. G) Schematic model of ASCT2
1239 and SMCTs in D-serine transport at different segments of proximal tubules. In physiological
1240 conditions, ASCT2 expression is less while SMCTs are abundant, suggesting that SMCTs
1241 mainly contribute to D-serine transport. In the IRI where SMCTs are reduced but ASCT2 is
1242 increased, a high affinity of D-serine transport reduces luminal D-serine.

1243 **Table 1**. Protein candidates for diagnosis of ischemia-reperfusion kidney injury

Protein	Name	Localization	Function/Roles	Application in kidney diseases[a]	Application in others[a]	4h/ sham	8h/ sham	References
Protein biomarkers previously predicted in kidney diseases								
CCN1 (CYR61)	IGF binding protein 10	Extracellular: ECM protein	Promotes chemotaxis, angiogenesis, cell adhesion, and tissue repair.	Diagnosis of IRI, renal injury, CKD	Tissue repair	41.4	29.9	Marx et al., 2018
LTF	Lactotransferrin	Extracellular: Enzyme	Multifunctional secreted protein involved in immune response to infection and injury.	High RNA expression in AKI transplantation	Immunotherapy, anti-inflammation	6.5	7.7	Famulski et al., 2013; Kruzel et al., 2017
FPR2 (ALX)	Formyl peptide receptor 2	PM: GPCR	Receptor of neutrophil chemotactic factors which promotes neutrophil activation.	Target of diabetic nephropathy treatment	Treatment of wound repair, Influenza	5.7	9.1	Luan et al., 2020
CYBB (NOX2)	Cytochrome B-245 β–chain	PM: Enzyme	Generates superoxide in phagocytes and emerge inflammation. Acts as a modulator of IRI and fibrogenesis.	Target of IRI treatment	Target for treatment of immunodeficiency diseases	2.2	2.7	Djamali et al., 2008; Karim et al., 2015
SERPINF1	Serpin family F member 1	Extracellular: Others	Neurotrophic protein inducing retinoblastoma cell differentiation.	Prognosis of acute rejection, CKD		1.9	1.7	Lu et al., 2016; Makridakis et al., 2020
C5AR1	Complement C5a receptor 1	PM: GPCR	Activates chemotaxis and superoxide production. Promote inflammation and injury.	Indicator and treatment target of renal injury, fibrosis	Pathogenesis of inflammatory diseases	1.6	2.0	Tang et al., 2018; Zheng et al., 2008
Protein biomarkers newly predicted in this study								
DCTN4	Dynactin subunit 4	Nucleus	Component of dynein-dynactin complex.	[DCTN4 mutation associated with infection in Citric Fibrosis]	-	2.6	2.8	Emond et al., 2012
LDLR	LDL receptor	PM: Carriers	Rate-limiting step for cholesterol synthesis. Modulated by PCSK9	[PCSK9 is a diagnostic marker for nephrotic syndrome]	Treatment of dyslipidemia	2.5	4.6	Shen et al., 2020; Shrestha et al., 2019
BTF3	Basic TF 3	Nucleus: Regulator	General transcription factor forming a complex with RNA polymerase II	-	[Associated with several cancer types]	2.4	2.4	Zhang et al., 2019
ARL3	ADP ribosylation factor-like 3	Cytoplasm: Enzyme	Small GTP-binding protein essential for cilia biogenesis and cytokinesis.	[ARL3 involve in kidney development]		2.4	2.3	Schrick et al., 2006
ZFP36L1 (BRF1)	ZFP36-like 1	Nucleus: Regulator	RNA-BP that promotes ARE-mediated RNA decay. Mediate HIF1a degradation.	-	Tumor suppressor	2.3	2.7	Sanduja et al., 2011
TPT1	Fortilin	Cytoplasm	Promote cell growth and regeneration, and host defense mechanism	-	Marker for cell viability	2.1	2.2	Pinkaew and Fujise, 2017
CDA	Cytidine deaminase	Cytoplasm: Enzyme	Deaminate cytidine to uridine. Highly express in leukocyte and enable TLR8 response.	-	[Associated with TLR8 function]	2.0	2.1	Furusho et al., 2019
PAFAH1B2	PAF-AH subunit β	Cytoplasm: Enzyme	A HIFα targeting gene involved in development, inflammation, cancer.	-	[Target of cancer treatment]	1.9	2.0	Ma et al., 2018
RPSA	Ribosomal protein SA	Cytoplasm: Regulator	Component of 40S ribosome. Functions as laminin receptor for cell adhesion	-	Target of cancer therapy	1.8	1.7	DiGiacomo and Meruelo, 2016
PIEZO1	Piezo-type mechanosensitive ion channel 1	Cytoplasm: Ion channel	Mechano-sensing cation channel activated for vascular remodeling and development.	[Control intraluminal pressure and urine flow]	Mechano-stress sensor	1.8	2.2	Martins et al., 2016
EIF3D	eIF3 subunit D	Cytoplasm: Regulator	Component of eIF3 specifically initiates mRNA involved in cell proliferation		[Highly detected in cancers]	1.8	1.7	Yin et al., 2018
OCLN	Occludin	PM: Tight junction	A tight junction protein, a substrate of MMP9. Associates with metastasis, inflammation, and repair	Loss and repair in tight junction membranes during IRI	-	1.7	1.7	Lee et al., 2011

PM: Plasma membrane
[a]Square brackets: Prediction

1244 **Table 1 (continued)**. Protein candidates for diagnosis of ischemia-reperfusion kidney injury

Protein	Name	Localization	Function/Roles	Application in kidney diseases[a]	Application in others[a]	4h/ sham	8h/ sham	Refs
Protein biomarkers newly predicted in this study								
PCOLCE	Procollagen C-endopeptidase enhancer	Extracellular: Others	Binds to procollagen and enhances procollagen C-proteinase activity.	highly detected in CKD	[Highly detected in liver fibrosis]	1.6	2.0	Özkan et al., 2019
RPS27A	Ribosomal protein S27a	Cytoplasm	Component of Ubiquitin and 40S ribosome	[Target of MSC for diabetic nephropathy]	[Highly detected in cancers]	1.5	1.6	Yang et al., 2018
KCNAB2	K^+ channel subunit β-2	PM: Ion channel	K^+ channel regulating nerve signaling. KCNAB2 inhibition attenuates brain hypoxia.	-	Target for treatment of brain hypoxia	1.5	2.6	Wei et al., 2003
ESYT1	Extended synaptotagmin 1	Cytoplasm: Adaptor	Transports lipid between adjacent membranes or exocytosis to compensate for plasma membrane lipid change.	-	-	1.5	1.6	Saheki et al., 2016
APOA2	Apolipoprotein A2	Extracellular: Transporter	Component of HDL. Transports oxidized phospholipids in anti-inflammation.	Altered in kidney diseases	Prognosis of cancer progression	1.5	2.4	Kovacevic et al., 2017; Vaziri, 2016
SLC15A2	Peptide transporter 2	PM: Transporter	Peptide and drug transporter in proximal tubule cells.	[Participate in drug delivery and accumulation of toxicants]	-	0.7	0.6	Kamal et al., 2008
SLC19A3	Thiamine transporter 2	PM: Transporter	Reuptakes Thiamine. Malfunction of THTR2 associated with thiamine deficiency.	[Glucose in diabetes and CKD reduces THTR2 expression]	-	0.6	0.5	Bukhari et al., 2011
GPC4	Glypican 4	PM: Receptor	Heparan sulfate proteoglycan that modulates HGF signal to renal tubule formation	[important for renal tubule formation]	[Tumor suppressor]	0.6	0.6	Karihaloo et al., 2004
SLC5A8	Na^+/mono-carboxylate transporter 1	PM: Transporter	Transports lactate, pyruvate, butyrate, and short chain fatty acids. Target of NSAIDs.	[Lactate is prognosis marker of inflammation]	Tumor suppressor	0.6	0.6	Ganapathy et al., 2008
PLXDC2 (TEM7R)	Plexin domain containing 2	PM: Receptor	Receptor of pigment epithelium derived factor.	-	[Expressed in Ischemic stroke]	0.5	0.6	Cheng et al., 2014
SLC22A7	Organic anion transporter 2	PM: Transporter	Transports multiple substances and creatinine from blood to renal epithelia.	[Creatinine is a biomarker for IRI and kidney diseases]		0.5	0.6	Chu et al., 2016; Shen et al., 2017
CYB5B	cytochrome B5 type B	Mitochondria: Enzyme	Membrane-bound hemoprotein in electron transport chain			0.5	0.6	James et al., 2012
SLCO4C1	Organic anion transporter M1	PM: Transporter	Transports uremic toxin from blood to renal epithelia.	[Increase SLCO4C1 attenuates CKD]	Treatment of hypertension, inflammation	0.5	0.5	Suzuki et al., 2011
AQP7	Aquaporin 7	PM: Transporter	Transports glycol. Activates insulin secretion and regulates glucose and lipid metabolism.	[High urine glycerol is observed in acute renal failure]		0.5	0.5	Rodríguez et al., 2011; Sohara et al., 2006
SLC2A5	Glucose transporter 5	PM: Transporter	Fructose transporter. Expression is altered by diabetes and inflammation	-	-	0.4	0.6	Douard and Ferraris, 2008
CMKLR1	Chemerin receptor	PM: GPCR	A GPCR which modulates signals to reduce immune response and enhance angiogenesis	[Chimerin is induced in fibrosis rat model]	Treatment of inflammation	0.4	0.6	Mocker et al., 2019

PM: Plasma membrane
[a]Square brackets: Prediction

1245

1246 **Table 2**. Candidate transporters from mass spectrometry analysis of the BBMVs from IRI
1247 mouse kidneys. The list is arranged by the fold change.

Transporters	Accession	log_2 fold 4h IRI/ sham	p-value of 4h IRI/ sham	log_2 fold 8h IRI/ sham	p-value of 8h IRI/ sham	Peptides	Score Mascot	Abundance in sham[a]
				Transport proteins found to be increased				
Slc7a1/Cat1	Q09143	0.8	0.12	1.3	0.01	1	131	2.6E+06
Slc1a5/Asct2	P51912	0.4	0.10	0.7	0.09	4	767	1.5E+07
				Transport proteins found to be decreased				
Slc36a1/Pat1	Q8K4D3	-1.2	0.08	-1.0	0.12	3	103	5.4E+06
Slc2a5/Glut5	Q9WV38	-1.2	0.01	-0.8	0.04	2	1,140	6.5E+07
Slco4c1/Oatp-m1	Q8BGD4	-1.1	0.00	-0.9	0.00	9	4,011	1.5E+08
Slc22a13/Oat10	Q6A4L0	-1.1	0.03	-0.8	0.03	15	5,948	5.6E+08
Slc22a7/Oat2	Q91WU2	-0.9	0.00	-0.6	0.02	13	6,100	4.3E+08
Slc6a18/B^0at3	O88576	-0.8	0.17	-0.6	0.25	11	4,310	2.1E+08
Slc5a8/Smct1	Q8BYF6	-0.8	0.05	-0.7	0.02	25	26,044	2.9E+09
Slc15a2/Pept2	Q9ES07	-0.7	0.01	-1.1	0.05	9	2,379	4.6E+07
Slc5a12/Smct2	Q49B93	-0.6	0.01	-0.9	0.01	12	4,725	1.6E+08
TMEM27/ Collectrin[b]	Q9ESG4	-0.4	0.01	-0.1	0.17	9	23,686	3.3E+09

[a]Median from n = 3
[b]Collectrin is a regulatory protein for B^0at3 function

1248

1249 **Supplement Figures**

Figure supplement 1: Wiriyasermkul, et al.

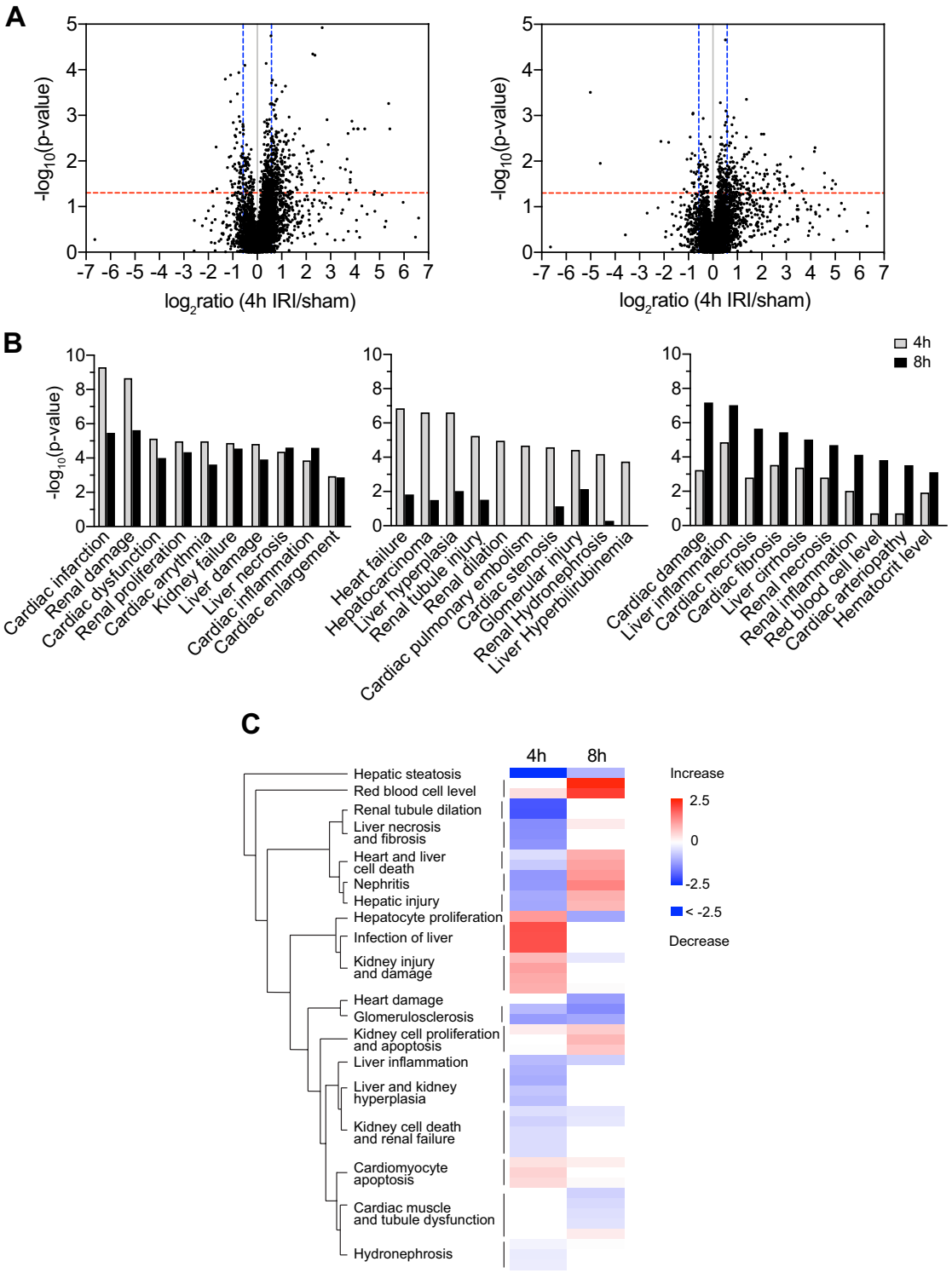

1250 **Figure supplement 1: Proteome of BBMVs and pathologies of mouse kidney IRI**

1251 A) Volcano plots of proteome identified from renal BBMVs of the IRI model. The $\log_2$ fold of
1252 4h IRI/sham (left) or 8h IRI/sham (right) were plotted against $-\log_{10}$ of p-value. Blue lines
1253 indicate protein fold change of 1.5 ($\log_2$ fold change = 0.58) and red line indicates p-value of
1254 0.05 ($-\log_{10}$ p-value = 1.3). One protein which is out of range is omitted for resolution purpose.
1255 B) Top-10 organ pathologies that are presented in both 4h and 8h IRI (left), dominant in 4h IRI
1256 (middle), and dominant in 8h IRI (right). C) Hierarchical heatmap of organ pathologies
1257 corresponding to B). Colors indicate predicted pathologies (z-score).

Figure supplement 2: Wiriyasermkul, et al.

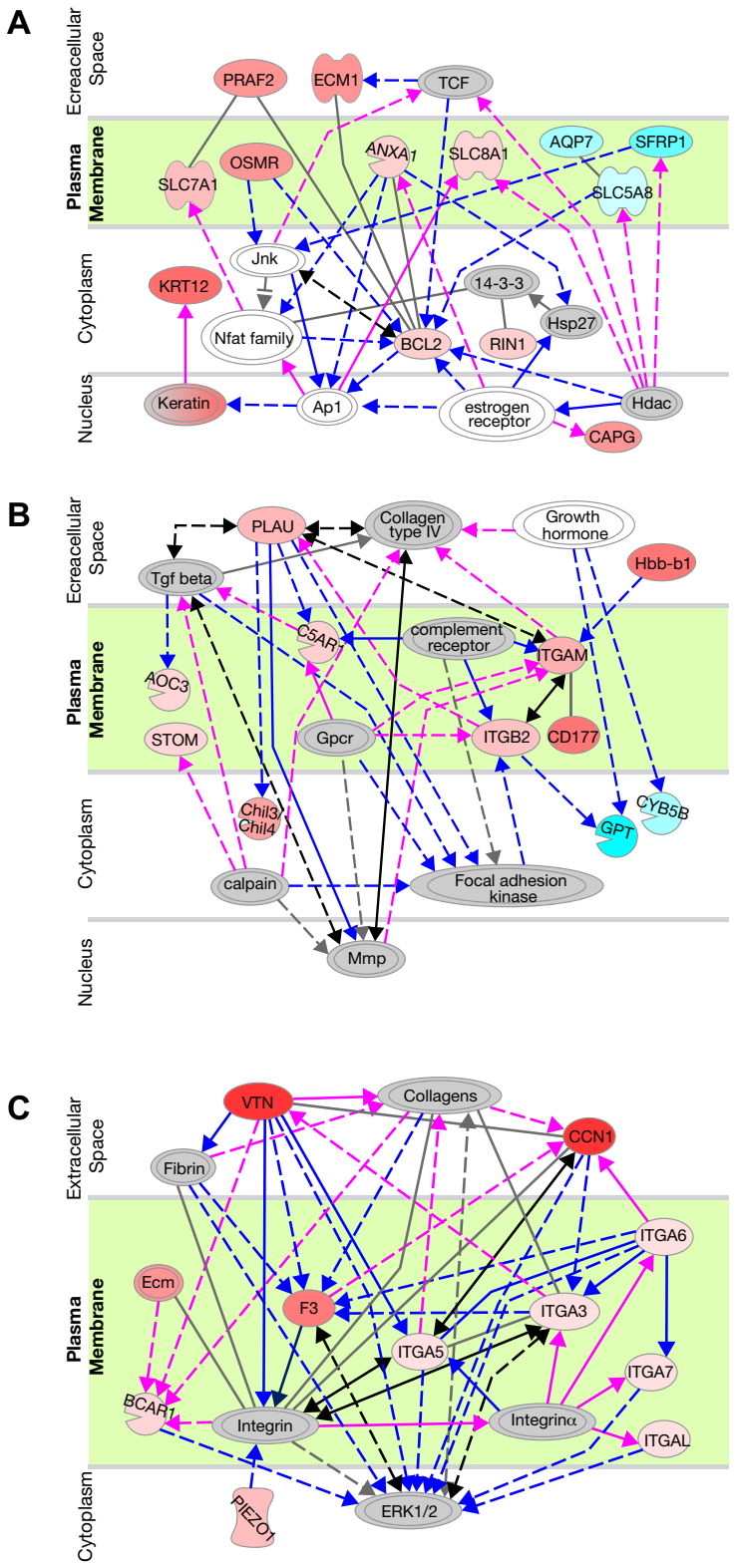

1258 **Figure supplement 2: Predicted pathways in response to 8h IRI**

1259 Identified proteins from renal BBMVs, which are significantly altered more or less than 1.5-
1260 fold change (p-value < 0.05) in 8h IRI, were curated into networks by IPA and literature. A –
1261 C networks indicate the proteins which are highly altered at 8h compared to 4h IRI. Protein
1262 expressions that are upregulated and downregulated are shown in red and cyan, respectively,
1263 with intensity shading corresponding to the degree of fold change. Proteins are shaped by
1264 categories and double cycles indicate protein complexes. Solid and dash lines represent direct
1265 and indirect interactions, respectively. Lines are colored for contrast observation in which blue
1266 and magenta lines imply activation to regulators and targeting proteins, respectively. A)
1267 Network involved in connective tissue development and function via ANXA1 and BCL2
1268 regulators. B) Network involved in cell-cell interaction and system development. C) Network
1269 involved in cell morphology, cell-cell interaction, and movement via Integrin signaling.

Figure supplement 3: Wiriyasermkul, et al.

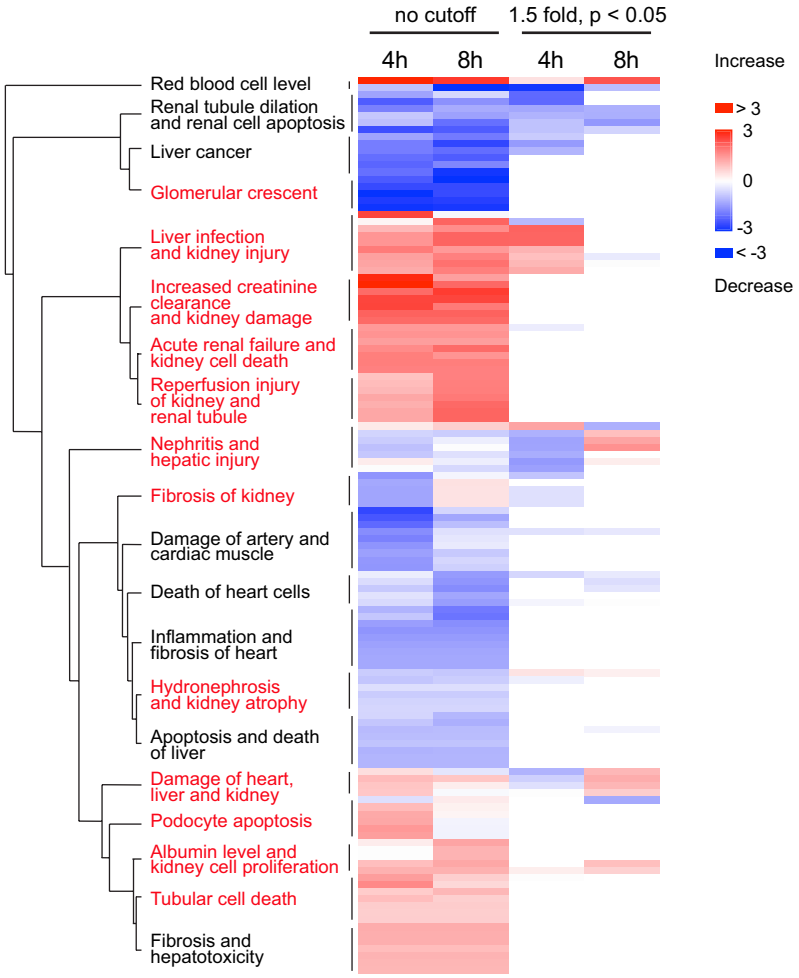

Figure supplement 3: Hierarchical heatmap of abnormalities from all identified proteins. Heatmap of all proteome with no cut-off value compared to data from the cut-off values of 1.5-fold change and 0.05 p-value (1.5 fold, $p < 0.05$). The abnormalities highlighted in red are those involved with kidney. Colors indicate predicted pathologies (z-score).

Figure supplement 4: Wiriyasermkul, et al.

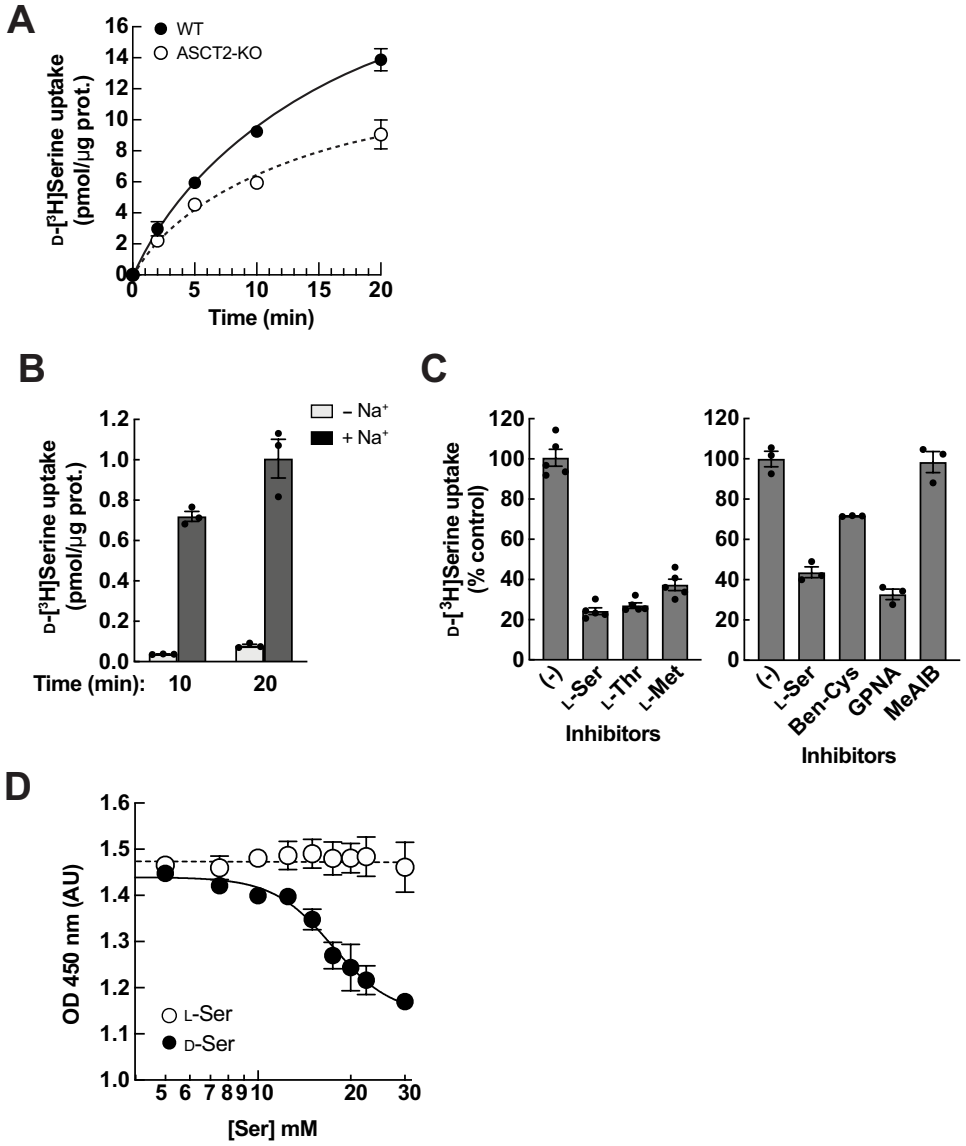

Figure supplement 4: Characterization of ASCT2 as a D-serine transporter in HEK293 cells

A) Time course of 100 µM D-[^{3}H]serine transport (10 Ci/mol) was measured in wild-type (WT) and *ASCT2*-knockout (ASCT2-KO) HAP1 cells. D-[^{3}H]Serine transport in the cells was measured in PBS pH 7.4. n = 3. B) Transport of 10 µM D-[^{3}H]serine was measured for 10 or 20 min in HEK293 cells in the presence or absence of Na^+. n = 3. C) Inhibition of D-[^{3}H]serine

1280 transport by several compounds. The uptake was measured for 10 min in PBS buffer. Left: 5
1281 μM D-[^{3}H]serine uptake was measured in the presence or absence of 2 mM L-amino acids. n =
1282 4. Right: 2 μM D-[^{3}H]serine uptake was measured in the presence or absence of 1 mM
1283 inhibitors; Ben-Cys: *S*-benzyl-L-cysteine, a non-specific inhibitor of ASCT2; GPNA: L-γ-
1284 glutamyl-*p*-nitroanilide, an inhibitor of ASCT2, SNATs and LATs; MeAIB: 2-
1285 (methylamino)isobutyric acid, a system A inhibitor. n = 3. D) Cell-growth measurement (XTT
1286 assay) of HEK293 cells treated with either L-serine (opened circles) or D-serine (closed circles)
1287 at different concentrations for two days. In contrast to L-serine which did not alter cell viability,
1288 D-serine reduced cell growth in a concentration-dependent manner. D-Serine inhibition curve
1289 was fitted to non-linear regression of $\log_{10}$[D-Ser] v.s. cell growth, resulting in IC_{50} of 17.4 mM
1290 and minimum growth at OD 450 nm of 1.15 AU. n = 3 - 5.

Figure supplement 5: Wiriyasermkul, et al.

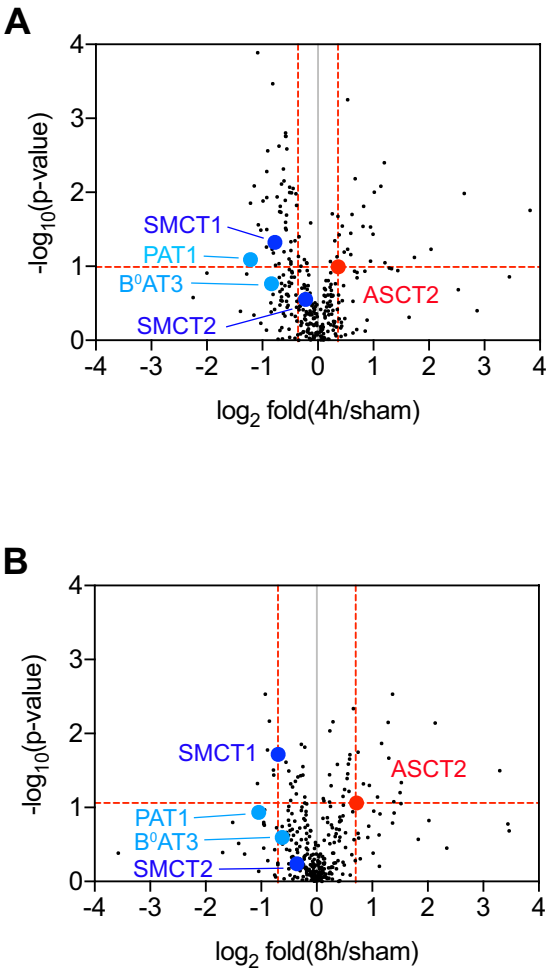

Figure supplement 5: SMCTs, PAT1, and B^0AT3 in the volcano plots of membrane transport proteins

Volcano plot of 319 membrane transport proteins is identical to the plot presented in Figure 4A. Position of SMCT1, SMCT2, PAT1, and B^0AT3 are indicated.

Figure supplement 6: Wiriyasermkul, et al.

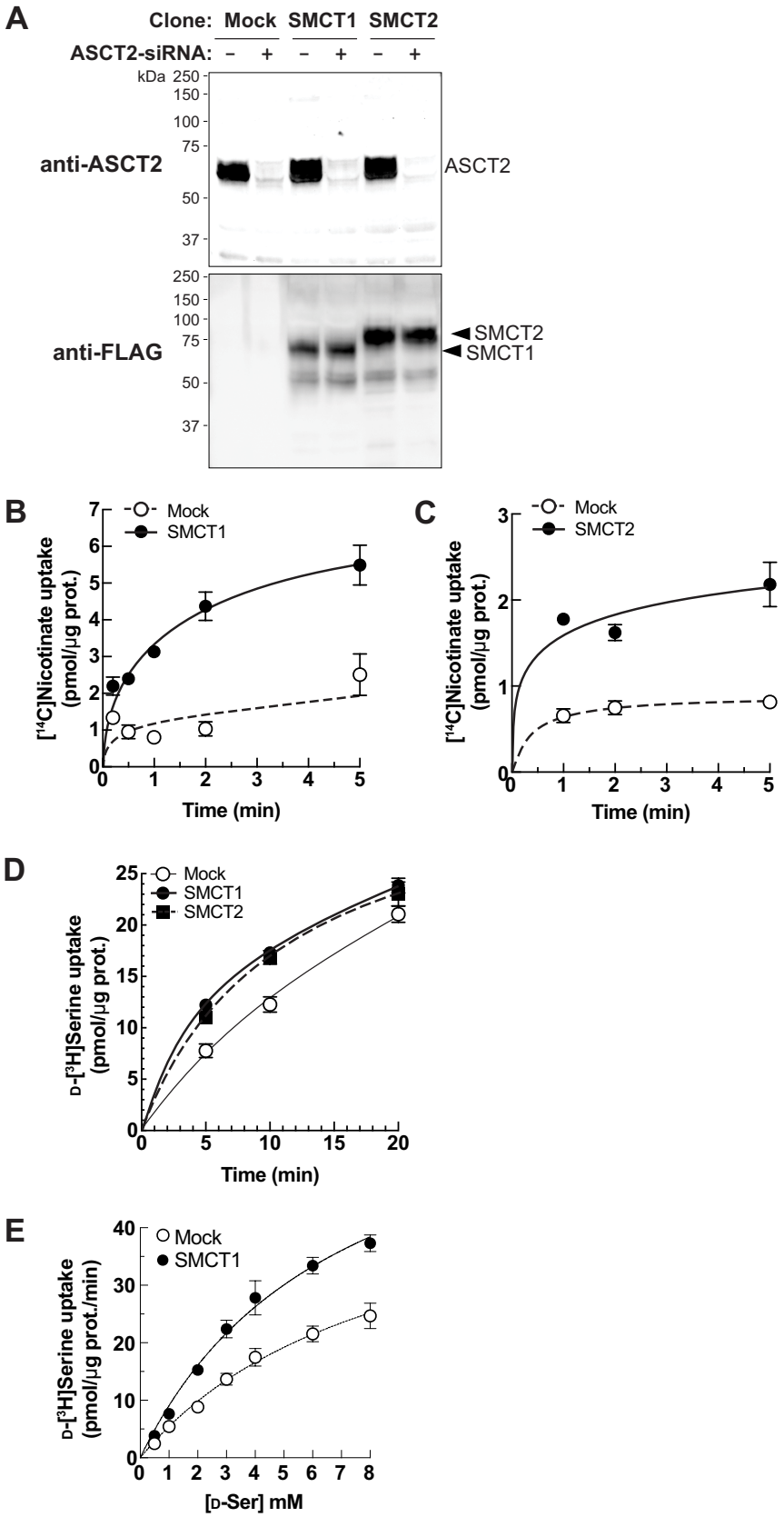

1295

1296 **Figure supplement 6: SMCT1 and SMCT2 function in FlpInTR-SMCT1 and FlpInTR-**
1297 **SMCT2 stable cell lines**

1298 A) Western blot of membrane fractions from FlpInTR-Mock, -SMCT1, and -SMCT2 cells with
1299 ASCT2-siRNA transfection. Flp-In T-REx 293 stably expressing SMCT1 (SMCT1) and
1300 SMCT2 (SMCT2), as well as Mock, were transfected with ASCT2-siRNA for two days.
1301 Membrane proteins were extracted from crude membrane fractions and subjected to Western
1302 blot analysis. ASCT2 knockdown efficiency was evaluated by anti-hASCT2 antibody.
1303 Expression of SMCT1 and SMCT2 were verified by anti-FLAG antibody. B – C) Evaluation
1304 of SMCT1 and SMCT2 function by transport assay. Time course of 50 μM [^{14}C]nicotinate
1305 uptake was measured for 0.5 – 5 min in FlpInTR-SMCT1 (B) and FlpInTR-SMCT2 (C) cells,
1306 compared to mock cells (Mock). n = 3. D) Time course of 100 μM D-[^{3}H]serine uptake in
1307 FlpInTR-SMCT1 (SMCT1), FlpInTR-SMCT2 (SMCT2), and Mock cells. The experiment was
1308 carried out in a similar way to experiment in Figure 6A except that the cells were not subjected
1309 to ASCT2 knockdown. n = 4. E) Raw data of Figure 6C before subtraction with the uptake data
1310 in Mock cells. D-[^{3}H]serine uptake in FlpIn293TR-SMCT1 compared to FlpIn293TR-Mock
1311 cells. The uptake values were fitted to Michaelis-Menten plot. n = 3 – 4.

Figure supplement 7: Wiriyasermkul, et al.

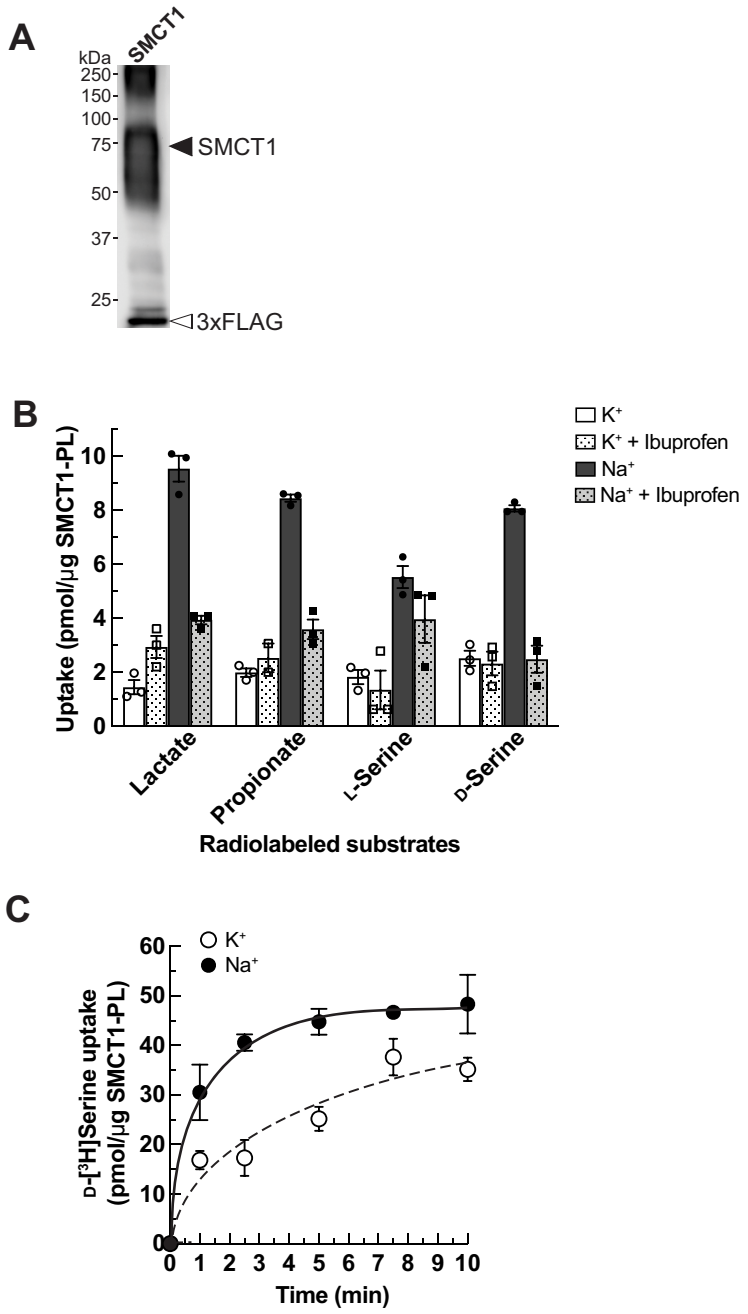

Figure supplement 7: Purification of SMCT1 and functional characterization

A) Western blot of purified SMCT1 from pCMV14-SMCT1-transfected Expi293F cells. The protein was detected by anti-FLAG antibody. The closed arrowhead indicates purified SMCT1, whereas the opened arrowhead is 3xFLAG peptides for the elution of the purified SMCT1. The bands above 250 kDa probably include SMCT1, which is aggregated at the top of SDS-

1317 polyacrylamide gel. B) Raw data of the ibuprofen effect presented in Figure 7B before
1318 subtraction with the uptake in K^+-buffer. Uptake of [^{3}H]lactate, [^{3}H]propionate, L-[^{3}H]serine,
1319 and D-[^{3}H]serine (all 50 μM) in SMCT1 proteoliposomes (SMCT1-PL). The uptake was
1320 measured in the Na^+ buffer (Na^+) or Na^+-free buffer (K^+) in the presence or absence of 1 mM
1321 ibuprofen. n = 3. C) Raw data of D-[^{3}H]serine transport in SMCT1-PL presented in Figure 7C
1322 prior to subtraction with the uptake in K^+-buffer. Time course of D-[^{3}H]serine (200 μM)
1323 transport was measured in the SMCT1 proteoliposomes in Na^+-buffer (Na^+) or Na^+-free buffer
1324 (K^+).

Figure supplement 8: Wiriyasermkul, et al.

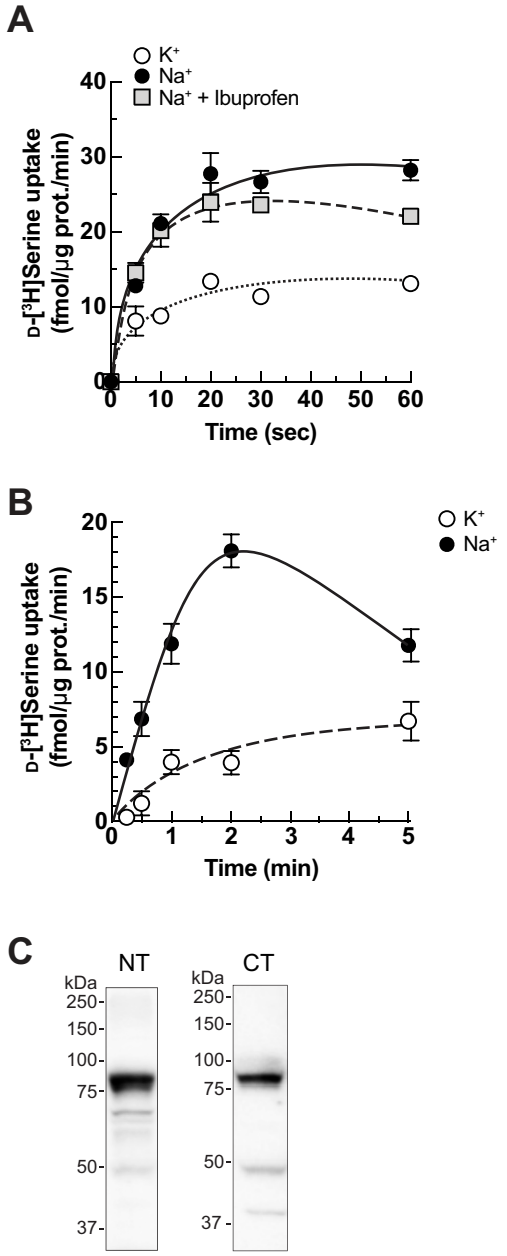

Figure supplement 8: D-Serine transport and expression of Asct2 in mouse BBMVs

A) Raw data of Figure 8A: D-[^{3}H]Serine transport in BBMVs preloaded with 4 mM L-glutamine. Time course of 10 µM D-[^{3}H]serine transport in L-glutamine-preloaded BBMVs in Na^+-buffer (Na^+) or Na^+-free (K^+) buffer in the presence or absence of 1 mM ibuprofen. n = 3 – 4. B) Time course of 10 µM D-[^{3}H]serine transport in BBMVs without preloading at longer

1330 time points. The transport was measured in Na^+-buffer (filled circles) or Na^+-free buffer
1331 (opened circles). n = 4. C) Western blot of Asct2 in mouse kidney BBMVs using anti-
1332 mAsct2(NT) (left) or anti-mAsct2(CT) (right) antibodies.

1333 **Table supplement 1. List of proteins identified from proteome analysis of BBMVs from**
1334 **IRI mouse kidneys.**
1335 *Table supplement 1 is provided as an excel sheet which is submitted separately as a*
1336 *supporting file.*
1337
1338
1339
1340

1341 **Table supplement 2**. Plasma membrane amino acid transporters identified from mass
1342 spectrometry of HEK293 membrane fraction

Transporter	Accession	Peptides	PSMs	Score Mascot	Abundance
SLC1A3/EAAT1	P43003	1	4	167	1.20E+07
SLC1A5/ASCT2	Q15758	5	15	221	1.68E+08
SLC3A2/4F2hc	J3KPF3	15	46	815	3.62E+08
SLC6A15/B^0AT2	Q9H2J7	2	2	46	1.28E+07
SLC7A1/CAT1	B2R728	2	7	83	4.94E+07
SLC7A6/y^+LAT2	Q92536	1	1	31	7.15E+06
SLC38A2/SNAT2	A8K6H9	1	2	88	2.82E+07
SLC38A9/SNAT9	Q8NBW4	1	1	0	1.33E+07

1343

Figure 1: Wiriyasermkul, et al.

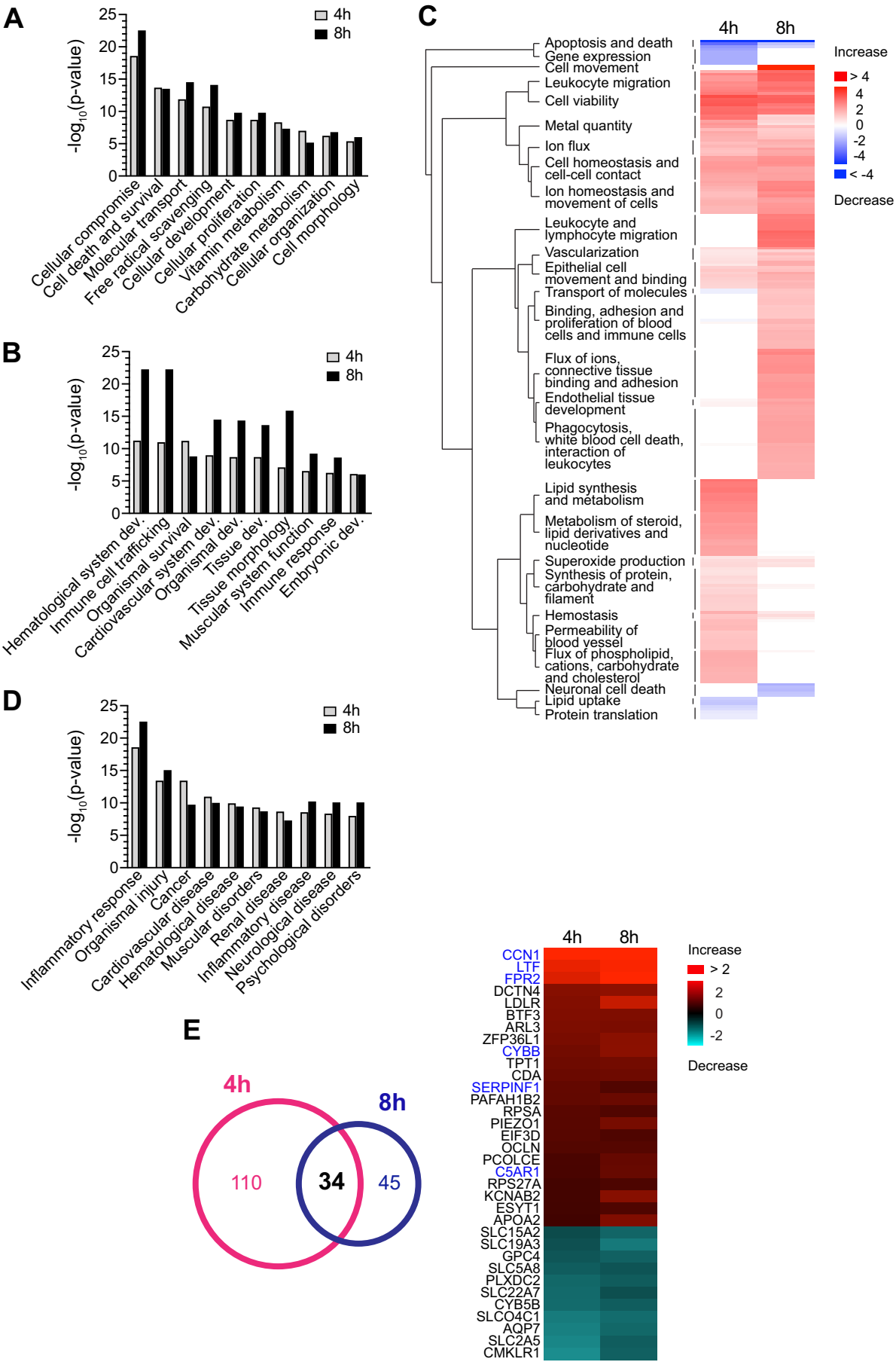

Figure 2: Wiriyasermkul, et al.

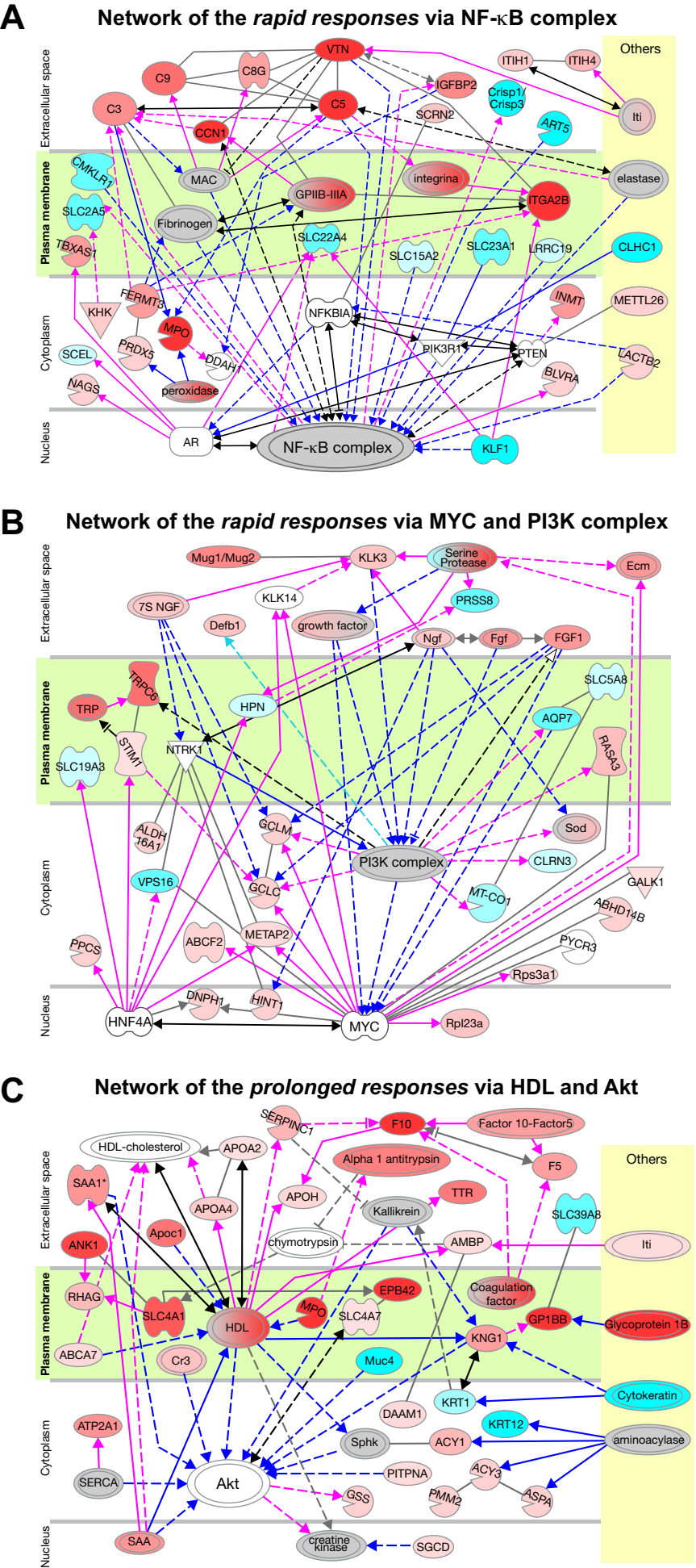

Figure 3: Wiriyasermkul, et al.

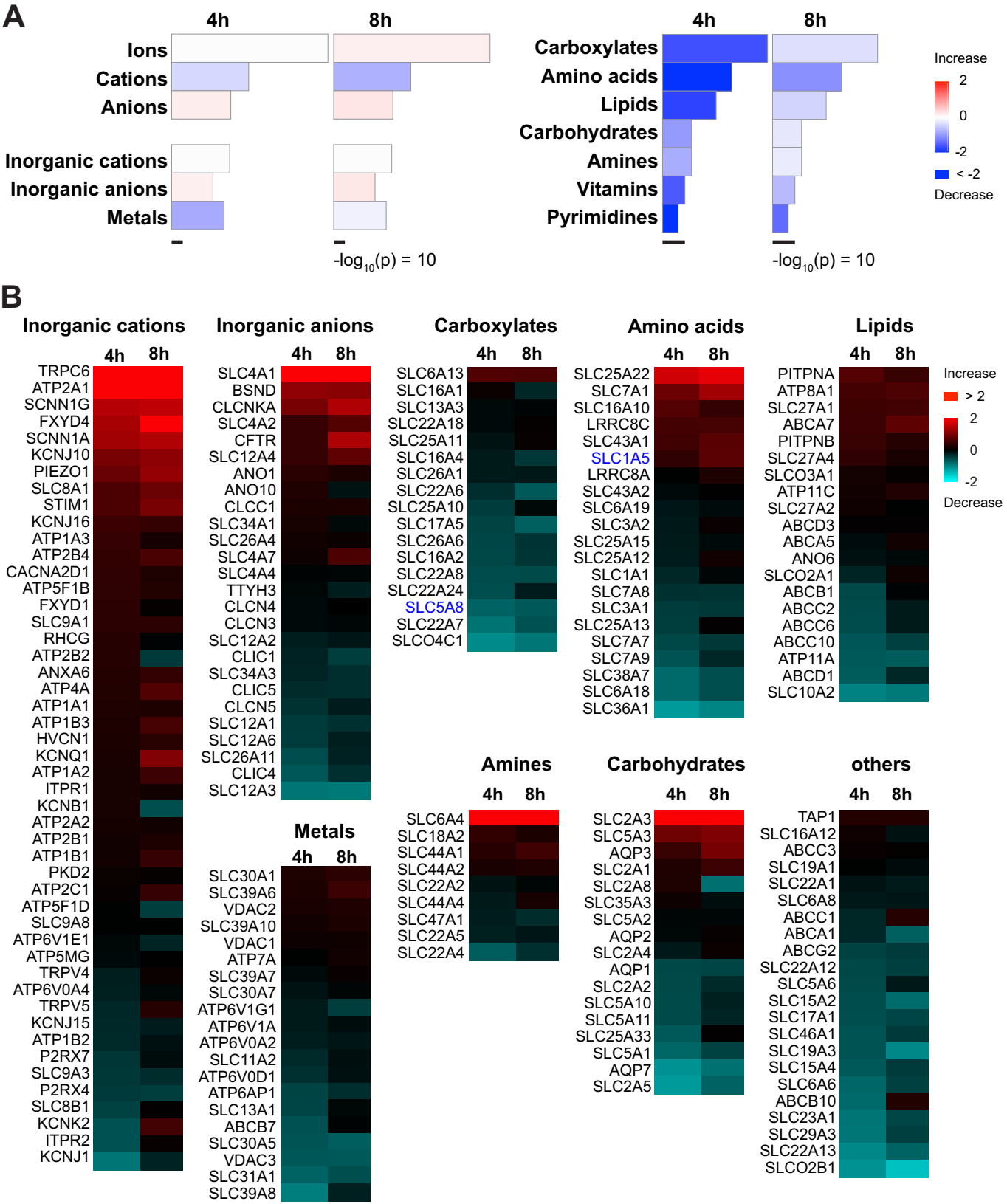

Figure 4: Wiriyasermkul, et al.

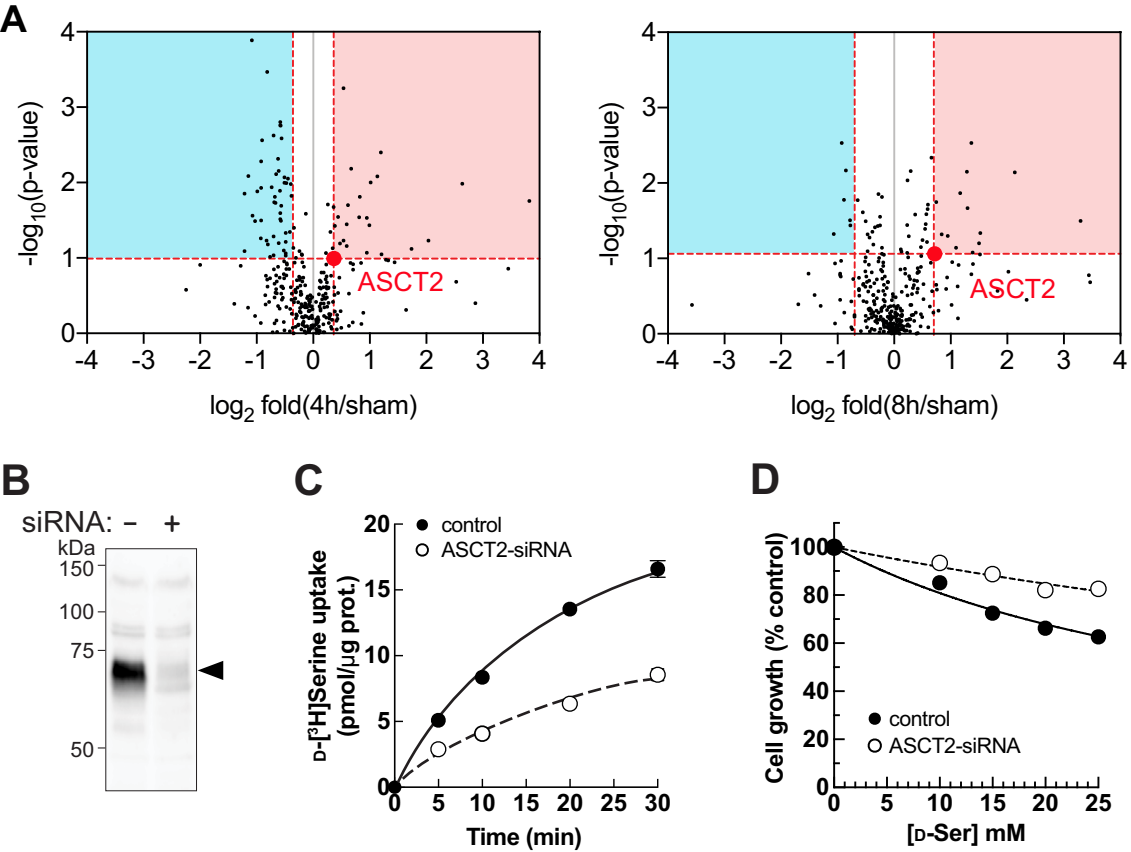

Figure 5: Wiriyasermkul, et al.

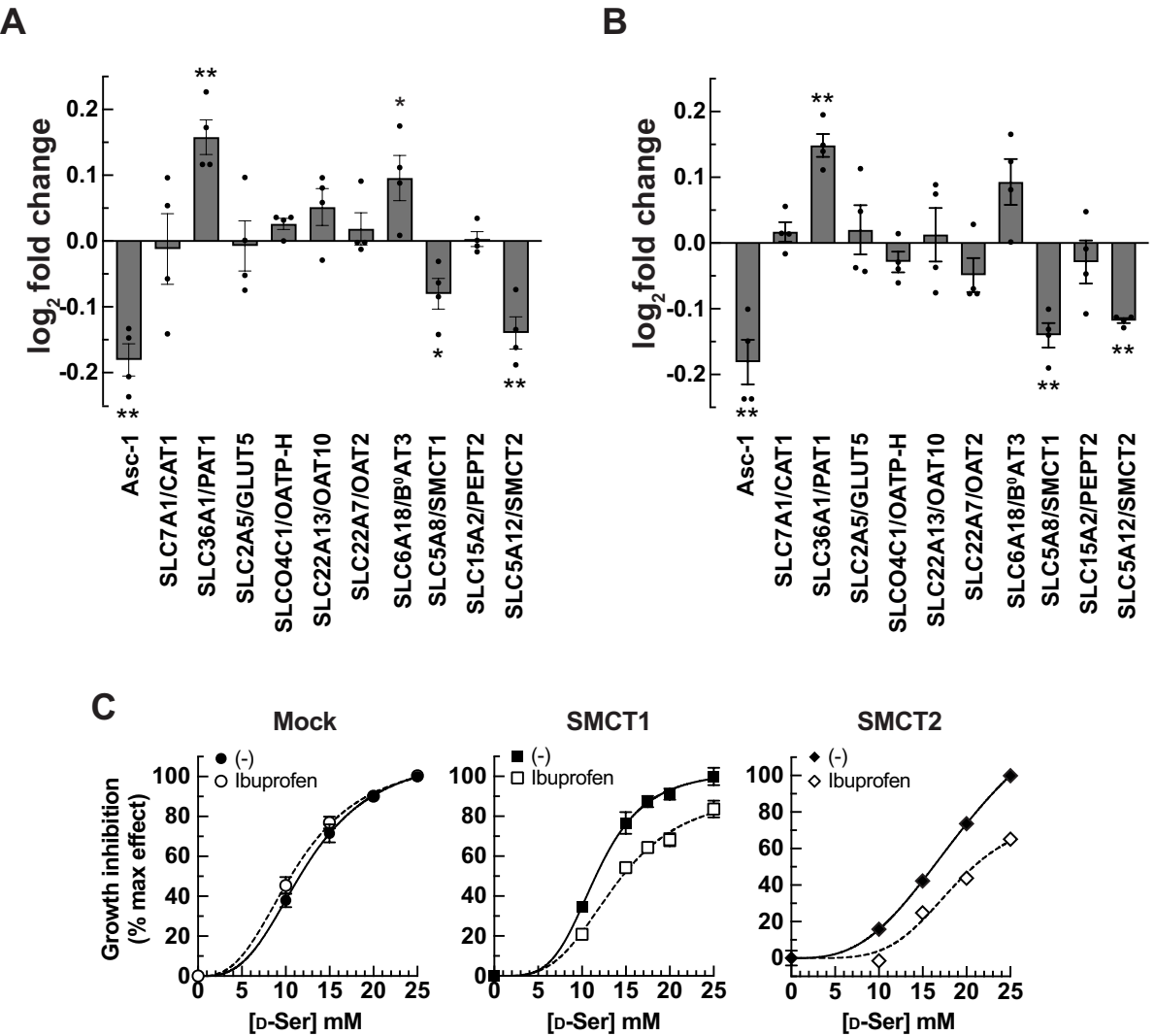

Figure 6: Wiriyasermkul, et al.

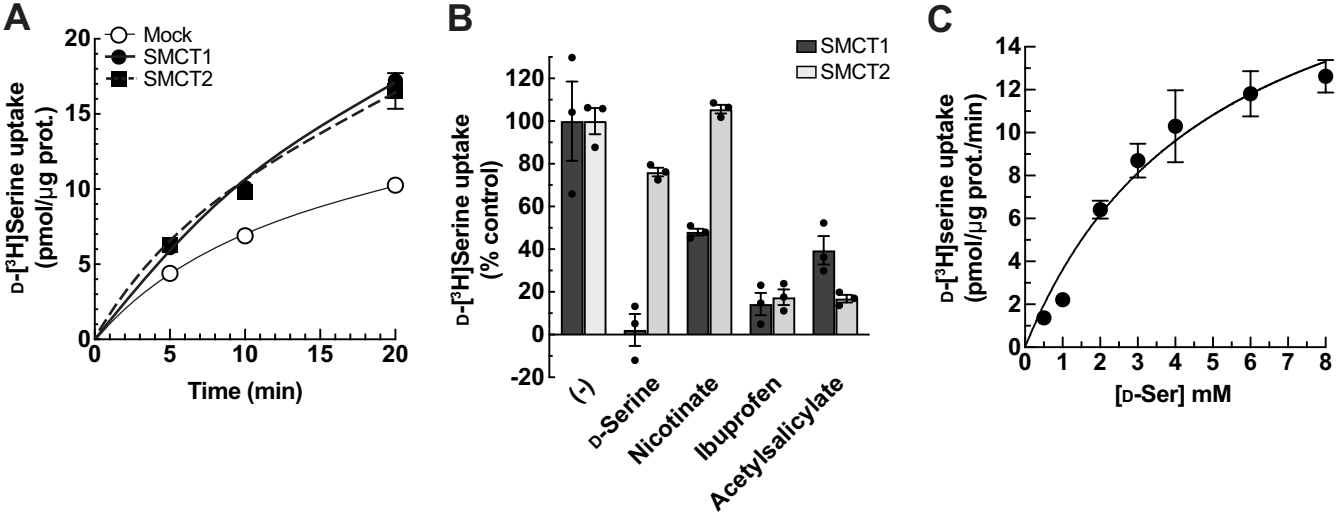

Figure 7: Wiriyasermkul, et al.

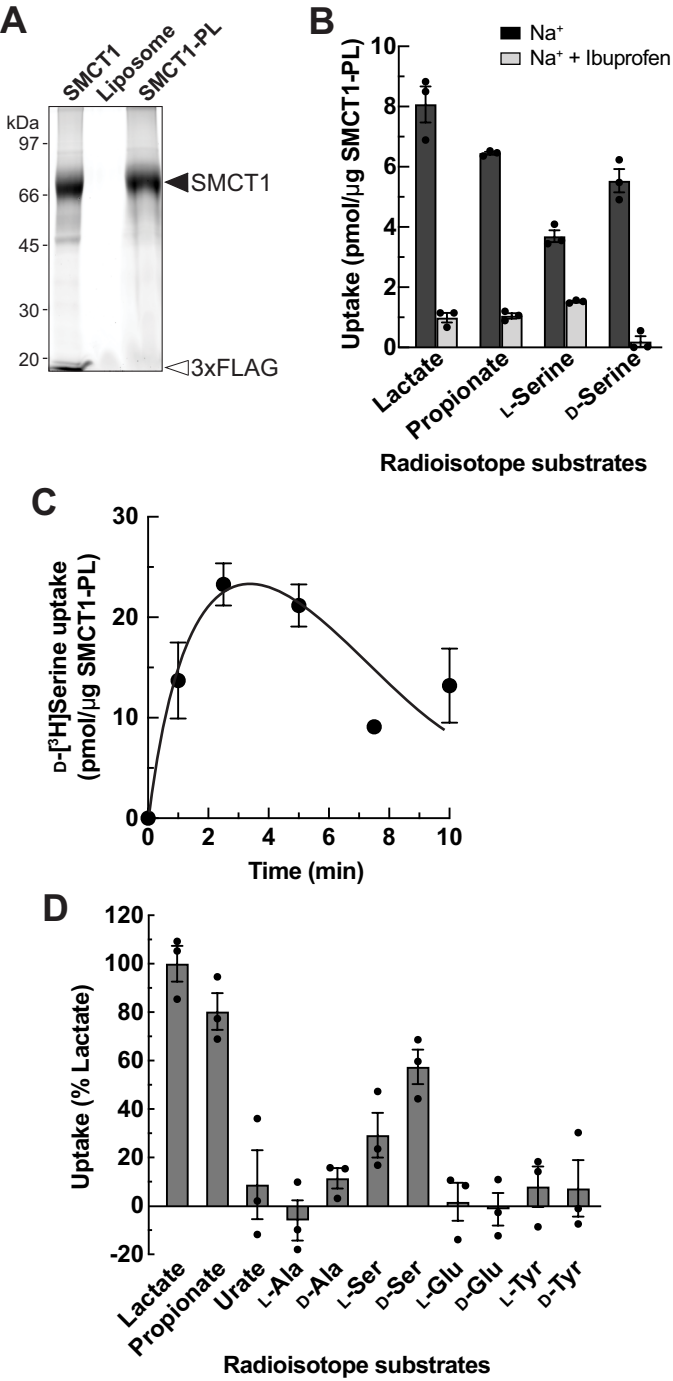

Figure 8: Wiriyasermkul, et al.

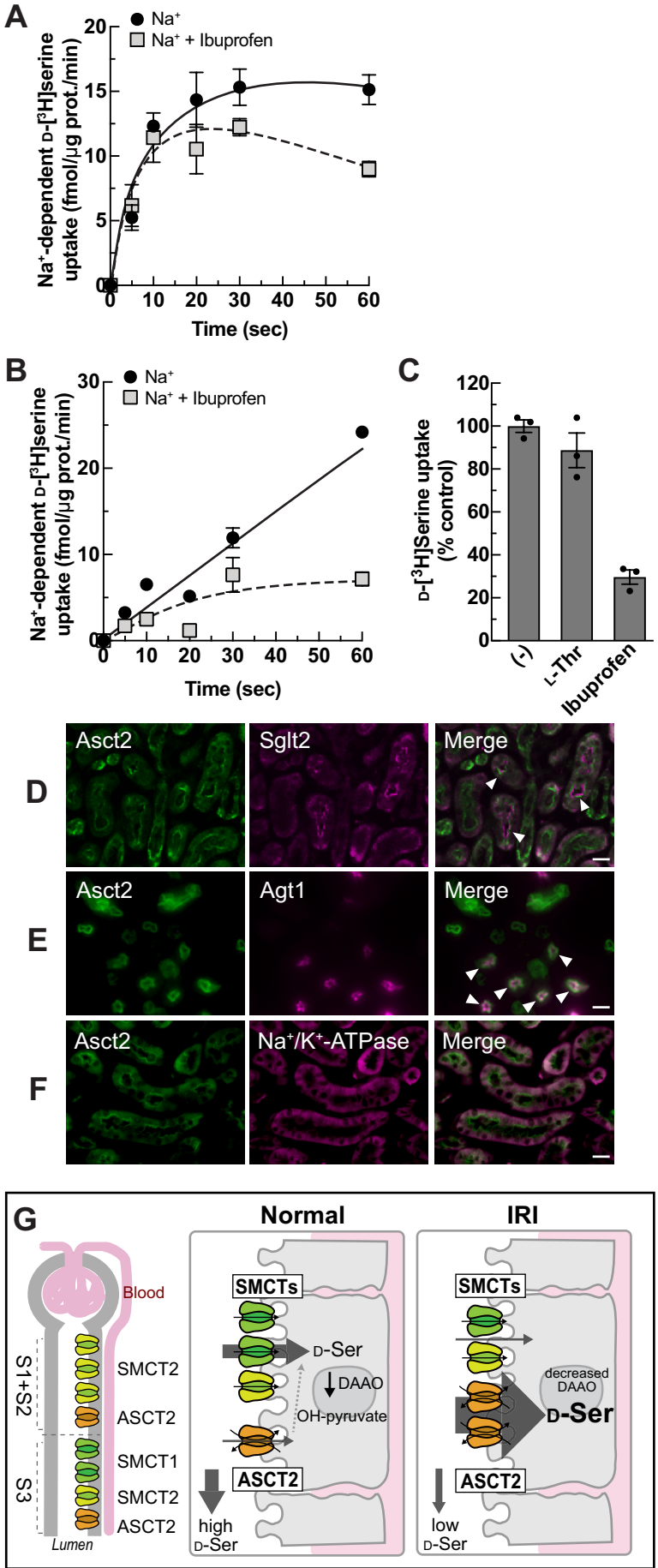

Figure supplement 1: Wiriyasermkul, et al.

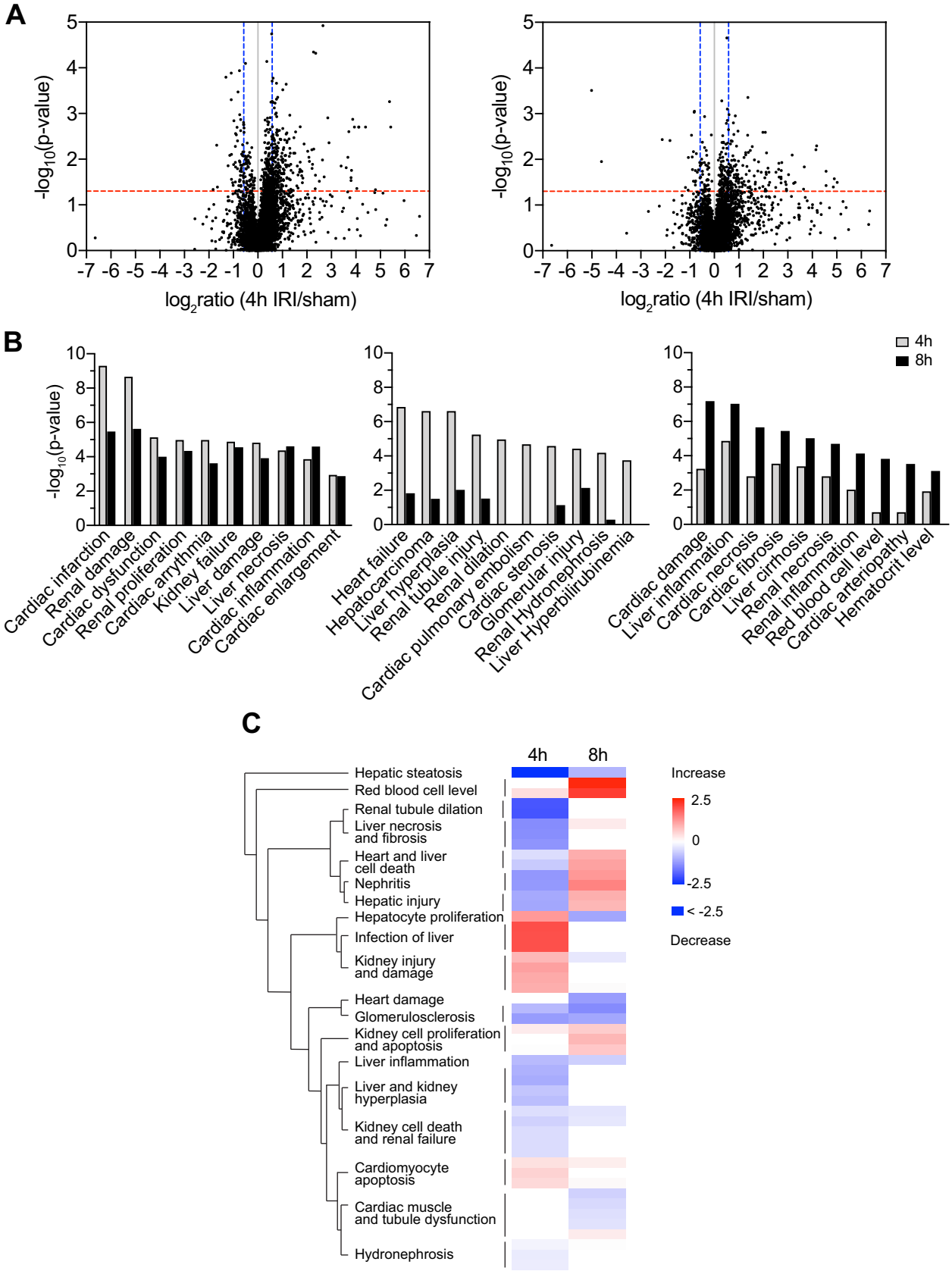

Figure supplement 2: Wiriyasermkul, et al.

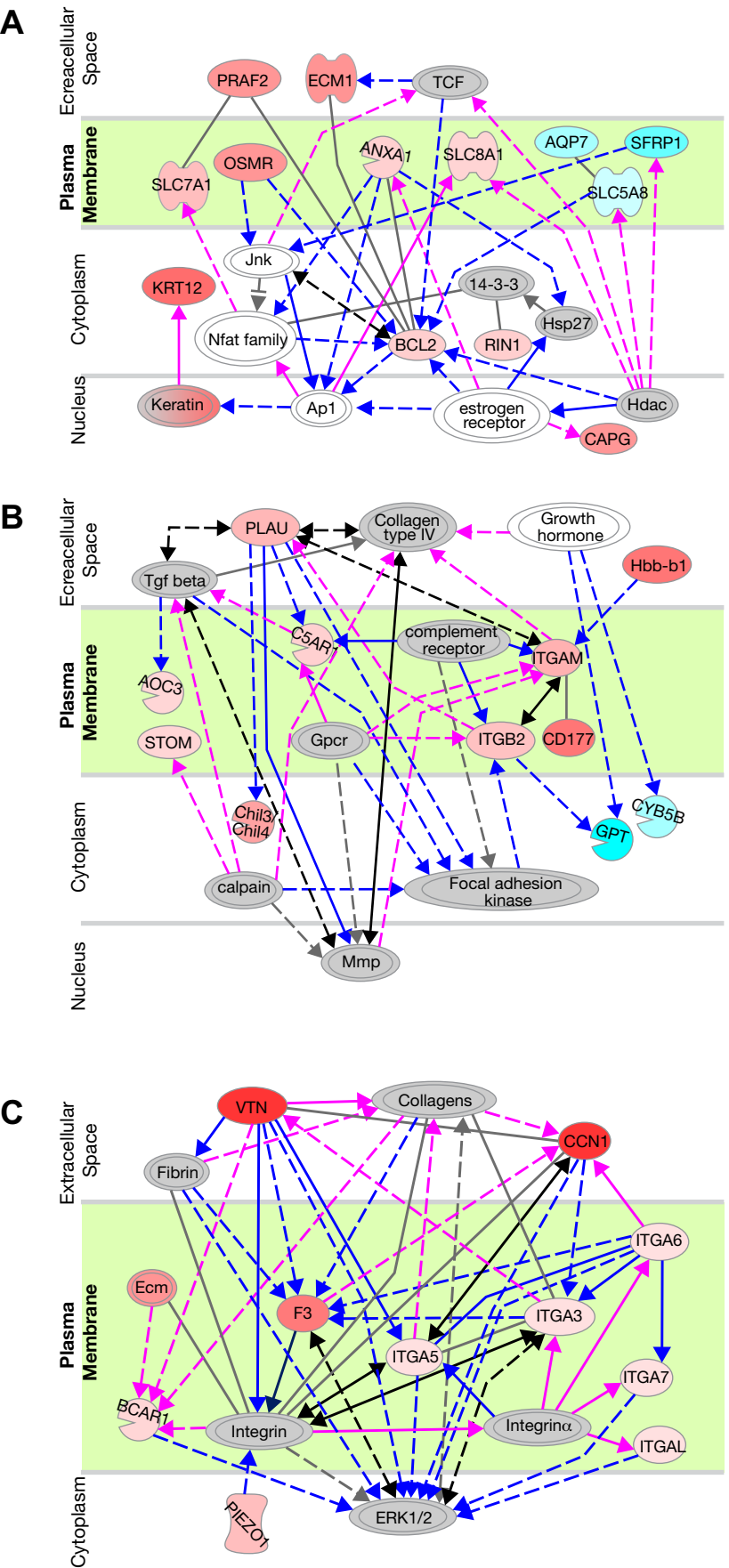

Figure supplement 3: Wiriyasermkul, et al.

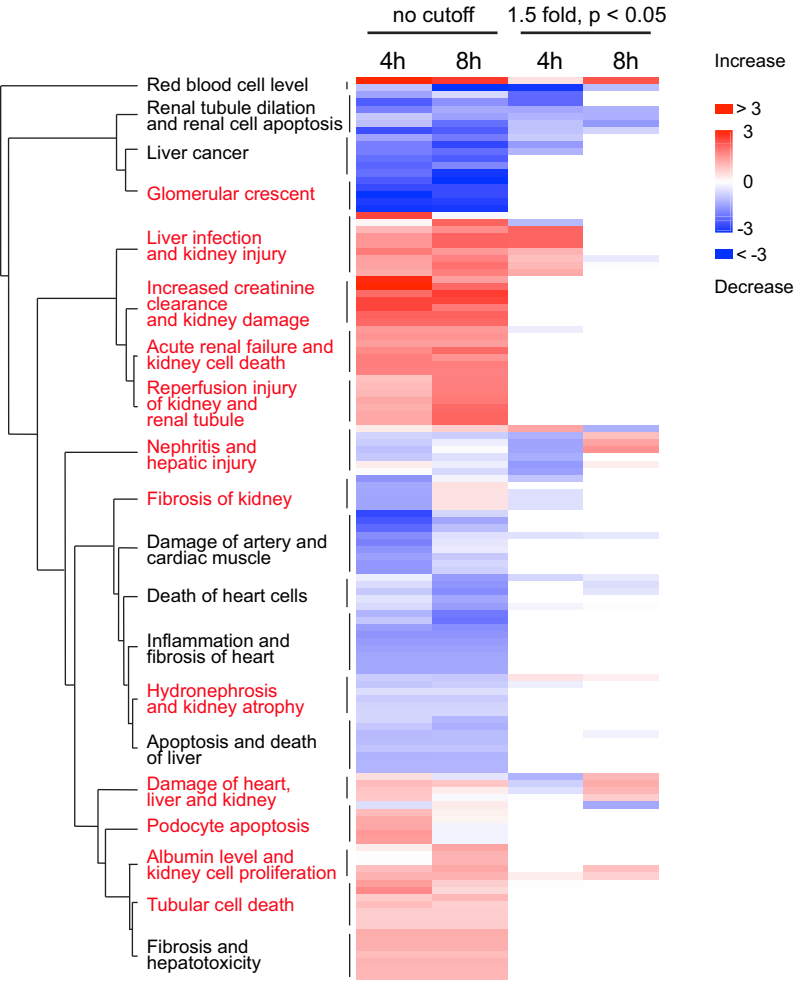

Figure supplement 4: Wiriyasermkul, et al.

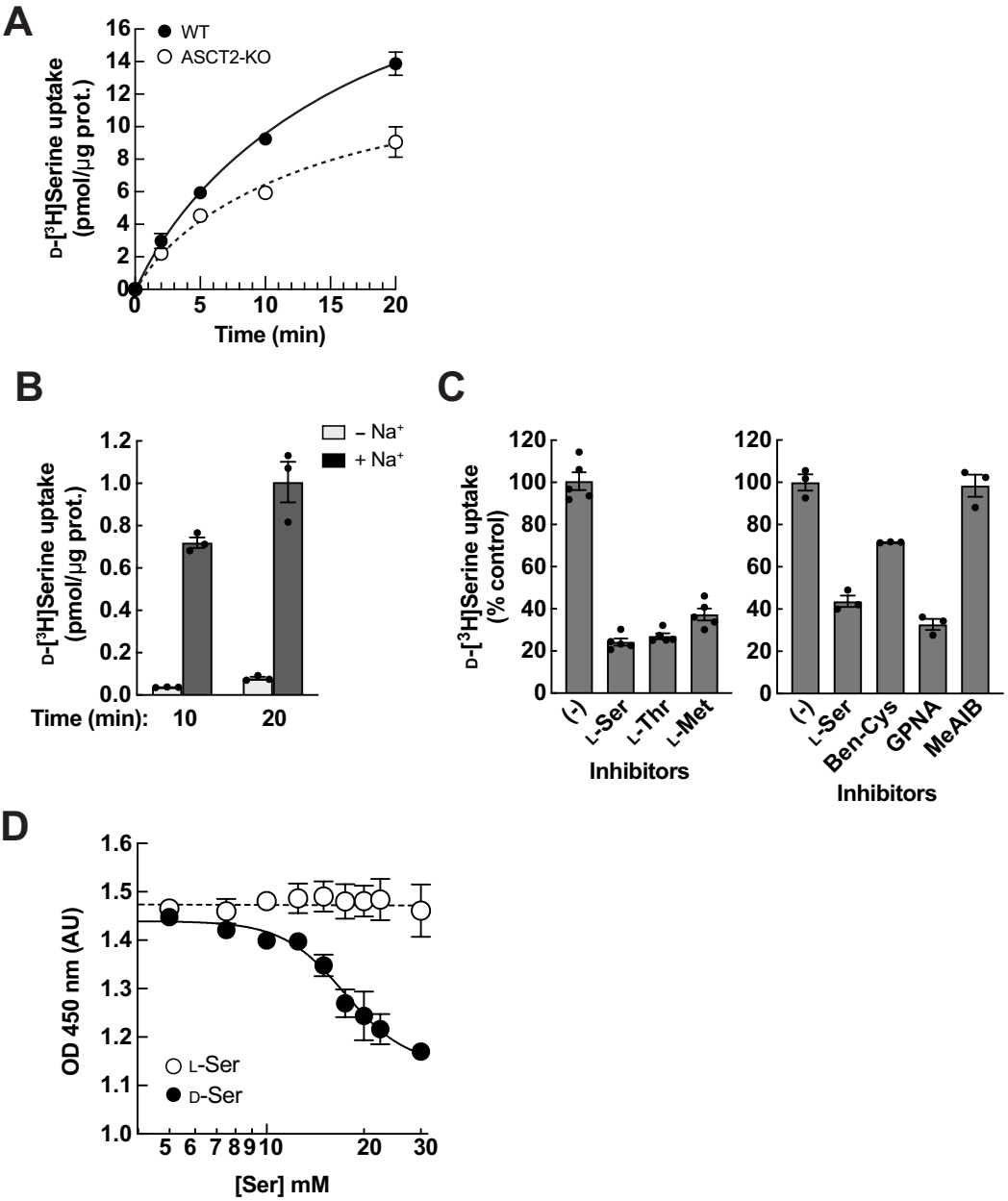

Figure supplement 5: Wiriyasermkul, et al.

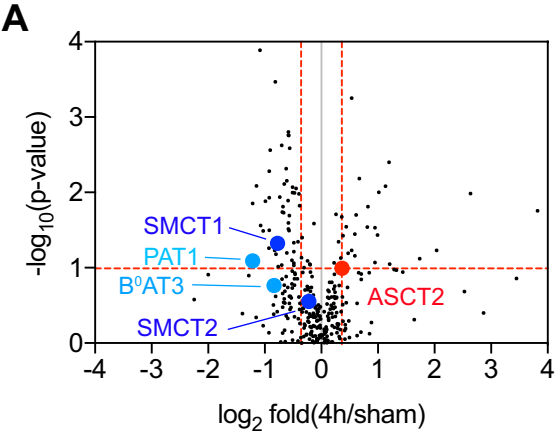

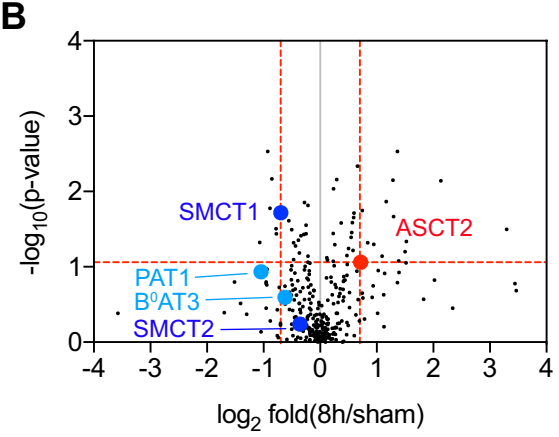

Figure supplement 6: Wiriyasermkul, et al.

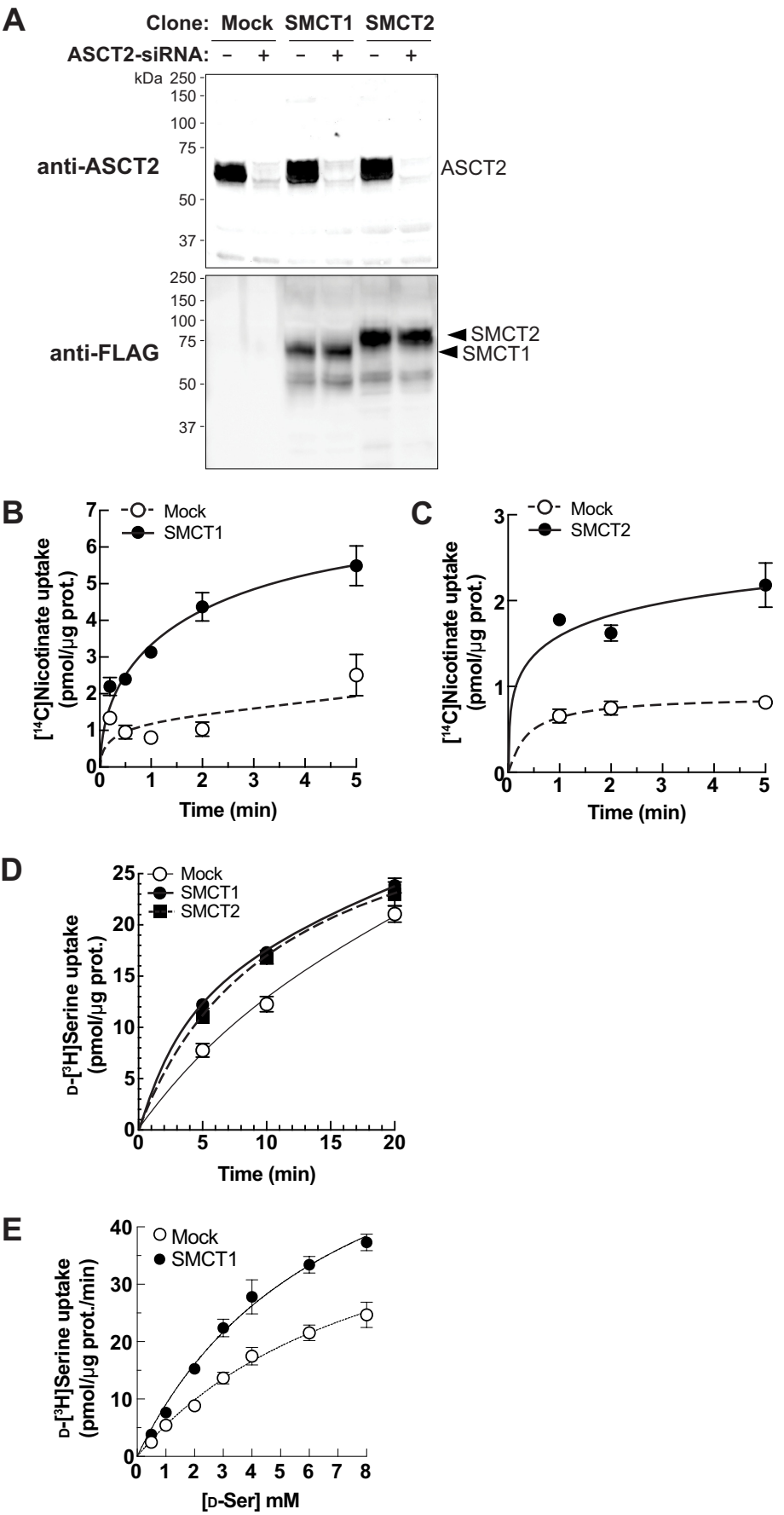

Figure supplement 7: Wiriyasermkul, et al.

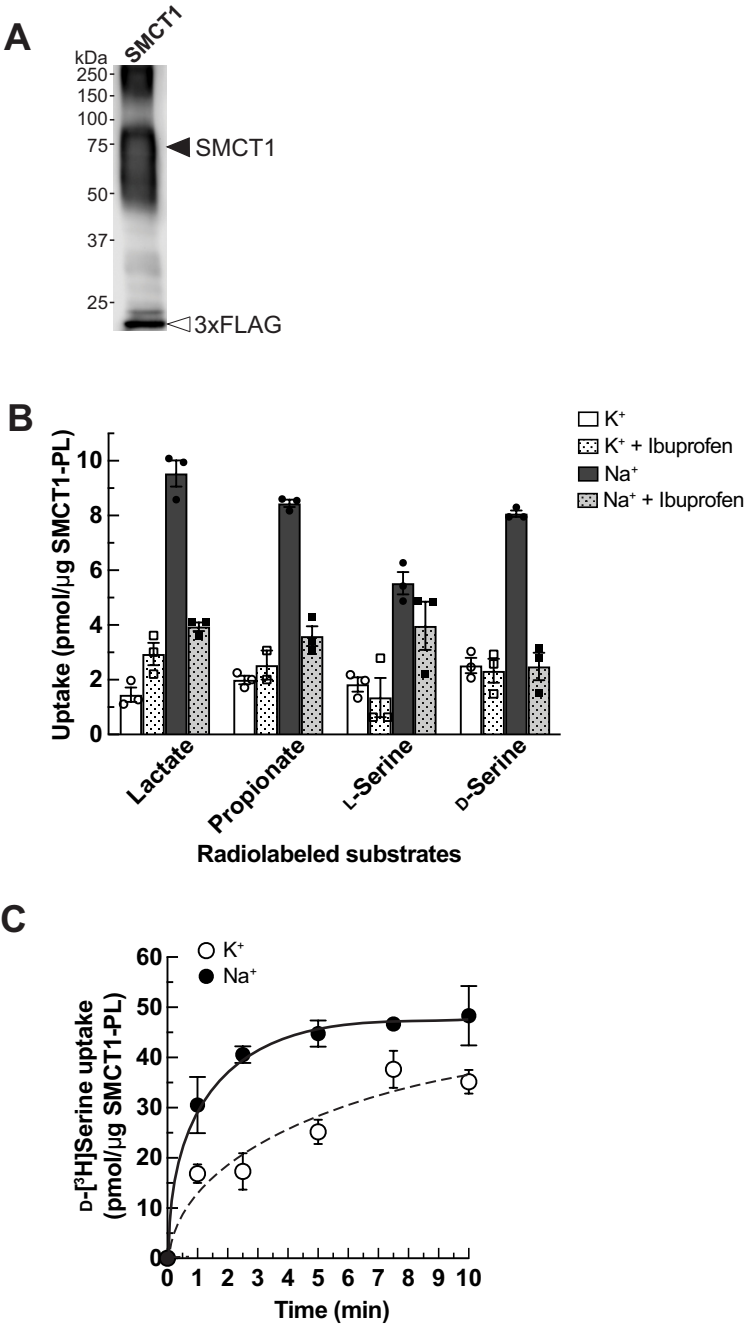
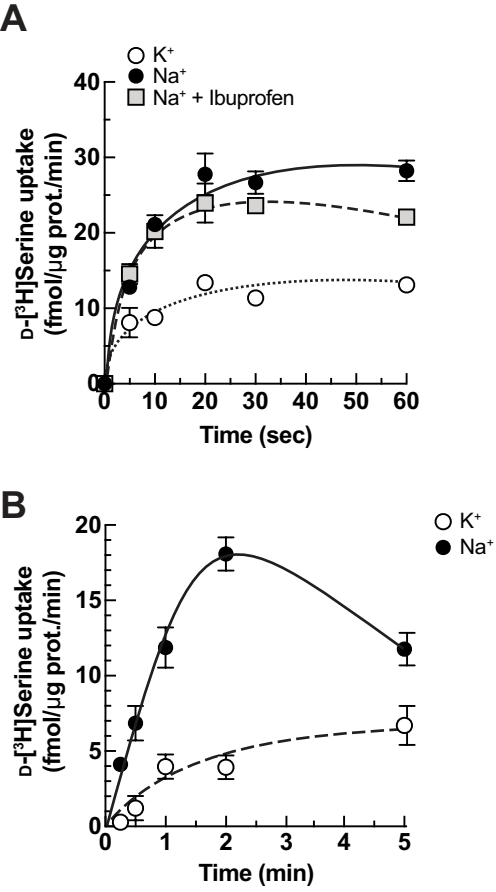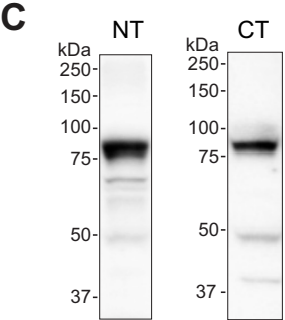
Figure supplement 8: Wiriyasermkul, et al.